ABSTRACT

Title of dissertation:	HYBRIDIZATION AND ENHANCEMENT PROCESSES IN QUASI-TWO DIMENSIONAL SUPERCONDUCTORS
	Zachary M. Raines, Doctor of Philosophy, 2019
Dissertation directed by:	Professor Victor M. Galitski Department of Physics

Superconductivity is a field with a great many branches and applications. In this dissertation, we focus on two specific processes in superconductors – light-induced enhancement and hybridization of collective modes – in two types of quasi-two dimensional materials – either the loosely coupled planes of a layered superconductor or a superconducting thin film.

Motivated by experiments in the cuprates that have seen evidence of a transient superconducting state upon optical excitation we study the effects of inter-plane tunneling on the competition between superconductivity and charge order. We find that an optical pump can suppress the charge order and simultaneously enhance superconductivity, due to the inherent competition between the two. Taking into account that the charge order empirically shows a broad peak in c-axis momentum, we consider a model of randomly oriented charge ordering domains and study how interlayer coupling affects the competition of this order with superconductivity.

Also in the cuprates, several groups have reported observations of collective modes of the charge order present in underdoped cuprates. Motivated by these experiments, we study theoretically the oscillations of the order parameters, both

in the case of pure charge order, and for charge order coexisting with superconductivity. Using a hot-spot approximation we find in the coexistence regime two Higgs modes arising from hybridization of the amplitude oscillations of the different order parameters. We explore the damping channels of these hybrid modes.

As another means of enhancing superconductivity we consider coupling a two-dimensional superconducting film to the quantized electromagnetic modes of a microwave resonator cavity. We find that when the photon and quasiparticle systems are out of thermal equilibrium, a redistribution of quasiparticles into a more favorable non-equilibrium steady-state occurs, thereby enhancing superconductivity in the sample, a fluctuation analog of a phenomenon known as the Eliashberg effect.

Finally, following the recent success of realizing exciton-polariton condensates in cavities, we examine the hybridization of cavity photons with two types of collective modes in superconductors. Enabled by the recently predicted and observed supercurrent-induced linear coupling between these excitations and light, we find that significant hybridization between the superconductor's collective modes and resonant cavity photons can occur.

HYBRIDIZATION AND ENHANCEMENT PROCESSES IN QUASI-TWO DIMENSIONAL SUPERCONDUCTORS

by

Zachary Mark Raines

Dissertation submitted to the Faculty of the Graduate School of the
University of Maryland, College Park in partial fulfillment
of the requirements for the degree of
Doctor of Philosophy
2019

Advisory Committee:
Professor Victor M. Galitski: Chair
Professor Alexey Gorshkov
Professor Richard Greene
Professor Jay Deep Sau
Professor John Weeks

Dedication

To my grandparents, who always believed I would get here.

Acknowledgements

The road up to and through graduate school has been a long one. I have not arrived at this point on my own and I would be remiss if I didn't mention those who helped me along the way.

I am grateful to my advisor, Victor Galitski, without whom this dissertation would not exist. In particular I am appreciative of his patience through my somewhat lengthy graduate school career, and for his advocacy on my behalf.

Throughout my time in graduate school I have benefited greatly from my interactions with my colleagues. Valentin Stanev and Andrew Allocca in particular played an outsized role in the work presented in this dissertation, both through contributed research and helpful advice. Andrew in particular deserves credit for having survived many years sharing an office with me.

I am thankful to Prof. Mohammad Hafezi for the enlightening discussions throughout the work leading to Chapters 4 and 5. Jonathan Curtis also deserves credit for his creative contributions to Chapter 4, as well as the many (sometimes heated) conversations that ultimately made Chapters 4 and 5 better works.

My family has had a large impact on my life and the course I've taken. I would like to thank my Dad for his advice and counsel regarding my academic journey and for encouraging me to achieve my goals. I would also like to thank my Mom for her support and for always believing in me.

To my friends, thanks for the support and the good times. Thank you to everyone I've worked with over the years.

A special thanks to Natalie, for taking the time to read through drafts of my work – especially the early versions – and for being supportive throughout my graduate school career. You helped me back up when I fell down, pushed me when I wasn't sure I could do it, and always made me smile.

Table of Contents

List of Tables

List of Figures

List of Abbreviations

Abbreviation	Description
BCS	**B**ardeen-**C**ooper-**S**chrieffer
BDW	**b**ond-**d**ensity-**w**ave
BS	**B**ardasis-**S**chrieffer
dFF-DW	**d**-**f**orm-**f**actor **d**ensity **w**ave
DOS	**d**ensity **o**f **s**tates
dSC	**d**-wave **s**uper**c**onductivity
EM	**E**lectro**m**agnetic
GL	**G**inzburg-**L**andau
JPR	**J**osephson **p**lasmon **r**esonance
KNLσM	**K**eldysh **N**on-**L**inear **σ** **M**odel
LBCO	**L**anthanum-**B**arium-**C**opper-**O**xide
LESCO	**L**anthanum-**E**uropium-**S**trontium-**C**opper-**O**xide
LSCO	**L**anthanum-**S**trontium-**C**opper-**O**xide
NESS	**n**on-**e**quilibrium **s**teady **s**tate
NLσM	**N**on-**L**inear **σ** **M**odel
RPA	**r**andom **p**hase **a**pproximation
THz	**T**erra**h**ertz
YBCO	**Y**ttrium-**B**arium-**C**opper-**O**xide

List of Symbols

Name	Symbol	Description
Electron operator	$c^{\dagger}_{n_1, n_2, \ldots}$	Electron creation operator for the state described by quantum numbers $n_1, n_2, \ldots$
Fine structure constant	α	$\alpha = e^2 / \hbar c$ (in Gaussian units). $\alpha^{-1} = 137.035999139(31)$
Heaviside function	Θ	$\Theta(x) = (1 + \operatorname{sgn} x)/2$
Fermi function	n_F	$n_F(x) = \left(1 - \exp(x/T)\right)^{-1}$
Bogoliubov quasiparticle DOS	ρ_{BQP}	$\rho_{\mathrm{BQP}} = \epsilon / \sqrt{\epsilon^2 - \Delta^2}$
Inelastic Relaxation time	τ_{in}	The charactestic time over which quasi-particle energy changes due to scattering with e.g. phonons

List of Publications

This dissertation is based on the following publications

1. Z. M. Raines, V. G. Stanev, and V. M. Galitski, "Enhancement of superconductivity via periodic modulation in a three-dimensional model of cuprates", Phys. Rev. B **91**, 184506 (2015)

2. Z. M. Raines, V. G. Stanev, and V. M. Galitski, "Hybridization of Higgs modes in a bond-density-wave state in cuprates", Phys. Rev. B **92**, 184511 (2015)

3. J. B. Curtis, Z. M. Raines, A. A. Allocca, M. Hafezi, and V. M. Galitski, "Cavity quantum Eliashberg enhancement of superconductivity", Phys. Rev. Lett **122**, 167002 (2019)

4. Z. Raines, *Phase pinning and interlayer effects on competing orders in cuprates*, 2018, arXiv:1809.06879 [cond-mat.supr-con]

5. A. A. Allocca, Z. M. Raines, J. B. Curtis, and V. M. Galitski, "Cavity superconductor-polaritons", Phys. Rev. B **99** (2019)

6. Z. Raines, A. A. Allocca, and V. Galitski, "Cavity Higgs-polaritons", In Preperation (2019)

Chapter 1: Introduction[1]

Superconductivity has been of profound interest since its discovery over a century ago [1], due both to its practical applications and the mystery of the mechanism behind its striking behavior. Indeed, while phenomenological description of the superconducting state was put forth by the London brothers [2] and Ginzburg and Landau [3] it took more than 45 years before the microscopic Bardeen-Cooper-Schrieffer (BCS) theory of superconductivity was developed [4]. In combination with pioneering works by Bogoliubov [5], Valatin [6], Abrikosov [7], Gor'kov [8, 9] and many others, it now became possible to theoretically study a wealth of phenomena related to superconductivity.

The discovery, three decades later, of the cuprate high temperature superconductors [10], opened up consideration of a wider array of superconducting systems and therefore more phenomena to investigate. Since then many families of superconductor have been discovered with a panoply of properties and underlying mechanisms, the nature of which is still an active area of research.

Of particular interest are the collective modes of superconductors and the interaction of the materials with electromagnetic fields, given the central role both of these play in the defining features of superconductivity [11]. In this dissertation, we study a selection of electromagnetic effects in superconductors focusing on externally driven enhancement of superconductivity and the behavior of collective modes. In what follows the systems playing host to these effects will be quasi-two dimensional superconductors: either the layered superconducting copper-oxide planes of a cuprate high-temperature superconductor, or a thin-film BCS superconductor inside a photonic cavity.

---

[1]Parts of this introduction are adapted from the works listed in the List of Publications. Those published in Physical Review B and Physical Review Letters are © American Physical Society.

1.1   Overview of dissertation

The structure of this dissertation is as follows. In Chapter 2, we investigate photo-induced enhancement of superconductivity in hole-doped cuprates. Motivated by pump-probe experiments described in Section 1.2.2, we study the effects of a light driven modification of interlayer structure on superconductivity in cuprates. Specifically, our focus is on the role of competition between superconductivity and experimentally observed coexistent charge order.

Chapter 3 then considers the same system for the purposes of investigating the amplitude collective modes of the competing orders. In this chapter, we calculate the dispersion relation and character of amplitude modes of the coexistent charge order and superconductivity. In particular, we investigate the emergence of a hybridized sub-gap amplitude mode.

Following this we turn our attention to coupled photonic cavity-superconductor systems for the remainder of the dissertation. In Chapter 4, we propose a means of enhancing superconductivity via coupling to a suitably engineered photon reservoir. We show how, in analogy with the Eliashberg effect discussed in Section 1.2.1, a photon bath can modify superconductivity by changing the occupation probabilities of Bogoliubov quasi-particles.

Finally, in Chapter 5 we investigate the possibility of hybridizing collective modes of superconductors with photons to form superconductor-polaritons. Such hybrid light-matter excitations are especially of interest due to the possibility of their condensation at high temperatures, similar to the examples discussed in Section 1.3.2.

In the rest of this chapter, we give a brief introduction to the background and formalism of the aforementioned topics in order to provide context for the treatment that follows.

1.2 Light induced enhancement of superconductivity

1.2.1 The Eliashberg Effect

At the simplest level, one expects the introduction of external Electromagnetic (EM) fields to be detrimental to superconductivity, either due to heating or through depletion of the condensate. There are, however, notable experimentally observed exceptions to this notion.

The first of these dates back to the 1960s, when enhancement of the critical current was observed for superconducting junctions subjected to microwave radiation [12, 13]. Several years later Eliashberg [14] proposed a theory explaining the effect as a redistribution of quasi-particles in the non-equilibrium steady state (NESS). The Eliashberg – or Wyatt-Dayem – effect[2] can be understood simply from the BCS gap equation

$$\frac{1}{g} = \int \frac{\mathrm{d}\mathbf{k}}{(2\pi)^d} \frac{1 - 2n(E_{\mathbf{k}})}{E_{\mathbf{k}}} \tag{1.1}$$

and the Boltzmann equation

$$\dot{n} + \mathbf{v} \cdot \boldsymbol{\nabla}_r n + \mathbf{F} \cdot \boldsymbol{\nabla}_p n = I_{\mathrm{coll}}[n]. \tag{1.2}$$

We begin by rewriting Eq. (1.1) in the quasi-classical approximation

$$\frac{1}{g\nu} = \int_{\Delta}^{\infty} \mathrm{d}\epsilon \frac{1 - 2n(\epsilon)}{\sqrt{\epsilon^2 - \Delta^2}} \tag{1.3}$$

where Δ is the BCS gap and ν is the density of states at the Fermi surface. Because the quasi-particle density of states (DOS) $\rho_{\mathrm{BQP}} = \epsilon/\sqrt{\epsilon^2 - \Delta^2}$ is sharply peaked near the gap edge $\epsilon \sim \Delta$, these low-energy particles matter most for determining the gap strength. Note that the left side of Eq. (1.3) is independent of the driving field. Thus,

---

[2]The Eliashberg effect should not be confused with the Migdal-Eliashberg theory of strong-coupling phonon-mediated superconductivity.

any change to n must cause a change in Δ to leave the integral invariant, as this is the only other free parameter. If the occupation of quasi-particles is redistributed such that particles near the gap edge are pushed to higher energies, this will have a similar effect to cooling the system, as in both cases the density of most relevant quasi-particles is depleted. This is the root of the Eliashberg effect. Concretely, we can consider the Ginzburg-Landau (GL) equation including the modification of the distribution function (c.f. Ivlev, Lisitsyn, and Eliashberg [15])

$$\frac{T_c - T}{T_c} - \frac{7\zeta(3)}{8\pi^2}\frac{\Delta^2}{T_c^2} - 2\int_\Delta^\infty \frac{d\epsilon}{\sqrt{\epsilon^2 - \Delta^2}} n_1(\epsilon) = 0. \tag{1.4}$$

where $n_1 = n - n_F$ is the deviation from the equlibrium Fermi occupation function. To lowest order in the correction $\delta\Delta = \Delta - \Delta_0$ and n_1 we then have

$$\frac{7\zeta(3)}{4\pi^2}\frac{\Delta_0\delta\Delta}{T_c^2} - 2\int_{\Delta_0}^\infty \frac{d\epsilon}{\sqrt{\epsilon^2 - \Delta_0^2}} n_1(\epsilon) = 0. \tag{1.5}$$

or

$$\frac{\delta\Delta}{\Delta_0} = \frac{T_c}{T_c - T}\int_{\Delta_0}^\infty \frac{d\epsilon}{\sqrt{\epsilon^2 - \Delta_0^2}} n_1(\epsilon) \tag{1.6}$$

where we have used the equilibrium GL equation to re-express Δ_0 in terms of T_c. We can see from Eq. (1.6) that for $T < T_c$ the enhancement of Δ is proportional to the depletion of n_1 scaled by the DOS factor $(\epsilon^2 - \Delta^2)^{-1/2}$.

To see how this happens we consider the uniform NESS in the absence of external forces.[3] The Boltzmann equation then simply becomes $I_{\text{coll}}[n] = 0$. The collision integral can be broken up into contributions leading to thermalization – due to i.e. phonons – which we treat here in the relaxation approximation and a contribution

---

[3]We include the external microwave field in the collision integral.

from the microwave field.

$$I_{\text{coll}}[n] \approx -\frac{n - n_F}{\tau_{\text{in}}} + I_{\text{coll}}^{\text{MW}}[n, \mathbf{A}]. \tag{1.7}$$

Here τ_{in} is the (inelastic) relaxation time. For the case where the final distribution is close to the Fermi distribution, we can linearize Eq. (1.7) in the deviation $n_1 = n - n_F$ and obtain

$$n_1 \approx \tau_{\text{in}} I_{\text{coll}}^{\text{MW}}[n_F, \mathbf{A}]. \tag{1.8}$$

$I_{\text{coll}}^{\text{MW}}$ can be calculated using the quasi-classical equations for a superconductor i.e. Usadel equation [16, 17] or Keldysh Non-Linear σ Model (KNLσM) [18, 19]. Doing so one finds

$$
\begin{aligned}
I_{\text{coll}}^{\text{MW}}[n_F] = \frac{2\alpha D}{c} \\
\times \Big[(1 - n_F(\epsilon) - n_F(\omega - \epsilon)) P(\epsilon, \omega - \epsilon) \rho_{\text{BQP}}(\omega - \epsilon) \Theta(\epsilon - \Delta) \Theta(\omega - \Delta - \epsilon) \\
+ (n_F(\epsilon + \omega) - n_F(\epsilon)) L(\epsilon, \epsilon + \omega) \rho_{\text{BQP}}(\epsilon + \omega) \Theta(\epsilon - \Delta) \\
+ (n_F(\epsilon) - n_F(\epsilon - \omega)) L(\epsilon - \omega, \epsilon) \rho_{\text{BQP}}(\epsilon - \omega) \Theta(\epsilon - \omega - \Delta) \Big]
\end{aligned} \tag{1.9}
$$

where D is the diffusion constant, α is the fine-structure constant, and $(L/P)(x, y) = 1 \pm \Delta^2/(xy)$ are coherence factors arising from the Bogoliubov rotation of the electron operators. We can identify each of the three terms: pair production and recombination, upward scattering, and downward scattering, respectively. The linearized correction due to Eq. (1.9) is plotted in Fig. 1.1. The most salient feature is that for a range of driving frequencies $\omega_{\text{min}} < \omega \lessgtr 2\Delta$ the correction n_1 is negative for electron energies $\epsilon \sim \Delta$ near the gap edge. We, therefore, see an enhancement of superconductivity.
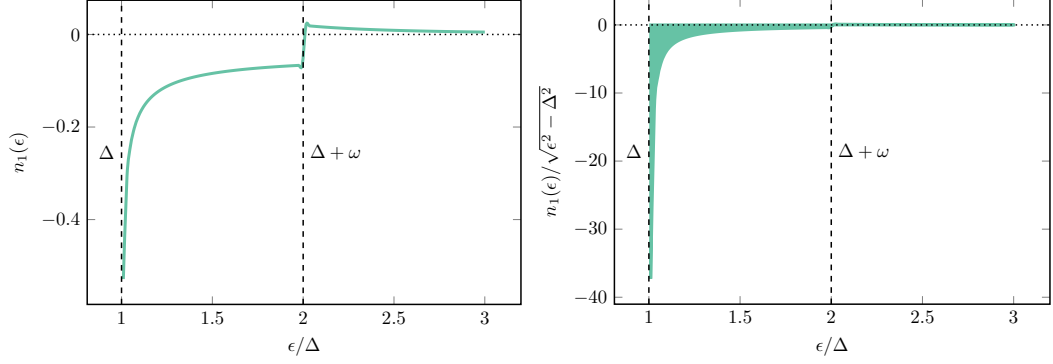
Figure 1.1: (a) Correction to the distribution function due to the collision integral in Eq. (1.9). (b) The correction scaled by the DOS factor $1/\sqrt{\epsilon^2 - \Delta^2}$. The area under the curve is negative, indicating with Eq. (1.6) that $\delta\Delta > 0$ and superconductivity is enhanced.

1.2.2 Transient enhancement of pairing in cuprates

Separate from the established physics of the Eliashberg effect (c.f. Section 1.2.1) the last decade has seen the advent of a new series of experiments showing evidence of photon-induced enhancement of superconductivity. In 2011, a transient Josephson plasmon resonance (JPR) feature was observed in pump-probe reflectivity measurements of Lanthanum-Europium-Strontium-Copper-Oxide (LESCO) following mid-infrared excitation of the sample [20]. Additionally, the onset of the JPR coincides with the emergence of a $1/\omega$-like dependence of the imaginary part of the optical conductivity $\mathrm{Im}\,\sigma(\omega)$ at low frequencies and a strong decrease of $\mathrm{Re}\,\sigma(\omega)$ at low frequencies. The strength of this dependence can of course be related to the superfluid density via the Kramers-Kronig relations

$$\mathrm{Im}\,\sigma(\omega) = \frac{1}{\pi}\int \mathrm{d}\omega' \, \frac{\mathrm{Re}\,\sigma(\omega')}{\omega - \omega'} \implies \mathrm{Im}\,\sigma(\omega) = \frac{e^2\rho_s}{mc\omega} + \mathcal{O}(\omega). \qquad (1.10)$$

where ρ_s is the superfluid density. The quantity $\lim_{\omega\to 0} \omega\,\mathrm{Im}\,\Delta\sigma(\omega)$ – where $\Delta\sigma(\omega)$ is the difference of the conductivity from the equilibrium state – is seen to follow mean field-like square root temperature dependence with a T_c approaching room temperature [21].

In contrast to the Eliashberg effect, the response seen in these experiments exhibited a sharp frequency dependence, with the JPR appearing only when the pump pulse was resonant with a particular lattice phonon. Subsequently, these experiments were repeated in other materials, including Yttrium-Barium-Copper-Oxide (YBCO) [21–24], Lanthanum-Barium-Copper-Oxide (LBCO) [25], and K_3C_{60} [26]. Specifically in YBCO, resonant X-ray spectroscopy suggested that coexisting charge order is suppressed in the same region of the phase diagram where superconductivity is enhanced in the optical excitation experiments [24]. This suggests that the experimental drive may be enhancing superconductivity by melting a competing instability in cuprates. This possibility is investigated in Chapter 2.

1.3   Hybridization of Collective Modes

1.3.1   d-form-factor density wave order in cuprates

Despite the decades of intense research efforts, superconductivity in cuprates remains a profound mystery. However, recently there has been a lot of progress in clarifying and refining the phase diagram of these materials experimentally [27, 28]. In particular, there is growing evidence of a charge order existing in the pseudogap state of several cuprate families [24, 29–34], which also coexists and competes with superconductivity at lower temperatures. Furthermore, it appears that this order has a non-trivial d-wave phase factor [33–35], implying that within a one-band model of copper sites it describes ordering entirely on the links. For this reason it has been dubbed bond-density-wave (BDW) or d-form-factor density wave (dFF-DW).[4]

One model for such order is a density-wave instability emerging from nesting of the Fermi surface [36, 37]; this is the model we employ in this dissertation. A detailed examination of the instability is given in Sections 2.2 and 2.3, but a few salient details are described here. The model we use is a 1-band model of cuprates, and as

---

[4]This is not to be confused with the similarly named *d-density wave.*

mentioned above, while the observed charge oscillation is physically on the oxygen sites of the copper-oxide plane, within the model it is described by a modulation on the links of the lattice – a spatial variation of the hopping between copper sites. Explicitly, the mean field Hamiltonian is

$$H = \sum_{ij} \left(t_{ij} + \phi_{ij} \cos\left(\mathbf{Q} \cdot \frac{\mathbf{r}_i + \mathbf{r}_j}{2} \right) \right) c_{i\sigma}^\dagger c_{j\sigma} + h.c., \tag{1.11}$$

where $c_{i\sigma}^\dagger$ is the electron creation operator for site i with spin σ. Here the charge order ϕ_{ij} has structure

$$\phi_{ij} = \phi_0 \begin{cases} 1 & \mathbf{r}_i - \mathbf{r}_j = \pm a\hat{x} \\ -1 & \mathbf{r}_i - \mathbf{r}_j = \pm a\hat{y} \\ 0 & \text{otherwise} \end{cases} \tag{1.12}$$

with a being the lattice constant. That is, the form factor is non-zero only for nearest-neighbors and has opposite signs on x-links and y-links.

The $dFF - DW$ order, being a complex order parameter in the usual Landau paradigm, has a nominally gapless phase mode and a massive amplitude mode. The fact that this order competes with superconductivity suggests a coupling between the dFF-DW and superconductor order parameters. This in turn indicates that there should be a coupling between the collective modes of the two orders, a topic which is the subject of Chapter 3.

1.3.2 Light-matter hybridization: Polaritons

Beyond enhancement of the superconducting state, there are other avenues for interfacing superconductors with light. Specifically, one can also consider how the fluctuation modes of the material hybridize with light. There is general precedent

for looking at hybrid light-matter excitations in semiconductors and metals in the well studied exciton-polaritons [38], surface-plasmon-polaritons [39, 40], phonon polaritons [41, 42], and others. In this section, we give a brief introduction to the notion of polaritons. For thorough overview of the field we refer the reader to Carusotto and Ciuti [43].

Generally polaritons are considered in a Hamiltonian framework, where a matter mode is coupled linearly to photons through a dipole coupling.

$$H = \begin{pmatrix} \Omega_{\text{matter}} & g \\ g & \omega_{\mathbf{q}} \end{pmatrix}. \tag{1.13}$$

Typically the dispersion of the matter excitation can be ignored as the velocity of the mode is much less than the speed of light. The eigenstates of this Hamiltonian are polaritons, whose existence can most easily be seen by the avoided crossing in the photonic dispersion such as in Fig. 1.2

Much work has recently focused cavity exciton-polaritons, that is polaritons formed from cavity-confined photons and the excitons of a material (e.g. a semi-conductor quantum well) placed within the cavity. A major appeal of this construction is that the polaritons have small effective mass and thus high Bose condensation temperatures. Cavity exciton-polariton condensation has in fact been observed up to room temperature [44, 45].

Another appeal of cavity polaritons is that their overlap with the cavity photons means they can be observed as signatures in the electromagnetic behavior of the cavity. In fact, the dispersion of the polaritons can be imaged by mapping the energy of photons injected into the cavity as a function of in plane momentum [46, 47].
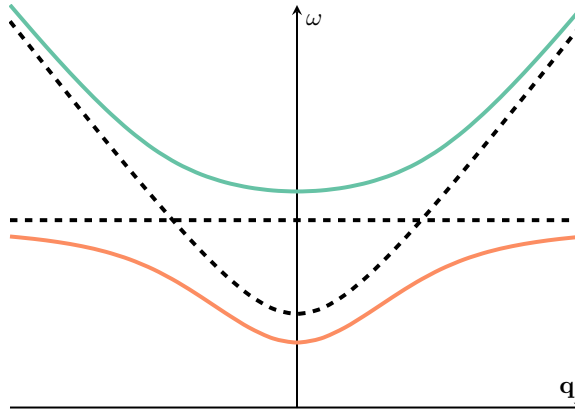
Figure 1.2: Dispersion of a matter excitation (e.g. an exciton) and a cavity photon (dashed lines) and the polariton states formed from them (solid lines).The resulting polaritons have an effective kinetic mass much smaller than that of the original matter excitation.

1.4 Formalism: Keldysh Field Theory

In this section, we introduce the Keldysh formalism for many body systems used in Chapters 3 and 4. We give here a brief overview of the technique and its accompanying notation. For a fuller introduction we refer the reader to Rammer and Smith [48], Altland and Simons [49], Kamenev [50], and Morawetz [51].

In any Green's function treatment of condensed matter theory one must encode in the formalism both the single-particle states of the system and the occupation of these states. In equilibrium formalisms, the latter information is redundant and so a complete theory can be written in terms of a single type of Green's function e.g. the Feynman (time-ordered) or Matsubara (imaginary-time) Green's functions. However, in the general case, the density matrix of the system is an additional quantity to be solved for and so must be encoded into the variables of the system. This can be done in a compact manner by introducing an auxiliary Green's function to keep track of the density matrix in the system. In the Keldysh formalism, we therefore enlarge our Green's function space to include three types of Green's function, the retarded, advanced, and Keldysh Green's functions. The retarded

and advanced components are redundant, but their inclusion allows for a matrix formalism which follows the usual Feynman rules and automatically maintains the appropriate analytic properties of the correlators in the theory.

Below we briefly outline obtaining the analog Keldysh field integral corresponding to a Gaussian zero-temperature action to illustrate the general approach. Then in Section 1.4.1 we employ these techniques to derive the KNLσM of disordered superconductors which will be used in Chapters 4 and 5.
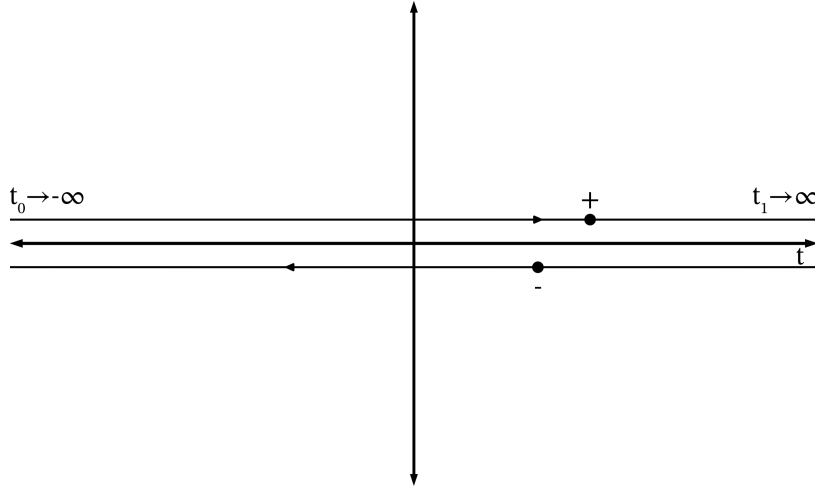
Figure 1.3: The Schwinger-Keldysh contour in the complex time plane. Time ordering of operators on this contour allows for a coherent state functional integral construction which can encode the non-equilibrium properties of the density matrix. The retarded, advanced, and Keldysh Green's functions can be obtained as expectations values of operators on different parts of the contour.

Let us begin with the usual $T = 0$ time-ordered coherent state functional integral

$$\langle\cdots\rangle_{T=0} = \int \mathcal{D}[\chi, \bar{\chi}](\cdots) \exp\left[i \int_{-\infty}^{\infty} \mathrm{d}t \, \underbrace{\bar{\chi}\big(i\partial_t - \hat{H}\big)\chi}_{S}\right]. \tag{1.14}$$

To express the analogous Keldysh theory we begin by taking the above theory on the time contour from $t = -\infty$ to $t = \infty$ and extending it to a complex time

contour containing forward and backward branches as in Fig. 1.3

$$S = \int_{-\infty}^{\infty} dt\, \bar{\chi}\big(i\partial_t - \hat{H}\big)\chi \rightarrow \oint_{\mathcal{C}} dt\, \bar{\chi}\big(i\partial_t - \hat{H}\big)\chi. \tag{1.15}$$

$\oint_{\mathcal{C}}$ denotes integration over the Keldysh contour. By defining fields on the upper and lower branches of the contour, this can again be written as an integral over the real time axis

$$S = \int_{-\infty}^{\infty} dt\, \Big[\bar{\chi}_+\big(i\partial_t - \hat{H}\big)\chi_+ - \bar{\chi}_-\big(i\partial_t - \hat{H}\big)\chi_- \Big] \tag{1.16}$$

where $\chi_\pm$ is a field on the upper/lower contour as shown in Fig. 1.3. From these operators one can define four types of correlators

$$\begin{aligned}
iG^T &= \big\langle \chi_+\bar{\chi}_+ \big\rangle & iG^{\tilde{T}} &= \big\langle \chi_-\bar{\chi}_- \big\rangle \\
iG^> &= \big\langle \chi_-\bar{\chi}_+ \big\rangle & iG^< &= \big\langle \chi_+\bar{\chi}_- \big\rangle,
\end{aligned} \tag{1.17}$$

the time-ordered, anti-time-ordered, greater, and lesser Green's functions, respectively. Due to the boundary conditions of the field integral, these functions are not all independent. It is therefore convenient to perform a change of basis on our field operators; the most useful choice of basis differs for bosons and fermions. For bosons, one performs the Keldysh rotation

$$\begin{pmatrix} \phi_c \\ \phi_q \end{pmatrix} = \frac{1}{\sqrt{2}} \begin{pmatrix} 1 & 1 \\ 1 & -1 \end{pmatrix} \begin{pmatrix} \phi_+ \\ \phi_- \end{pmatrix} \tag{1.18}$$

to the basis of *classical* and *quantum* components. In terms of these fields the action is

$$S = \int dt\, \bar{\phi}\hat{G}^{-1}\phi \tag{1.19}$$

defining a matrix Green's function

$$\check{G} = \begin{pmatrix} \hat{G}_K & \hat{G}_R \\ \hat{G}_A & 0 \end{pmatrix}. \tag{1.20}$$

with retarded (advanced) Green's functions $i\hat{G}_{R(A)} = \left\langle \phi_{cl(q)} \bar{\phi}_{q(cl)} \right\rangle$ satisfying $G_R^\dagger = G_A$, and the anti-Hermitian Keldysh Green's function $i\hat{G}_K = \left\langle \phi_{cl} \bar{\phi}_{cl} \right\rangle$.

For fermions we can use the fact that $\bar{\psi}$ and ψ are actually unrelated Grassman fields to instead perform the Larkin-Ovchinnikov change of basis

$$\begin{pmatrix} \psi_1 \\ \psi_2 \end{pmatrix} = \frac{1}{\sqrt{2}} \begin{pmatrix} 1 & 1 \\ 1 & -1 \end{pmatrix} \begin{pmatrix} \psi_+ \\ \psi_- \end{pmatrix} \tag{1.21}$$

$$\begin{pmatrix} \bar{\psi}_1 & \bar{\psi}_2 \end{pmatrix} = \frac{1}{\sqrt{2}} \begin{pmatrix} \bar{\psi}_+ & \bar{\psi}_- \end{pmatrix} \begin{pmatrix} 1 & 1 \\ -1 & 1 \end{pmatrix} \tag{1.22}$$

leading to a fermionic action

$$S = \int \mathrm{d}t\, \bar{\psi} \check{G}^{-1} \psi \tag{1.23}$$

with

$$\check{G} = \begin{pmatrix} \hat{G}_R & \hat{G}_K \\ 0 & \hat{G}_A \end{pmatrix}. \tag{1.24}$$

Finally, in both the fermionic and bosonic cases we can parameterize the anti-Hermitian Green's function in terms of a Hermitian function $\hat{F}$

$$\hat{G}_K = \hat{G}_R \hat{F} - \hat{F} \hat{G}_A. \tag{1.25}$$

The retarded and advanced functions describe the states of the system, with $\mathrm{tr} \left[\hat{G}_R - \hat{G}_A \right] = -2\pi i \mathcal{A}$ giving the spectral function $\mathcal{A}$ from which can be extracted the DOS

$\rho(\omega) = \int_{\mathbf{q}} \operatorname{tr} \mathcal{A}(\omega, \mathbf{q})$. The generalized distribution function $\hat{F}$ describes the occupation of states and in equilibrium is given by $\coth(\omega/2T)$ for bosons and $\tanh(\epsilon/2T)$ for fermions.

Functionally, then, the Keldysh formalism as employed in this dissertation comprises extending all fields with an extra matrix degree of freedom, $\hat{\chi}(\mathbf{r}, t) \to \hat{\chi}_\alpha(\mathbf{r}, t)$, in what we henceforth refer to as Keldysh space. This leads to an additional Keldysh space matrix structure for all Green's functions which can be treated via simple matrix multiplication. The analytic structure of the components of the matrix enforces that any product of matrix Green's functions will result in the same matrix form. The result is that the Keldysh matrix structure of the correlators keeps track of both the spectral and correlation aspects of the theory automatically with no other explicit work required in the calculation. The price that we have paid is the introduction of extra degrees of freedom, and new matrix structure in the coupling between bosonic and fermionic fields arising from the Keldysh rotations. Quantities of interest can be calculated in the usual manner of the functional integral

$$\left\langle \hat{\mathcal{O}} \right\rangle = \int \mathcal{D}[\bar{\chi}, \chi] \hat{\mathcal{O}} e^{iS_K[\bar{\chi}, \chi]}. \tag{1.26}$$

Typically, one is concerned with obtaining causal (retarded) objects.

1.4.1 Keldysh Non-Linear σ model

We now outline here a construction of the Keldysh Non-Linear σ Model (KNLσM), which will be used to obtain the results in Chapter 4. For more details on the KNLσM we refer the reader to Feigel'man, Larkin, and Skvortsov [18], Kamenev [50], and Kamenev and Levchenko [52].

The derivation of the σ model begins with a minimally coupled BCS action in the presence of a random impurity potential, which we have, as described above,

extended to the Keldysh contour

$$S = \oint_{\mathcal{C}} dt d\mathbf{x} \left[\bar{\psi} \left(i\partial_t - \hat{\epsilon} \left(-i\boldsymbol{\nabla} + \frac{e}{c}\mathbf{A} \right) + \mu - V_{\text{imp}} \right) \psi + \frac{\lambda}{\nu} \bar{\psi}_\uparrow \bar{\psi}_\downarrow \psi_\downarrow \psi_\uparrow \right]. \qquad (1.27)$$

Here $\hat{\epsilon}$ is the quasi-electron energy, μ the chemical potential, ν the density of states at the Fermi surface, λ the BCS coupling strength[5], and V_{imp} the impurity potential.

One now averages over Gaussian disorder which induces an effective disorder interaction in the usual manner

$$iS_{\text{dis}} = -\frac{1}{4\pi\nu\tau} \oint_{\mathcal{C}} dt dt' d\mathbf{x} \bar{\psi}(t)\psi(t)\bar{\psi}(t')\psi(t'). \qquad (1.28)$$

The bilinears $\bar{\psi}(t)\psi(t)$ describe rapidly varying modes on the scale of the impurities. However, the bilinears $\bar{\psi}(t)\psi(t')$ describe slowly varying degrees of freedom. Therefore a Hubbard-Stratonovich field Q dual to $\bar{\psi}(t)\psi(t')$ is introduced to decouple the disorder interaction. The BCS interaction is also decoupled via the Hubbard-Stratonovich field Δ in the usual fashion. Coupling to the A-field is handled via the paramagnetic coupling $\mathbf{j} \cdot \mathbf{A} \approx \frac{e}{c}\mathbf{v}_F \cdot \mathbf{A}$. At this point one performs the Larkin-Ovchinnikov rotation and integrates out the fermions. This leads to an action for the Hubbard-Stratonovich fields Q and Δ

$$iS = -\frac{\pi\nu}{8\tau} \text{Tr} \, \check{Q}^2 + \text{Tr} \ln \left[\check{G}^{-1} + \frac{i}{2\tau}\check{Q} - \frac{e}{c}\mathbf{v}_F \cdot \check{\mathbf{A}} + \check{\Delta} \right] \qquad (1.29)$$

where G is the Bogoliubov-de Gennes Green's function. Tr in the above indicates a trace over all indices: both matrix and space-time. The notation $\check{X}$ indicates a matrix in Nambu and Keldysh spaces. The matrix $\check{Q}$, describing the soft electronic degrees of freedom, is a function of position $\mathbf{r}$ and two time coordinates t, t'. One then performs an expansion about the saddle-point solution for Q as well as a

---

[5]In terms of the usual BCS coupling constant g, $\lambda = g\nu$.

gradient expansion. One notes that the $\text{Tr}\,\check{Q}^2$ vanishes on the soft manifold $\check{Q}^2 = \check{1}$
—where we must keep in mind that the unit matrix must have the proper analyticity
structure —indicating that such modes are massless.[6] The result of these expansions
along with the non-linear constraint gives the KNLσM

$$iS_{NLSM} = -\frac{\pi\nu}{8}\,\text{Tr}\left[D\left(\partial\check{Q}\right)^2 + 4i\left(i\hat{\tau}_3\partial_t\check{Q} + \check{\Delta}\check{Q}\right)\right] - i\frac{\nu}{2\lambda}\,\text{Tr}\,\check{\Delta}^\dagger\hat{\gamma}^q\check{\Delta}. \qquad (1.30)$$

where $D = v_F\tau_{\text{imp}}^2/2$ is the diffusion constant, $\nu = \nu_\uparrow + \nu_\downarrow$ is the total electronic
density of states at the Fermi surface, and λ is the strength of the BCS type coupling.
The photon field $\mathbf{A}$ couples to the model through the covariant derivative

$$\partial\check{X} = \nabla\check{X} - i\frac{e}{c}[\check{\mathbf{A}}, \check{X}]. \qquad (1.31)$$

All matrices in the model are 4×4 in the product of Keldysh and Nambu spaces.

We employ a slightly modified Non-Linear σ Model (NLσM) which includes
coupling to a thermal bath

$$iS_{NLSM} = -\frac{\pi\nu}{8}\,\text{Tr}\left[D\left(\partial\check{Q}\right)^2 + 4i\left(i\hat{\tau}_3\partial_t\check{Q} + i\frac{\gamma}{2}\check{Q}_{\text{rel}}\check{Q} + \check{\Delta}\check{Q}\right)\right] - i\frac{\nu}{2\lambda}\,\text{Tr}\,\check{\Delta}^\dagger\hat{\gamma}^q\check{\Delta}$$
$$(1.32)$$

In what follows we employ the conventions used in Ref. [52]. Explicitly

$$\check{Q}_{\text{rel}}(\epsilon) = \begin{pmatrix} 1 & 2F_{\text{eq}}(\epsilon) \\ 0 & -1 \end{pmatrix}_K \qquad (1.33)$$

$$\check{\mathbf{A}} = \sum_\alpha \mathbf{a}_\alpha\hat{\gamma}^\alpha \otimes \hat{\tau}_3, \qquad \check{\Delta} = \sum_\alpha \left(\Delta_\alpha\hat{\gamma}^\alpha \otimes \hat{\tau}_+ - \Delta_\alpha^*\hat{\gamma}^\alpha \otimes \hat{\tau}_-\right)$$

---

[6]This is a little subtle. For causality, the matrix $\check{1}$ must mean $\text{diag}\left(\hat{1}^R, \hat{1}^A\right)$ where the superscript
indicates the retarded/advanced unit function. The trace is then $\text{Tr}\{\check{1}\} = \text{Tr}\{\hat{1}^R\} + \text{Tr}\{\hat{1}^A\}$. The
vanishing of the trace is then a consequence of the proper regularization of $\hat{1}^{R/A}$. For more details
see [52].

where the index α runs over (cl, q) and $\gamma^{\mathrm{cl}} = \sigma^0$ and $\gamma^{\mathrm{q}} = \sigma^1$ are matrices in Keldysh space. We model inelastic relaxation through a linear coupling to a bath $\hat{Q}_{\mathrm{rel}}$ with temperature T [19]. This is equivalent to the relaxation $(1/\tau)$ approximation in the kinetic equation. In particular $\gamma = 1/\tau_{\mathrm{in}}$ is the inelastic scattering rate.

The saddle-point equations of Eq. (1.32) for Δ_q^* and $\check{Q}$ respectively correspond to the BCS gap equation and the Usadel equation [16] for the quasi-classical Green's function $\check{Q}$. In the absence of external field $\mathbf{A}$, the saddle point of $\check{Q}$ is

$$\partial\left(D\check{Q}\partial\check{Q}\right) + i\{i\hat{\tau}_3\partial_t, \check{Q}\} + i\left[i\tau_2\Delta_0 + i\frac{\gamma}{2}\check{Q}_{\mathrm{rel}}, \check{Q}\right] = 0 \qquad (1.34)$$

where we have assumed Δ_{cl} to be homogeneous and real. Assuming a homogeneous, steady state solution $\check{Q}_{\mathrm{sp}}(t - t')$ we may Fourier transform to obtain

$$i\epsilon[\hat{\tau}_3, \check{Q}(\epsilon)] + i[i\tau_2\Delta_0, \check{Q}(\epsilon)] + \gamma/2\left[\check{Q}_{\mathrm{rel}}(\epsilon), \check{Q}(\epsilon)\right] = 0. \qquad (1.35)$$

The saddle-point solution $\check{Q}_{\mathrm{sp}}$ will have the structure

$$\check{Q}_{\mathrm{sp}} = \begin{pmatrix} \hat{Q}_{\mathrm{sp}}^R & \hat{Q}_{\mathrm{sp}}^R\hat{F} - \hat{F}\hat{Q}_{\mathrm{sp}}^A \\ 0 & \hat{Q}_{\mathrm{sp}}^A \end{pmatrix}$$

as governed by fluctuation-dissipation.

1.4.2 Gaussian Fluctuations

Gaussian fluctuations about the saddle point can be parameterized in a number of ways, but in this dissertation we will use the exponential parameterization

$$\check{Q} = \check{U}\check{V}^{-1}e^{-\check{W}/2}(\hat{\sigma}_3 \otimes \hat{\tau}_3)e^{\check{W}/2}\check{V}\check{U}. \qquad (1.36)$$

with

$$\check{U}(\epsilon) = \begin{pmatrix} 1 & F_{\text{eq}}(\epsilon) \\ 0 & -1 \end{pmatrix}_K \otimes \hat{\tau}_0, \qquad \check{V}(\epsilon) = \begin{pmatrix} e^{\tau_1\theta/2} & 0 \\ 0 & e^{\tau_1\theta^*/2} \end{pmatrix}_K \qquad (1.37)$$

where the subscript K indicates that a matrix is in the Keldysh space. Here, $\theta(\epsilon)$ is a complex angle which is determined by the Usadel equation, and satisfies $\theta(-\epsilon) = -\theta^*(\epsilon)$. The matrices U and V are a change of basis which allows us to separate the equilibrium and saddle point properties from the fluctuation effects: U encodes the fluctuation dissipation relation, while V parameterizes the solution to the retarded Usadel equation. The matrix $\check{W}$ is then composed of fields multiplying the generators of the algebra of the target manifold of the theory. In particular, the matrix $\check{W}$ anticommutes with $\sigma_3\tau_3$ and for $\check{W} = 0$ Eq. (1.36) reduces to the saddle-point solution. By expanding the exponential in this parameterization we can capture the Gaussian fluctuations along the soft manifold. $\check{W}$ has 4 independent components that couple to the vector potential, explicitly,

$$\check{W}(\mathbf{r}, t, t') = i \begin{pmatrix} c_R(\mathbf{r}, t, t')\tau_1 & d_{cl}(\mathbf{r}, t, t')\tau_0 \\ d_q(\mathbf{r}, t, t')\tau_0 & c_A(\mathbf{r}, t, t')\tau_1 \end{pmatrix}_K, \qquad (1.38)$$

which we call the cooperon (c_R, c_A) and diffuson (d_{cl}, d_q) fields.

We now expand Eq. (1.32) to quadratic order in the cooperon and diffuson fields c and d, generating the quadratic diffusive action

$$iS_{cd} = \frac{\pi\nu}{4} \int \frac{d\epsilon}{2\pi} \int \frac{d\epsilon'}{2\pi} \, \text{tr} \left[\vec{d}_{\epsilon'\epsilon} \hat{\mathcal{D}}_{\epsilon\epsilon'}^{-1} \vec{d}_{\epsilon\epsilon'} + \vec{c}_{\epsilon'\epsilon} \hat{\mathcal{C}}_{\epsilon\epsilon'}^{-1} \vec{c}_{\epsilon\epsilon'} \right] \qquad (1.39)$$

where we have defined the vector notation

$$\vec{d} = (d^{cl}, d^q), \qquad \vec{c} = (c^R, c^A)$$

$$\hat{\mathcal{D}}_{\epsilon\epsilon'}^{-1} = \mathcal{D}_{\epsilon'\epsilon}^{-1}\sigma_+ + \mathcal{D}_{\epsilon\epsilon'}^{-1}\sigma_-, \qquad \hat{\mathcal{C}}_{\epsilon\epsilon'}^{-1} = \mathrm{diag}\left(\mathcal{C}_{\epsilon\epsilon'}^R, \mathcal{C}_{\epsilon\epsilon'}^A\right)^{-1},$$

(1.40)

and the diffuson and cooperon propagators

$$\mathcal{D}_{\epsilon\epsilon'}^{-1} = \mathcal{E}^R(\epsilon) + \mathcal{E}^A(\epsilon'), \qquad [\mathcal{C}^{R/A}]_{\epsilon\epsilon'}^{-1} = \mathcal{E}^{R/A}(\epsilon) + \mathcal{E}^{R/A}(\epsilon')$$

$$\mathcal{E}^R(\epsilon) = i\left(\epsilon + i\frac{\gamma}{2}\right)\cosh\theta_\epsilon - i\Delta\sinh\theta_\epsilon, \qquad \mathcal{E}^A(\epsilon) = \left(\mathcal{E}^R(\epsilon)\right)^*$$

(1.41)

where θ_ϵ is the spectral angle appearing in Eq. (1.37). We have thus arrived at a theory where the electronic behavior of the system is described in terms of low-lying diffuson and cooperon modes.

Chapter 2: Enhancement of superconductivity via periodic modulation in cuprate superconductors

This chapter is based upon Raines, Stanev, and Galitski [53] and Raines [54, ©
American Physical Society].

2.1 Overview

The past several years have brought exciting new experimental works in under-doped cuprates on transient states showing signatures of electron-electron pairing [20, 21, 23, 25]. In these experiments, the system is excited via mid-infrared laser pulses which drive phonon modes of the system and can lead to quasi-static changes of the lattice structure via non-linear phonon couplings [22]. Reflectivity measurements are taken as a function of time delay, from which the frequency dependent conductivity can be extracted. For times close to the pump, features reminiscent of superconductivity can be seen in the optical conductivity $\sigma(\omega)$, e.g. a $1/\omega$ divergence in $\operatorname{Im} \sigma(\omega)$ and Josephson plasmon resonances (JPRs) [24]. Furthermore, the nature of this enhancement seems to be different from the already well known effect due to quasi-particle photo-excitation [14, 15, 21, 55, 56]. While the traditional light induced enhancement (c.f. Section 1.2.1 and Chapter 4) occurs for light in the microwave region and has a broad frequency dependence, the effects observed in these non-linear phononics experiments occur for only a narrow frequency range in the mid-infrared, when the incident light is resonant with a particular phonon mode of the apical oxygens.

The nature of the photo-excitation employed in experiments, as well as previous theoretical works, have suggested that it is important to understand the effect of interlayer coupling. Indeed, several works have investigated these experiments and

proposed an increase of inter-layer coupling as one of the dominant effects [22, 57]. Specifically, one consequence of driving the c-axis phonon modes is a transient quasi-static modification of the interlayer spacing [22], leading to an enhancement of the hopping between the planes. Here we focus on its role in the competition between charge order and superconductivity to have a full understanding of the effects seen under mid-infrared excitation. In particular, one scenario suggests melting of the competing charge order [53, 58] via modulation of the interlayer coupling as the underlying mechanism, motivated in particular by the suppression of charge ordering peaks in X-ray coinciding with the transient pairing state [24].

To address this problem we start from the $t - J - V$ model of the quasi two dimensional CuO_2 planes [59, 60], which can naturally support the coexistence and competition between charge ordering and superconductivity [37, 61, 62]. This model is similar in spirit to previous studies of the cuprates e.g. Refs. [63–66]. Furthermore, we focus on the low energy physics of fermions near the so-called 'hot-spots', where the Fermi surface intersects the magnetic Brillouin zone [36, 67]. In particular, we consider ordering of the d-form-factor density wave type discussed in Section 1.3.1. We extend the model by introducing an effective Hamiltonian, describing stacked planes, coupled by a c-axis tunneling term t_z. Then we investigate the phase diagram of this extended model by utilizing a Landau expansion of the free energy. Quite surprisingly, we observe a non-monotonic behavior of the critical temperatures of the two orders with increasing t_z, and we provide an intuitive physical explanation of this interesting feature. Finally, we consider different effects of the photo-excitations of the system, particularly focusing on the role of the apical oxygens, which are thought to play a key role in the experiments [21–23]. We find that, quite generally, there is a parameter region where an optical pump can lead to a melting of the charge order and a corresponding enhancement in superconductivity, due to the competition between the two orders.

It should be noted that the $t-J-V$ model and its variants tend to have as their leading instability a (Q,Q) type in-plane ordering vector [37, 61, 68], with the $(Q,0)$ ordering vector seen in experiment [33] as a sub-leading instability (with both orders having predominantly d-wave symmetry). While several extensions of the model have been proposed as a way to stabilize the experimentally observed order [62, 69, 70], they introduce additional, and for our purposes unnecessary, complications. The physical content of our results lead us to expect that the qualitative behavior of the effects would be similar for the experimentally relevant $(Q,0)$ charge order.

Regarding the out-of-plane structure, while the c-axis momentum seen in experiments is peaked about $Q_z = \pi$, the feature is quite broad [30]. Along with scanning tunneling microscopy results [33], this suggests a picture of patches of in-plane order which are only weakly correlated between planes. Indeed the importance of defects in stabilizing the form of the order has been experimentally established [71]. We therefore extend consideration to the case where the local phase and orientation of charge order are pinned by e.g. lattice impurities or distortions. Taking this phase and orientation to be random variables, we consider the Landau theory obtained by averaging over all such regions in the system. In general, we find that when in-plane pinning of the charge order is taken into account an increase of interlayer coupling leads to a melting of charge order and an enhancement of superconductivity.

The outline of the chapter is as follows. In Section 2.2, we describe the $t-J-V$ model [59, 60] of the planes and consider the non-interacting susceptibility in the charge ordering channel to find the wavevector of the strongest instability. In Section 2.3, we consider the effect of interlayer tunneling in the case where charge order is constant along the c-axis. Then, in Section 2.5, we study the effect of charge order phase pinning of the competition between order. To this end we construct the averaged Landau free energy of competing superconductivity and order and study how interlayer coupling affects the competition between the two orders. Time-

dependent perturbation of the inter-layer coupling t_z is introduced in Section 2.6, and the high-frequency limit is studied. Finally, in Section 2.7, we summarize and discuss our results.

2.2 Model

In order to study the interplay of d-form-factor density wave (dFF-DW) and d-wave superconductivity (dSC) orders we employ a 2D $t - J - V$ model of a CuO_2 plane [37, 59, 60, 62]. It provides a natural platform for exploring the general features of the interaction and the coupling between these two orders within a single copper oxide plane. The Hamiltonian is

$$H = \sum_{i,j} t_{ij} c_{\sigma,i}^\dagger c_{\sigma,j} + \frac{1}{2} \sum_{\langle i,j \rangle} J\vec{S}_i \cdot \vec{S}_j + \frac{1}{2} \sum_{\langle i,j \rangle} V n_i n_j, \qquad (2.1)$$

where V and J are nearest neighbor interactions, $n_i = \sum_\sigma c_{i,\sigma}^\dagger c_{i,\sigma}$ is the charge density, and $\mathbf{S}_i = \frac{1}{2} \sum_\sigma c_{i,a}^\dagger \vec{\sigma}_{ab} c_{i,b}$ is the site spin density, with i and j being site indices, and σ, a, and b spin indices. The term t_{ij} contains nearest, next to nearest, and next to next to nearest hopping[1]. V describes the nearest-neighbor tail of the Coulomb repulsion, which tends to suppress the d-wave superconductivity and enhance the dFF-DW order. J is the usual nearest neighbor anti-ferromagnetic exchange interaction.

Of course, the pure $t - J$ model has been extensively used in the studies of cuprates as an effective one-band description of the CuO_2 planes [72]. It naturally leads to a d-wave superconductivity as its dominant instability. In order to have a region where superconductivity and dFF-DW order coexist the model can be extended by the introduction of V, which suppresses superconductivity and boosts the charge order – this is the rationale behind the $t - J - V$ model.

---

[1]In this work we used $t_1 = 430\,\text{meV}$, $t_2 = -0.32 t_1$, $t_3 = -0.5 t_2$, and $\mu = -1.1856 t_1$.

Table 2.1: Basis functions for factorization of nearest neighbor interactions categorized by the representation of D_4 to which they belong.

l	$f^l(\mathbf{k})$	Representation
1	$\cos k_x - \cos k_y$	B_1
2	$\cos k_x + \cos k_y$	A_1
3	$\sin k_x - \sin k_y$	E
4	$\sin k_x + \sin k_y$	

The nearest neighbor form of the interaction allows us to decompose the potential into a sum of factorizable potentials

$$J_{\mathbf{k}-\mathbf{k}'} = \frac{1}{2}J \sum_l f^l(k)f^l(k') \tag{2.2}$$

$$V_{\mathbf{k}-\mathbf{k}'} = \frac{1}{2}V \sum_l f^l(k)f^l(k'). \tag{2.3}$$

Here, the functions $f^l(k)$, listed in Table 2.1, form a basis of nearest neighbor in-plane interaction vertices which transform as representations of D_4 [70]. Since we are interested in dSC and dFF-DW we will be focusing on the terms containing $f^1(\mathbf{k}) = \cos k_x - \cos k_y$, which correspond to a $d_{x^2-y^2}$-like form factor. In real space such a form factor corresponds to the case where x-links and y-links have opposite signs. Self-energy effects due to interactions in other channels will be assumed to have already been taken into account in the free dispersion.

We may then undertake a decoupling in the dFF-DW and dSC channels. Due to the form of the interaction, we consider only layer-local order parameters. The superconducting order is taken to be d-wave and constant along the c-axis.

With these restrictions, at the mean-field level, we consider the order parameters

$$\phi(\mathbf{Q}) = \frac{g_\phi}{2} \sum_{\mathbf{k},\sigma} f^1(\mathbf{k}) \left\langle c^\dagger_{\mathbf{k}-\mathbf{Q}/2,\sigma} c_{\mathbf{k}+\mathbf{Q}/2,\sigma} \right\rangle$$

$$\Delta = \frac{g_\Delta}{4} \sum_{\mathbf{k},\sigma,\sigma'} f^1(\mathbf{k}) \left\langle c_{-\mathbf{k},\sigma}(-i\sigma^2_{\sigma\sigma'})c_{\mathbf{k},\sigma'} \right\rangle$$

(2.4)

where $g_{\phi,\Delta} = \frac{3J}{4} \pm V$ and $\langle \cdots \rangle$ indicates an ensemble average.
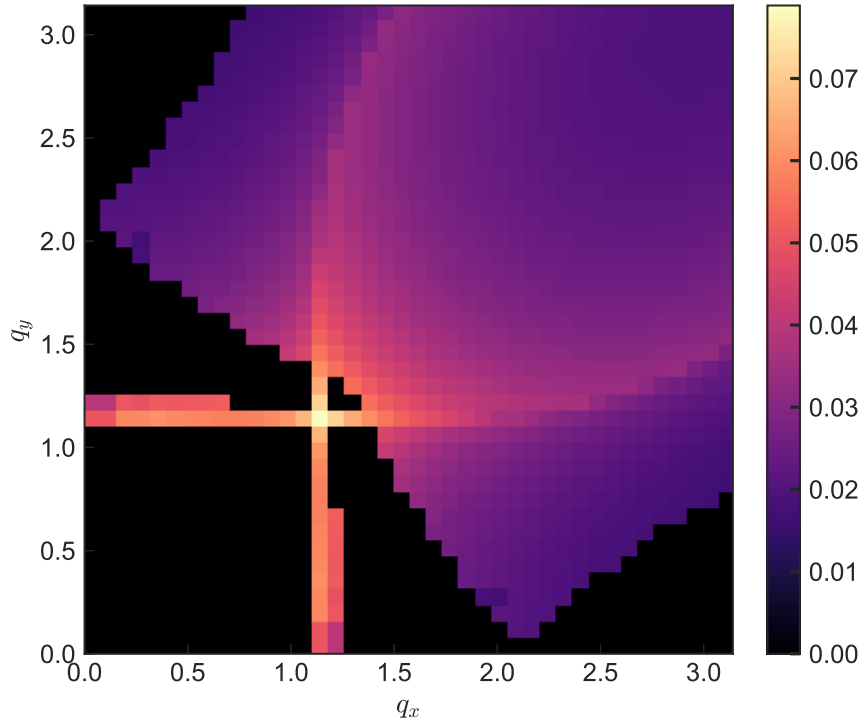
Figure 2.1: Maximum eigenvalue of the matrix density wave susceptibility $\hat{\Pi}_\phi$ as a function of in-plane ordering vector in the Brillouin zone. The strongest instability is generically at in-plane wavevector (Q, Q) with $Q \sim 1.14$ and out of plane wavevector $Q_z = \pi$.

Having defined the order parameters we can also define associated normal state susceptibilities in these channels. In particular, we define the matrix dFF-DW

susceptibility

$$\Pi(\mathbf{q})_{ij} = -\sum_{k}[f^1(\mathbf{k})]^2 \, \mathrm{tr}_{L,\sigma}\left[\hat{G}_0(\epsilon_n, \mathbf{k}+\mathbf{Q}/2)\hat{v}_i\hat{G}_0(\epsilon_n, \mathbf{k}-\mathbf{Q}/2)\hat{v}_j\right].\qquad(2.5)$$

where $\hat{G}_0$ is the non-interacting Green's function and $\sum_k$ includes an integral over in-plane momentum and a sum of the Fermionic Matsubara frequency ϵ_n.

In order to determine the in-plane charge-ordering wavevector, we calculated the susceptibility at various values of $\mathbf{Q}$ and compared the maximum eigenvalues. An intensity plot of the strongest instability by wavevector is shown in Fig. 2.1. For the in-plane component, we generically find the susceptibility to be greatest for a diagonal (Q, Q) nesting wavevector as is generally the case in such models [37, 61, 68].
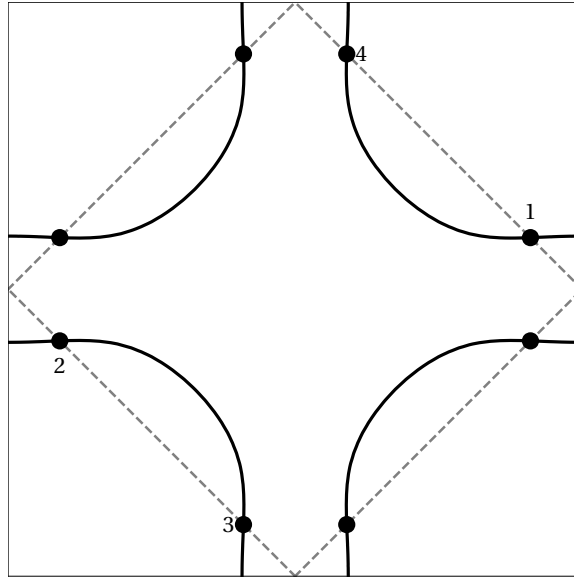
Figure 2.2: The leading instability has an in-plane ordering momentum which connects the 'hot-spots', the points where the Fermi surface intersects the magnetic Brillouin zone boundary, across the edge of the Brillouin zone, e.g. the hot-spots labeled 1 and 2. The symmetry of the problem allows the mean-field Hamiltonian at only hot regions 1 and 2 to be considered.

2.3   Hot-Spot model and the charge ordering instability
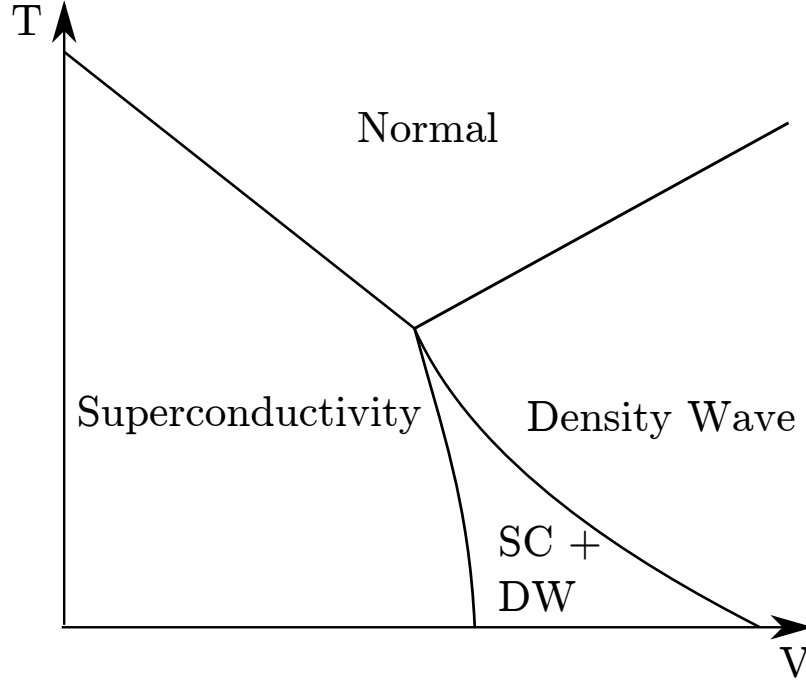
Figure 2.3: Schematic phase diagram of competing d-wave superconductivity and d-form-factor density wave. *V*, the nearest-neighbor Coulomb repulsion, acts as a tuning parameter for the relative strength of the two instabilities.

We now construct a low-energy effective model by restricting our attention to fermions living within a limited region surrounding 'hot-spots' – points where the Fermi surface intersects the magnetic Brillioun zone boundary, as depicted in Fig. 2.4 (such models have been introduced and used in a number of studies of charge order in cuprates [37, 61, 73, 74]). These points are of special interest because the Fermi surface is nested with wave-vector $\mathbf{K} = (\pi, \pi)$, and given the importance of anti-ferromagnetic spin fluctuations to pairing in the cuprates [37, 75, 76], we expect that the most relevant interactions will be those with exchanged momentum $\mathbf{K}$. Close to the hot-spots we can replace the interactions $J_{\mathbf{q}}, V_{\mathbf{q}}$ with constants $J_{\mathbf{K}}, V_{\mathbf{K}}$, and restrict the two unconstrained fermion momenta $\vec{k} - \vec{k}' = \vec{q}$ to lie in hot regions separated by $\mathbf{K}$.
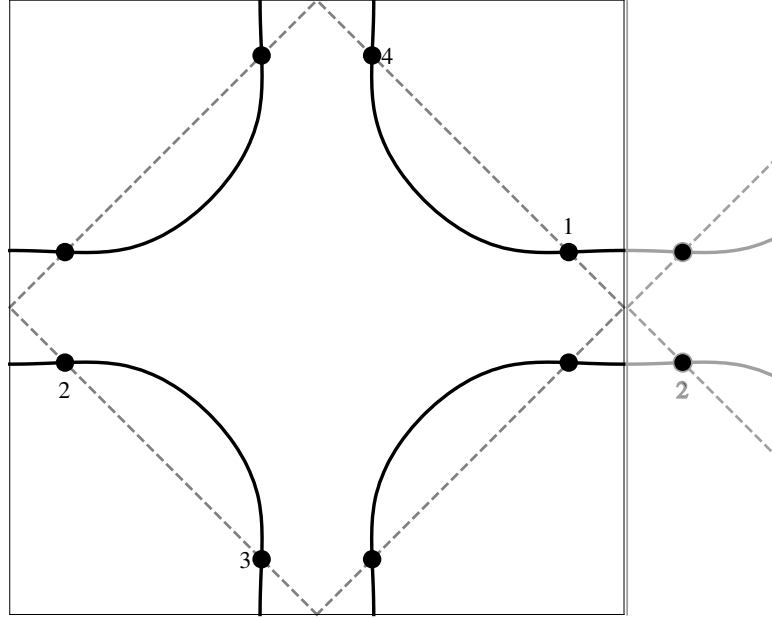
Figure 2.4: Hot-Spots exist where the Fermi surface intersects the magnetic Brillioun zone boundary. The charge ordering vectors are given by the separations between hot-spots 1 and 2 across the Brillouin zone border and the rotated vector $(Q, -Q)$.

Furthermore, we only consider a charge ordering instability with a diagonal (Q, Q) ordering vector and a d-wave form factor, as this is the strongest mean field instability. If we further enforce time reversal symmetry this allows us to concentrate our attention to four hot-spots. Having restricted our fermions to live within a range Λ of the hot-spots we obtain an effective Hamiltonian

$$H = \sum_{\mathbf{k},i} \xi_{i,\mathbf{k}} c^\dagger_{i,\mathbf{k},\sigma} c_{i,\mathbf{k},\sigma} + g^{abcd} \sum_{\mathbf{k},\mathbf{p}} \left[c^\dagger_{1,\mathbf{k},a} c_{2,\mathbf{k},d} c^\dagger_{4,\mathbf{p},c} c_{3,\mathbf{p},b} - c^\dagger_{1,\mathbf{k},a} c^\dagger_{2,-\mathbf{k},c} c_{4,-\mathbf{p},d} c_{3,\mathbf{p},b} \right],$$
(2.6)

where the interaction is

$$g^{abcd} = -\frac{1}{4} J_{\mathbf{K}} \vec{\sigma}_{ab} \cdot \vec{\sigma}_{cd} - V_{\mathbf{K}} \delta_{ab} \delta_{cd},$$
(2.7)

$\mathbf{k}$ and $\mathbf{p}$ are now the deviations from the hot-spots, $a-d$ are the electron spin indices, and i is now a hot-spot index (e.g. as shown in Fig. 2.2). Inversion symmetry allows

us to restrict attention to half of the hot-spots in the Brillouin zone.

At this point we undertake a mean field decomposition of the interaction (four-fermion) terms of the Hamiltonian simultaneously in the dFF-DW and dSC, where a d-wave form factor is assumed for both orders, by defining

$$i\sigma_{ab}^{y}\bar{\Delta} = -g_{\Delta}\sum_{\mathbf{k}}\left\langle c_{1,\mathbf{k},a}^{\dagger}c_{2,-\mathbf{k},b}^{\dagger}\right\rangle = g_{\Delta}\sum_{\mathbf{k}}\left\langle c_{3,\mathbf{k},a}^{\dagger}c_{4,-\mathbf{k},b}^{\dagger}\right\rangle, \tag{2.8}$$

and

$$\phi\delta_{ab} = -g_{\phi}\sum_{\mathbf{k}}\left\langle c_{1,\mathbf{k},a}^{\dagger}c_{2,\mathbf{k},b}\right\rangle = g_{\phi}\sum_{\mathbf{k}}\left\langle c_{3,\mathbf{k},a}^{\dagger}c_{4,\mathbf{k},b}\right\rangle, \tag{2.9}$$

where

$$\begin{aligned} g_{\Delta} &= \frac{1}{2}\sum_{a,b,c,d}g^{abcd}(i\sigma_{ac}^{y})(i\sigma_{db}^{y}) = \frac{3J}{4} - 4V \\ g_{\phi} &= \frac{1}{2}\sum_{a,b,c,d}g^{abcd}\delta_{ad}\delta_{bc} = \frac{3J}{4} + V, \end{aligned} \tag{2.10}$$

are the effective couplings in the superconducting and charge channels respectively. The order Δ is the projection of uniform d-wave superconductivity onto the hot-spots, and ϕ describes a d-wave charge order, that lives on the bonds between copper sites, and has modulation vector $\mathbf{Q}$ given by the separation between hot-spots. It is clear that V enhances superconductivity and simultaneously suppresses charge order. Because of the d-wave form factor of the order parameters, two of the remaining hot-spots become redundant and at the mean field level the behavior of the system may be described by a 4×4 Hamiltonian in hot-spot-Nambu space. Defining a Nambu spinor $\psi_{\vec{k}} = \left(c_{1,\vec{k},\uparrow}, c_{2,\vec{k},\uparrow}, c_{2,-\vec{k},\downarrow}^{\dagger}, c_{1,-\vec{k},\downarrow}^{\dagger}\right)^{T}$ the Hamiltonian takes the form

$$\mathcal{H} = \sum_{\mathbf{k}}\psi_{\mathbf{k}}^{\dagger}\hat{H}_{\mathrm{MF}}(\mathbf{k})\psi_{\mathbf{k}} + \frac{2}{g_{\Delta}}|\Delta|^{2} + \frac{2}{g_{\phi}}|\phi|^{2}, \tag{2.11}$$

where

$$
\hat{H}_{\mathrm{MF}}(\mathbf{k}) =
\begin{bmatrix}
\xi_1(\mathbf{k}) & \bar{\phi} & \Delta & 0 \\
\phi & \xi_2(\mathbf{k}) & 0 & \Delta \\
\bar{\Delta} & 0 & -\xi_1(\mathbf{k}) & -\bar{\phi} \\
0 & \bar{\Delta} & -\phi & -\xi_2(\mathbf{k})
\end{bmatrix},
\tag{2.12}
$$

and Δ and ϕ are the superconductivity and dFF-DW order parameters respectively.

Both order parameters are generally complex numbers, which we can write as $\Delta = |\Delta|e^{i\theta_\Delta}$ and $\phi = |\phi|e^{i\theta_\phi}$. However, since we can always remove the complex phases (at the mean-field level) via a gauge transformation[2] $c_1 \to c_1 e^{-i(\theta_\Delta - \theta_\phi)/2}$, $c_2 \to c_2 e^{-i(\theta_\phi + \theta_\Delta)/2}$, we will consider only real and non-negative values for ϕ and Δ in our analysis.

From Eq. (2.11) we can readily derive a Landau free energy for the Δ and ϕ orders. Evaluating $f = f_{MF} + \frac{1}{N} \langle H - H_{MF} \rangle_{MF}$, using the above decoupling and expanding to fourth order in the order parameters, we obtain

$$
f = \left[\frac{2}{g_\phi} - \Pi_\phi \right] \phi^2 + \left[\frac{2}{g_\Delta} - \Pi_\Delta \right] \Delta^2 + \beta_\phi \phi^4 + \beta_\Delta \Delta^4 + w\phi^2 \Delta^2,
\tag{2.13}
$$

with $w, \beta_\phi, \beta_\Delta > 0$. The exact expressions for the coefficients are given in Table 2.2. It is in fact possible to solve the mean field problem exactly via a sequence of Bogoliubov transformations. This method breaks down, however, once we introduce c-axis hopping or move beyond the hot-spot approximation, and so, in anticipation of this extension of the model, we have chosen instead to work with a Landau expansion, which will carry over to the more complicated cases.

In what follows we hold J fixed and use V to adjust the splitting between the superconducting and dFF-DW instabilities. Doing so, we obtain a phase diagram such as that in Fig. 2.5. In it we see the following easy-to-understand behavior:

---

[2]The ability to gauge away the phase degrees of freedom requires that we be considering only superconductivity and a single charge order and applies only to the hot-spot model at the mean field level.

Table 2.2: Microscopic expressions for coefficients of the Landau theory. n_F is the Fermi function and n'_F the derivative of the Fermi function with respect to energy.

Term	Expression
Π_Δ	$\int_{\mathbf{k}} \frac{1-2n_F(\xi_1)}{\xi_1}$
Π_ϕ	$2\int_{\mathbf{k}} \frac{n_F(\xi_2)-n_F(\xi_1)}{\xi_1-\xi_2}$
β_Δ	$\int_{\mathbf{k}} \frac{1}{2\xi_1^2}\left[n'(\xi) + \frac{1-2n_F(\xi)}{2\xi_1}\right]$
β_ϕ	$\int_{\mathbf{k}} \frac{1}{(\xi_1-\xi_2)^2}\left[n'(\xi_1) + n'(\xi_2) + 2\frac{n_F(\xi_2)-n_F(\xi_1)}{\xi_1-\xi_2}\right]$
γ	$2\int_{\mathbf{k}} \frac{1}{\xi_1(\xi_1-\xi_2)}\left[n'(\xi_1) + \frac{1-2n_F(\xi_1)}{2\xi_1}\right]$

Figure 2.5: Phase diagram of the 2D model, for fixed J. The regions are from left to right, dSC, dFF-DW + dSC, and dFF-DW, with the white region at the top being the normal phase. Note that the temperature does not extend down to $T = 0$ as the Landau theory is not valid in this limit.

when V is zero or very small the d wave superconductivity is the only relevant instability of the model. With V increasing, superconductivity is suppressed and eventually dFF-DW appears as the leading order. Notably, in the region where these instabilities are comparable there is a (rather narrow) coexistence phase. These features are consistent with previous studies of the model [37].

We expect this phase diagram to be strictly valid only close to T_c *and* in the region in which the critical temperatures of both orders are comparable. However, comparing the Landau expansion with the exact numerical mean-field solution shows that even for intermediate temperatures there is only a small, purely quantitative correction to the shape of the coexistence region.

2.4   Extension to stacked planes

Motivated by the experiments which have used optical excitation polarized along the c-axis to create transient states of enhanced superconductivity [21, 23, 25], we seek to extend the purely two-dimensional model from the previous section to include coupling between planes. The simplest model that encapsulates this behavior can be represented by the following Hamiltonian:

$$H_{3D} = \sum_l H_l + H_{\mathrm{T}}. \tag{2.14}$$

Here l is a layer index, and H_l is the single-layer Hamiltonian considered in Eq. (2.1). There are N_z copies of those, which are coupled via a c-axis tunneling term

$$H_{\mathrm{T}} = \sum_{\vec{k}_\parallel, k_z} c^\dagger_{\vec{k}_\parallel, k_z \sigma} t_z(\vec{k}_\parallel, k_z) c_{\vec{k}_\parallel, k_z, \sigma}, \tag{2.15}$$

where c-axis momentum k_z is conjugate to the plane index l.

In what follows we will consider and compare three different forms for the

tunneling t_z in Eq. (2.15). The exact expressions for each tunneling type are presented in Table 2.3. Type A tunneling (nearest neighbor hopping along the c-axis) we introduce mainly for its simplicity, type B comes from a one-band tight binding fit to band structure calculations for Lanthanum-Strontium-Copper-Oxide (LSCO) [77], and type C was proposed as an approximate tunneling form for several families of cuprate superconductor [78]. Despite the significant differences between these tunneling forms, it turns out that the effects we obtain are not specific to any of them, but are in all cases qualitatively similar.

Table 2.3: c-axis tunneling elements used in the calculation

Type	c-axis tunneling
A	$-2t_z \cos k_z$
B [77]	$-2t_z \cos\left(\frac{k_z}{2}\right)\left(\cos k_x - \cos k_y\right)^2 \cos\left(\frac{k_x}{2}\right)\cos\left(\frac{k_y}{2}\right)$
C [78]	$-2t_z \cos(k_z)(\cos k_x - \cos k_y)^2$

We now retrace the same steps as in Section 2.2. The derivation proceeds similarly, but there are some subtleties that need to be considered first.

Due to the model containing solely in-plane interactions, we only need to consider pairing of quasi-particles within the same plane. As a consequence of this, the order parameters do not depend on k_z and the vector $\mathbf{Q}$ which separates fermions contributing to pairing in the charge channel cannot change with k_z. Because of this restriction, we find that while at $k_z = 0$ superconductivity and dFF-DW pair the same points in the 2D Brillioun zone, this is no longer true for $k_z \neq 0$, $t_z \neq 0$. The particle and hole being paired in the dFF-DW channel must remain separated by $\vec{Q} = (Q, Q)$ even when the Fermi surface is no longer nested with this vector, as can be seen in Fig. 2.6. Superconductivity on the other hand continues to pair $\mathbf{k}$ and $-\mathbf{k}$ for all k_z. As a consequence, one has to be careful to define the hot regions properly in this case. There are several ways one might do so, but fortunately, as shown in Appendix A.1, they all lead to the same qualitative behavior.

That being the case, we implement the following procedure. At each k_z there is a region centered on where the 2D Fermi surface intersects the 2D magnetic Brillioun zone. ϕ now pairs quasi-particles separated by the fixed charge ordering vector and is only non-zero when the momenta of both fall within a hot region. With this procedure in place, the free energy takes the same form as Eq. (2.13) but with the coefficients now being the three dimensional integrals shown in Table 2.4. Here, we have made the simplifying assumptions that Δ and ϕ are not modulated along the c-axis.[3] As can readily be seen, the expressions in Table 2.4 reduce to those in Table 2.2 in the limit of no c-axis hopping.
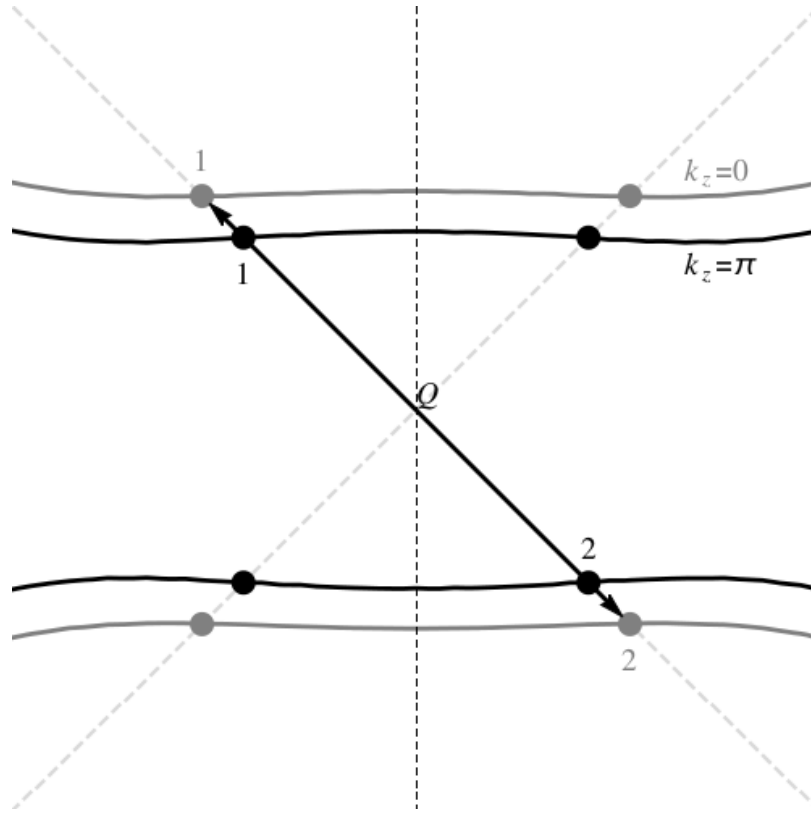
Figure 2.6: Bending of the Fermi surface as a function of c-axis angular momentum leads to a destruction of nesting away from $k_z = 0$. As the Fermi surface nesting vector is a function of k_z but the ordering vector $\mathbf{Q}$ is not, the Fermi surface cannot remain nested at $\mathbf{Q}$ for all k_z. This leads to a weakening of the dFF-DW nesting instability.

---

[3]As discussed above this is not the whole picture. We will investigate the extensions to non-trivial out of plane ordering vector in Section 2.5.

Table 2.4: Microscopic expressions for the coefficients of the Landau theory. ξ_{1-Q} is the energy at a point at the point $\vec{k}' = \vec{k} + \vec{k}_{\text{HS}} - \vec{Q}$. Primed integration indicates a restriction of the integral to regions where both $\vec{k}$ and $\vec{k}'$ lie within a hot region. The k_z integration is from $-\pi$ to π.

Term	Expression
Π_Δ	$\int_{\mathbf{k}} \frac{1-2n_F(\xi_1)}{\xi_1}$
Π_ϕ	$2\int_{\mathbf{k}}' \frac{n_F(\xi_{1-Q})-n_F(\xi_1)}{\xi_1-\xi_{1-Q}}$
β_Δ	$\int_{\mathbf{k}} \frac{1}{2\xi^2}\left[n_F'(\xi) + \frac{1-2n_F(\xi)}{2\xi}\right]$
β_ϕ	$\int_{\mathbf{k}}' \frac{1}{(\xi_1-\xi_{1-Q})^2}\left[n_F'(\xi_1) + n_F'(\xi_{1-Q}) + 2\frac{n_F(\xi_{1-Q})-n_F(\xi_1)}{\xi_1-\xi_{1-Q}}\right]$
γ	$2\int_{\mathbf{k}}' \frac{1}{\xi_1(\xi_1-\xi_{1-Q})}\left[n_F'(\xi_1) + \frac{1-2n_F(\xi_1)}{2\xi_1}\right]$

Using each of the three tunneling forms, we calculated the state which minimized the free energy for a range of T, V and t_z. The (Q, Q) order remains the leading charge instability at the quadratic level, so we again only decouple in this channel and the d-wave superconducting channel. The phase diagram for tunneling type B is presented on Fig. 2.7 (the other two types lead to qualitatively similar diagrams). We start (for $t_z = 0$) with the coexistence case in which dFF-DW is the leading instability. As we can see, for small but finite t_z the charge order is further enhanced at the expense of superconductivity. However, once t_z becomes sufficiently large, the tendency reverses, and superconductivity is boosted by the increase of three-dimensionality, until it becomes the leading instability.

To understand this peculiar shape of the phase diagram, we look at the quadratic coefficients in the free energy. The behavior of the superconducting coefficients, Π_Δ and β_Δ, can be explained entirely by the dependence of the density of states and bandwidth, $\rho(\xi, t_z)$ and $W(t_z)$. As can be seen in Fig. 2.8, these lead to only a small effect on the superconducting susceptibility. Thus, the features visible in Fig. 2.7 are mostly determined by the behavior of the charge instability and its indirect effect on superconductivity through the biquadratic term in the free energy.
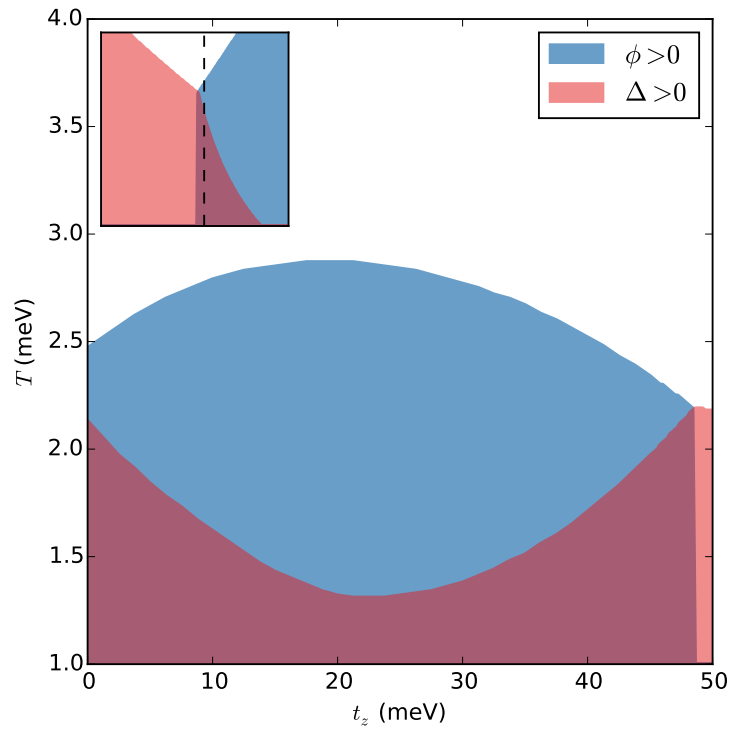
Figure 2.7: Phase diagram of a system of stacked planes at a fixed coupling strength for tunneling type B in Table 2.3. Types A and C exhibit qualitatively similar behavior, but with different scales on the t_z axis. The inset indicates where the starting point at $t_z = 0$ lies in $V - T$ plane of Fig. 2.5 ($V = 110 \, \text{meV}$).

The non-monotonic behavior of the charge susceptibility Π_ϕ can be understood as a competition of two effects. First, it is well known within this model that in the absence of Fermi surface curvature, the diagonal dFF-DW order exhibits a BCS type transition characterized by a logarithmic divergence. Curvature however cuts off the divergence of the logarithm and weakens the charge instability [36, 37, 79]. Specifically, we can write the dispersions as

$$\xi_1 = \xi_+ + \xi_- \tag{2.16}$$

$$\xi_2 = \xi_+ - \xi_- \tag{2.17}$$

In that case the charge susceptibility becomes

$$\Pi_\phi = \int_{\mathbf{k}} \frac{\sinh\frac{\xi_-}{2T}\cosh\frac{\xi_-}{2T}}{\xi_-[\sinh^2\frac{\xi_+}{2T} + \cosh^2\frac{\xi_-}{2T}]} \tag{2.18}$$

in the 2D limit. One can see clearly that in the limit that $\xi_+ \to 0$, the absence of curvature, the charge (particle-hole) instability becomes as strong as the superconducting (particle-particle) one, and for any non-zero ξ_+ the charge susceptibility is weaker compared to that of the BCS case.

As the c-axis hopping t_z increases the 2D curvature decreases. This is because the $k_z = 0$ component for all tunneling types is of the form $-t_z\eta(\mathbf{k}_\parallel)c^\dagger_{\mathbf{k}_\parallel}c_{\mathbf{k}_\parallel}$, with $\eta > 0$. Near the hot-spots this acts as an effective upward shift in the chemical potential, which moves the hot-spots such that ξ_+ is decreased relative to ξ_-. As a result, for increasing t_z, the $k_z = 0$ Fermi surfaces changes in such a way as to effectively enhance the charge instability. Fundamentally, this is a consequence of the effect of the tunneling term on the properties of the Fermi surface of each plane.

In opposition to the aforementioned effect, increasing t_z will lead to a progressive destruction of nesting away from $k_z = 0$, as depicted in Fig. 2.6. For $t_z = 0$, the Fermi surface is nested at the hot-spots for all k_z. However, as t_z increases the

Fermi surface warps more with k_z, decreasing the portion of the phase space for which there is approximate nesting, and thus weakening the charge susceptibility.

For small t_z the warping of the Fermi surface is small, and so the 2D decrease of curvature is nearly the same for a wide range of k_z values, leading to an overall strengthening of the charge instability. However, as t_z increases Fermi surface warping along the c-axis becomes more pronounced. As a consequence, the available phase space for charge ordering is substantially reduced, while at the same time the significance of the decreased curvature is lessened away from $k_z = 0$, together eventually causing a weakening of the charge ordering instability. The non-monotonic shape of the phase diagram can consequently be understood as demonstrating a crossover between regimes in which the 2D and the 3D effects of t_z dominate.

Interestingly, the value of t_z for which superconductivity reaches a minimum is of similar magnitude to the strength of c-axis hopping for various families of cuprates obtained as a fit to band structure [77]. Given this, if we imagine a system where t_z is near or greater than the point of minimum superconducting T_c in Fig. 2.7, then enhancements of t_z will generally lead to suppression of charge order and enhancement of superconductivity.

It should be noted that the effects demonstrated here are obtained within the grand canonical ensemble at fixed chemical potential. In anticipation of Section 2.6 the experimental program we envision comprises placing a sample in contact with its environment, which functions as a particle bath maintaining μ, and then applying perturbations that will lead to a change of t_z in the effective Hamiltonian. This, however, means that the volume enclosed by the Fermi surface is not constant and therefore average particle number is not conserved. If one were instead to consider a system where such a constraint were important this might change the behavior of the phase diagram at small t_z, where the effects are largely governed by the position of the $k_z = 0$ Fermi surface. However, larger t_z should still lead to Fermi
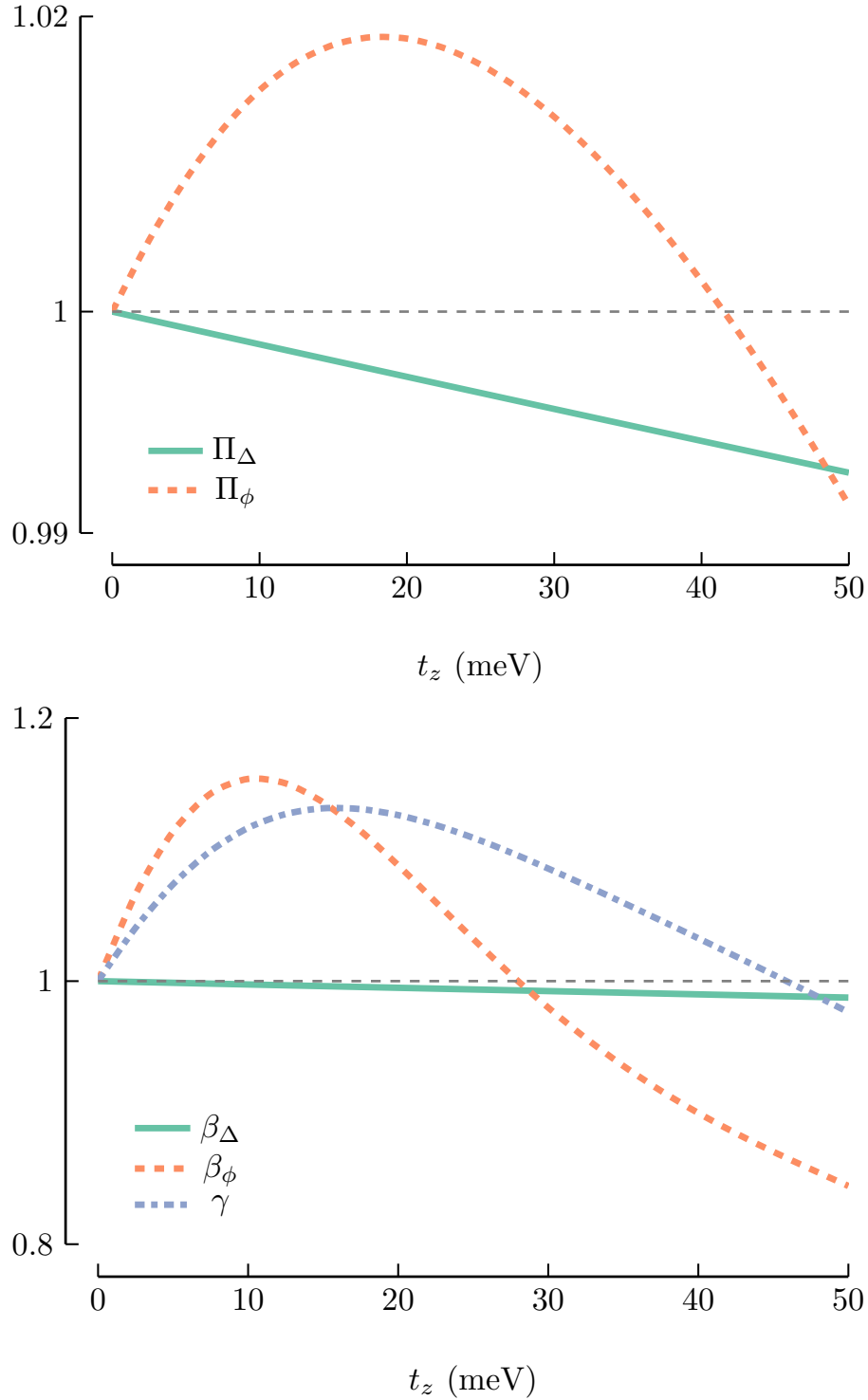
Figure 2.8: Quadratic susceptibilities and quartic coefficients of the Landau free energy as a function of t_z, scaled by their value at $t_z = 0$, for type B tunneling (at fixed temperature). Types A and C again exhibit similar behavior. Note that there is no significance to the crossing of lines for different coefficients, as the leading instability will be determined by $g\Pi$.

surface warping and thus the enhancement of superconductivity in that regime should remain. Therefore, while the 2D effects that are important predominantly at small t_z could be washed away, the suppression of charge order (via destruction of nesting), and thus the enhancement of superconductivity, appears much more robust.

2.5 Effects of phase pinning

As previously mentioned, the above argument is complicated by the possibility of a non-zero out-of-plane ordering vector. Due to the nearest neighbor nature of the inter-plane hopping, the Fermi surface is always nested perfectly at the wave vector $(0, 0, \pi)$. Therefore if the dFF-DW wavevector is (Q, Q, π) it will be largely unaffected by the change in interlayer tunneling, and the effect disappears.

The susceptibility analysis of Section 2.2 indeed confirms, that one can instead have an instability toward an order which oscillates with wavenumber π along the c-axis. Over a range of parameters, the strongest dFF-DW instability is overwhelmingly of such form. Nevertheless, there are reasons to believe that the experimental situation is a little more complicated. Empirically, the c-axis ordering vector Q_z of the density wave phase is broadly peaked around π, with a correlation length of approximately 0.6 lattice units [30]. Motivated by this we consider the case in which the interlayer ordering is not defined by a single wavevector. Instead, we propose a charge order $\phi_L = |\phi|e^{i\theta_L}$ at in-plane wavevector $\mathbf{Q}_L$, where the relative phase $\theta = \theta_1 - \theta_2$ in between two layers and the relative orientation $\mathbf{Q}_1 \cdot \mathbf{Q}_2 \in \{0, Q^2\}$ of the ordering vector on the layers are taken to be random variables determined by disorder. To study this more quantitatively we restrict our attention to $t - J - V$ model of two coupled planes. We model each Cu-O plane as a $t - J - V$ model [37, 59, 60, 62] on a square lattice, setting the lattice constant a to 1. Our model takes

the form $H = H_0 + H_{\text{int}}$. The free part is given by

$$H_0 = \int_{\mathbf{k}} \psi_{\mathbf{k}}^\dagger \left(\xi_{\mathbf{k}} \hat{\Lambda}_0 + t_{\mathbf{k}} \hat{\Lambda}_1 \right) \otimes \hat{\sigma}_0 \psi_{\mathbf{k}}$$

$$t_{\mathbf{k}} = t_z (\cos k_x - \cos k_y)^2 / 4 \tag{2.19}$$

where Λ_i are Pauli matrices acting in the layer space and σ_i act in the spin space. where $\xi_{\mathbf{k}}$ is as in Section 2.2 and t_k describes the hopping between layers [78, 80]. As before, we add to this the layer-local interactions

$$H_{\text{int}} = \frac{1}{2} \sum_{\langle i,j \rangle} \sum_L \left(V n_{i,L} n_{j,L} + J \mathbf{S}_{i,L} \cdot \mathbf{S}_{j,L} \right). \tag{2.20}$$

where L is a layer index.

For the model under consideration, the Landau free energy generically takes the form

$$\mathcal{F}_O[\theta] = \alpha_\Delta |\Delta|^2 + \beta_\Delta |\Delta|^4 + \alpha_{\phi,O}[\theta]|\phi|^2 + \beta_{\phi,O}[\theta]|\phi|^4 + \gamma_O[\theta]|\phi|^2|\Delta|^2, \tag{2.21}$$

where θ is as above, $O = \|, \perp$ is the relative orientation of the ordering vectors in the two planes, and Δ and ϕ are the superconducting and density wave order parameters, respectively. The coefficients may be calculated diagrammatically from the free particle action and depend parametrically on the interlayer couplings through the single-particle dispersion. The microscopic expressions for the Landau coefficients are given in Appendix A.2. We again find $\gamma > 0$, indicating competition between the two orders. For purposes of calculation it is useful to express the coefficients as a power series in $\cos(\theta)$

$$c_\|(\theta) = \sum_n c^{(n)} \cos^n \theta, \qquad c_\perp = \frac{1}{2\pi} \int_0^{2\pi} d\theta c_\|(\theta) \tag{2.22}$$

where $c \in \{\alpha, \beta, \gamma\}$ and for a term including ϕ^m the coefficients $c^{(n)} = 0$ for $n > m/2$. This form allows moments of the terms to be calculated easily in terms of the circular moments $\left\langle e^{in\theta} \right\rangle_\theta$.

The corresponding saddle-point equations admit three non-trivial solutions: a superconducting phase, a density wave phase, and a coexistent phase:

$$|\Delta| = \sqrt{-\frac{\alpha_\Delta}{2\beta_\Delta}}, \ \phi = 0$$

$$\Delta = 0, \ |\phi| = \sqrt{-\frac{\alpha_\phi}{2\beta_\phi}} \tag{2.23}$$

$$|\Delta| = \sqrt{\frac{2\beta_\phi \alpha_\Delta - \gamma \alpha_\phi}{\gamma^2 - 4\beta_\Delta \beta_\phi}}, \ |\phi| = \sqrt{\frac{2\beta_\Delta \alpha_\phi - \gamma \alpha_\Delta}{\gamma^2 - 4\beta_\Delta \beta_\phi}}.$$
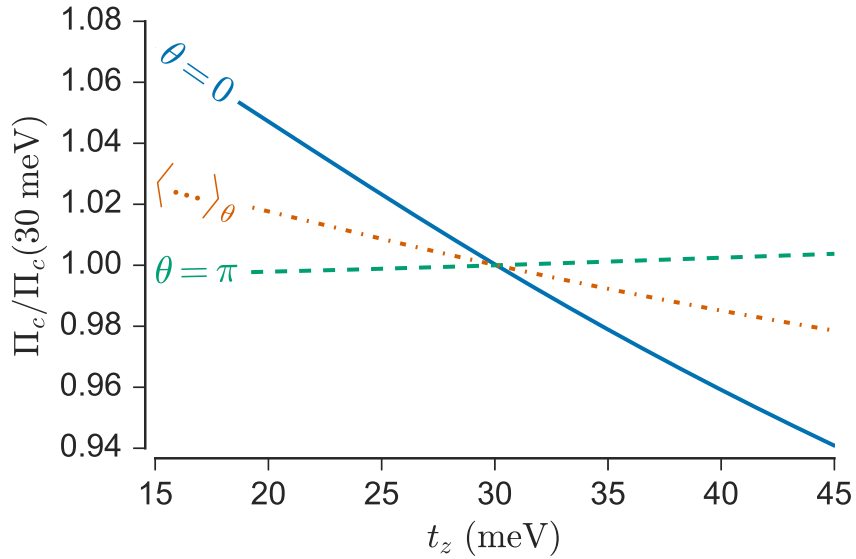
Figure 2.9: Charge susceptibility as a function of interlayer coupling for relative phase $\theta = 0$ (solid blue), $\theta = \pi$ (dashed green), and averaged with respect to θ (orange dot-dashed). Notably, there is little effect for $\theta = \pi$, while for $\theta = 0$ there is a noticeable suppression of charge ordering. The averaged case sits somewhere between the two, but the suppression of charge order is still significant.

To understand the effect of increased c-axis coupling on the dFF-DW we first consider the effect on the charge susceptibility $\Pi_\phi = -\alpha_\phi + \frac{1}{g_\phi}$, where g_ϕ is the

strength of the interaction in the dFF-DW channel. As can be seen in Fig. 2.9, increasing t_z leads to a notable suppression for order at $\theta = 0$ while $\theta = \pi$ sees a slight enhancement (due to the change in carrier density at fixed chemical potential [53]).

Now let us look at the averaged susceptibility. We take the relative orientation of the wave-vectors to obey a Bernoulli distribution, where alignment has probability p, and we take θ to be distributed according to a wrapped normal distribution[4]with mean $\mu = \pi$, and standard deviation σ

$$P[\theta] = \frac{1}{\sigma\sqrt{2\pi}} \sum_{k=-\infty}^{\infty} \exp\left(-\frac{(\theta - \mu + 2\pi k)^2}{2\sigma^2}\right). \qquad (2.24)$$

This is the simplest extension of a Gaussian distribution to a periodic variable. Our choice of distribution corresponds to the approximation that the relative phase is mostly determined by its first and second moments. Here, we have set the mean of the distribution to π to reflect both the fact that this is the energetically favored orientation in absence of disorder and that this is experimentally observed to be the peak ordering vector.

After the averaging process, we find

$$\overline{\Pi}_\phi = \sum_O \int_0^{2\pi} d\theta P[\theta] P[O] \Pi_\phi[O, \theta] = \Pi_\phi^{(0)} + \frac{1}{2}\left(\frac{1}{2} + e^{-\sigma^2/2}\cos\mu\right)\Pi_\phi^{(1)} \qquad (2.25)$$

with $\Pi^{(i)}$ defined as in Eq. (2.22).

As is shown in Fig. 2.9 the averaged susceptibility, like the $\theta = 0$ case, shows a noticeable decrease as t_z is increased, indicating a melting of charge order. Minimizing the averaged free energy density $\bar{F}$ we find that an increase in interlayer coupling leads to an observable melting of dFF-DW and a concomitant enhance-

---

[4]The wrapped normal distribution is a straightforward extension of the normal distribution to a periodic variable. It is a close cousin of the Von Mises distribution, which is the eigendistribution of diffusion for a periodic variable with a harmonic confinement but is somewhat more analytically convenient. We have explicitly checked that there is no qualitative difference between the results for the two distributions.
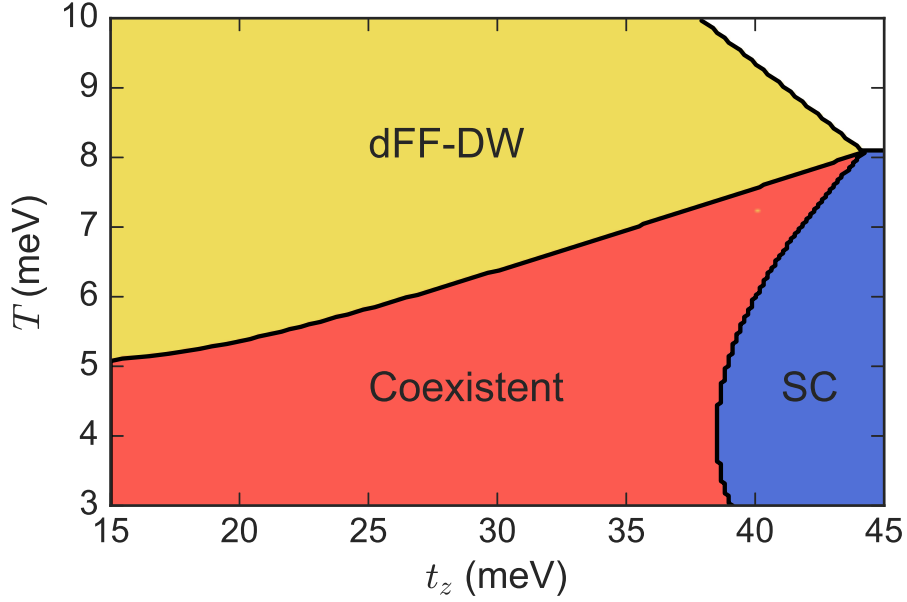
Figure 2.10: Phase diagram as a function of interlayer coupling t_z and temperature T for a fixed value of interaction strength. Increasing t_z leads to a suppression of charge ordering and a coinciding enhancement of superconductivity.

ment of superconductivity as can be seen in Fig. 2.10. In fact, tuning of interlayer coupling at fixed temperature can tune between charge-ordered, coexistent, and superconducting phases.

Changing the variance of the phase leads to a quantitative difference but results are qualitatively similar. In particular, we considered various values of σ with the dFF-DW ordering temperature at $t_z = 30\,\text{meV}$ held fixed. As shown in Fig. 2.11 for a wide range of σ an increase in interlayer tunneling leads to a melting of dFF-DW and an associated enhancement of dSC. The salient point is that pinning of the dFF-DW phase in general frustrates the interlayer ordering of the density wave state which would otherwise make it insensitive to changes in interlayer coupling. So while, in an idealized system the interlayer coupling strength should not appreciably affect the competition between dFF-DW and dSC order, in a realistic system an increase of the interlayer coupling generically leads to a melting of dFF-DW and enhancement of dSC. One way to visualize this effect is that domains with distinct
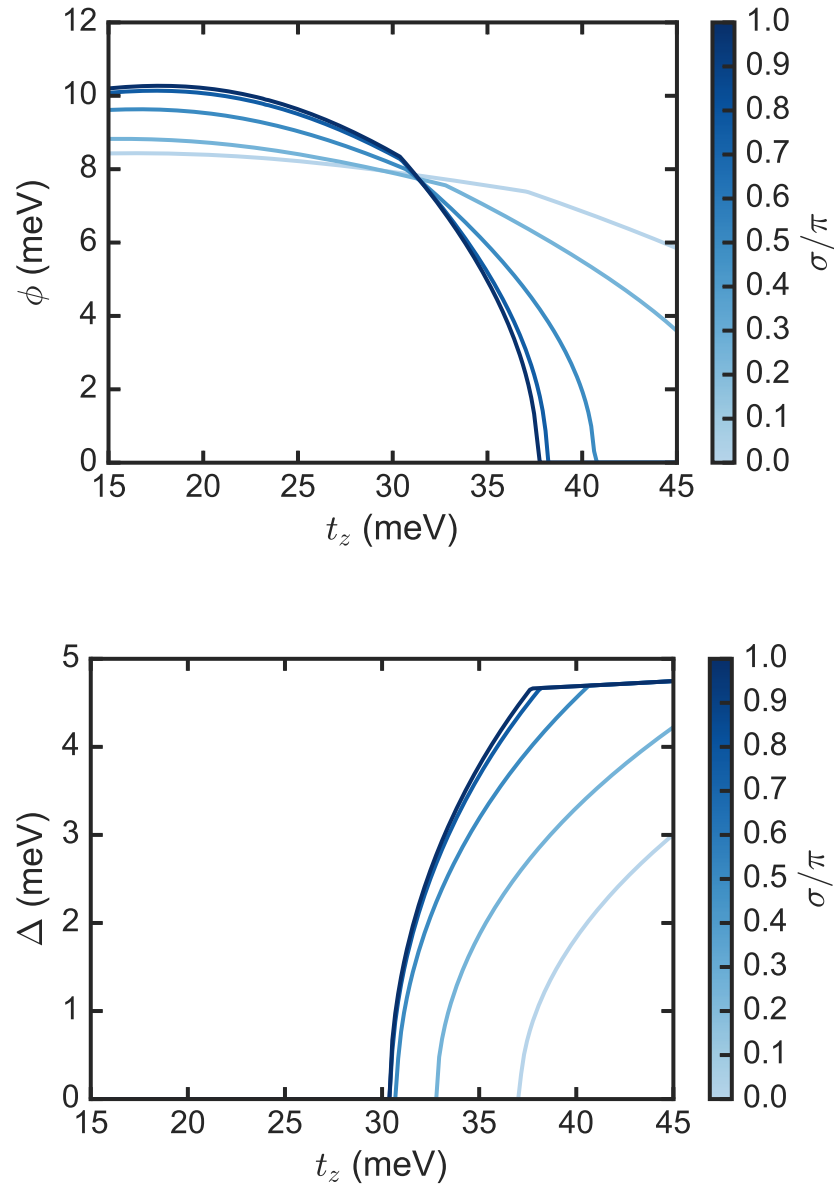
Figure 2.11: dFF-DW order parameter ϕ (top) and superconducting order parameter Δ (bottom) vs interlayer coupling for various values of σ, the standard deviation of the interlayer dFF-DW phase difference. The coupling constants of the model have been normalized to keep the bare charge ordering temperature at $t_z = 30\,\text{mev}$ fixed. Increasing t_z in general leads to a melting of dFF-DW and enhancement of dSC with the effect becoming more pronounced as σ is increased.

phase differences form and these domains are susceptible to melting to different degrees. Such a picture is consistent with experiments where inhomogeneous enhancement of electron-electron pairing is observed [22], as one might expect from inhomogeneous melting of dFF-DW domains.

2.6 Enhancement of superconductivity via periodic modulation

It has been argued that in YBCO the c-axis vibrations, induced by the external field, can change the equilibrium lattice structure [22]. The result is a transient shift of the CuO_2 planes – the intra-bilayer distance increases, while the inter-bilayer one decreases. In our model this would lead to effectively bringing the layers closer. Intuitively, it is clear that this should lead to enhancement of the inter-plane coupling t_z. In this the role of the apical oxygen seems quite significant; previous experimental works have found that there is a range of dopings for which the inter-layer hopping exhibits a roughly exponential dependence on the hole-doping [81] while the bond length between the plane copper and the apical oxygen exhibits a roughly linear dependence on doping through the same region [82]. A natural interpretation is that the hopping exhibits an exponential dependence on an effective barrier width d:

$$t_z = Ae^{-\alpha d}, \tag{2.26}$$

where d is approximately linear in the distance between the plane and the apical oxygen [81, 83]. Thus, decreasing the interlayer distance leads to an *exponential* increase of the c-axis tunneling.

There is a second, more subtle, way in which driving the apical oxygens can enhance the interlayer tunneling. Let us consider a vibration of these ions *without* change of their equilibrium positions. Then, in line with the above reasoning, we can model the effect of harmonic oscillations of the apical oxygen on t_z as oscillations

of the effective barrier width, leading to a time dependent hopping element

$$t_z(t) = Ae^{-\alpha d(t)} = t_{z0} \exp[-\alpha d_1 \cos(\Omega t)], \qquad (2.27)$$

where $d(t) = d_0 + d_1 \cos(\Omega t)$, and $t_{z0} = Ae^{-\alpha d_0}$.

Let us consider the high frequency limit. Then, we expect that the quasi-particles will see an effective time averaged Hamiltonian. While in experiment the frequencies are not extremely high, we consider this limit as a particularly simple case, from which we may extract relevant qualitative trends. More formally, we can obtain a Floquet Hamiltonian related to the time dependent hoppings. The stroboscopic dynamics of the system will be governed by this Floquet Hamiltonian, which can be obtained as series in $1/\Omega$ via a Magnus expansion of the time evolution operator [84]. For a high frequency oscillation, we keep only the first term of this expansion, which is just the time-dependent Hamiltonian averaged over one period. In this case the Floquet Hamiltonian is the original Hamiltonian (Eq. (2.14)), but with the modification

$$t_z \to \langle t_z(t) \rangle = \Omega \int_0^{\frac{2\pi}{\Omega}} \frac{dt}{2\pi} t_z(t) = t_{z0} I_0(\alpha d_1), \qquad (2.28)$$

where I_0 is the modified Bessel function of the first kind. I_0 is bounded below by 1, and increases monotonically with the magnitude of d_1. Therefore, within this approximation, any oscillation of the apical oxygens unavoidably leads to enhancement of the effective c-axis tunneling t_z. This can be easily understood from the exponential dependence of the tunneling on the apical oxygen position: in the tail of the exponent, a stronger enhancement is obtained from decreasing the argument than the suppression when increasing it at π/Ω time later. Thus, the tunneling amplitude is, on average, enhanced. Note that this observation is rather general, and likely applicable well beyond the region of validity of the high-frequency approximation used above.

By using data from Refs. [81, 82] we can obtain an estimate to the magnitude of both the oscillatory enhancement and the slower, quasi-static, effect[5]. Assuming an oscillation distance of $d_1 \sim 4.5 \, \text{pm}$, as is observed in the experiments discussed in Ref. [22], we find approximately a 55% enhancement of t_z in the steady state average. This in turn may lead to a few percent up to around a 40% enhancement in the superconducting T_c depending where in the non-monotonic structure of Fig. 2.7 the sample is before perturbation. A stronger effect is the shift of the equilibrium position of the apical oxygen. A quasi-static shift of the apical oxygen position by 2.4 pm (again see Ref. [22]) can increase t_z by as much as 110%, subsequently enhancing T_c by up to about 60%. The difference in magnitudes arises from the fact that the quasi-static shift of the apical oxygens produces a direct increase of t_z, whereas oscillation leads to an imperfect cancellation of weaker and stronger tunneling at different times in a period due to the nonlinear dependence of t_z on d_1. These effects provide a qualitative picture of a possible mechanism underlying the explanation given in Ref. [22].

2.7 Discussion and Conclusion

The primary motivation for this investigation came from the recent experiments on transient enhancement of superconductivity in the cuprates via mid-infrared optical excitations [21–23, 25]. To model these experiments we considered an extension of the $t - J - V$ model of cuprates to three dimensions, and the effects of this three-dimensionality on the competition between superconductivity and bond

---

[5]As discussed in Ref. [81], we may relate their measurements of the integrated c- spectral weight N_{eff}^c to the c-axis tunneling strength via the c-axis plasma frequency. If we take the exponential behavior of this quantity to be dominated by the c-axis tunneling with form $t_z \propto e^{-\alpha d(x)}$, with d the Cu(1)-O(4) (in-plane copper to apical oxygen) bond length, we may write $N_{\text{eff}}^c \sim A e^{-2\alpha d(x)}$, where A is effectively a constant. The data in Ref. [81] is for N_{eff}^c as a function of doping, but Ref. [82] provides data showing a quasi-linear dependence of the Cu(1)-O(4) bond length on doping. Thus, we model $d(x) = d_0 - \eta x$ with x the hole doping. We may now obtain a rough estimate of $\eta \approx 0.075 \, \text{Å}$ and $\alpha \approx 31 \, \text{Å}^{-1}$ by approximating the data points presented in figures in Refs. [81, 82] in order to reproduce the observed data.

density wave orders. We showed that for our extended model, increased inter-plane tunneling leads to a suppression of charge ordering, and a coinciding enhancement of superconductivity due to the inherent competition between the two orders. The evolution of charge order takes place in two steps, corresponding to the regions where 2D and 3D effects of increased interlayer coupling, respectively dominate. The primary effect of interest is that the charge instability is sensitive to the c-axis curvature of the Fermi surface, which destroys nesting at the charge ordering vector. This effect is generic across several tunneling forms proposed for various cuprate materials. Notably the presence of phase pinning of the dFF-DW is essential to this effect.

These results provide a physical picture explaining the enhancement of superconductivity by the decrease of the inter-bilayer distance, caused by optical excitation. We further showed that periodic oscillations of the apical oxygens (identified in the experiments as important) can also lead to an effective increase of the inter-layer coupling. Both these effects indirectly promote superconductivity via a suppression of the competing charge ordering. We believe that the mechanism presented here could play a significant part in the observed enhancement of superconductivity and could be useful in pursuing new ways to raise T_c. Other mechanisms have been proposed with regard to these experiments: the suppression of phase fluctuations [57, 85] as well as the usual enhancement of superconductivity due to microwave stimulation [14] could certainly play a complementary role.

While the c-axis curvature effects seem to be too weak to explain the observed enhancement of superconducting correlations alone, there are still other theoretical [58] and experimental [24] reasons to believe that melting of charge order plays an important role. Other explanations have been considered for this effect such as redistribution of spectral weight [57], suppression of superconducting phase fluctuations [86], or other routes to melting of dFF-DW order [58]. Most likely the

complete explanation is some combination of factors, with a number of these frameworks forming complementary rather than competing mechanisms.

At the end, let us also note that this work considers only the mean field behavior of such a system. As is well known, fluctuations play an extremely important role in the superconducting transition of cuprates [87–89]. Nevertheless, we expect that the effects discussed here on a mean field level will remain important in a more complete description of the system (entering through the relevant energy scales, for example). The mean field theory presented in this paper is only the first necessary step in the study of these effects, and including fluctuations is an important direction for future work.

Chapter 3: Hybridization of Higgs mode in a bond-density-wave state

This chapter is based upon Raines, Stanev, and Galitski [90, ©️ American Physical Society], published in Physical Review B.

3.1 Overview

Recently, several groups employed time-domain reflectivity [91] as a tool to study the charge order seen in cuprates [92–95], and, in particular, its collective modes. In some cases they were able to extract the amplitude and phase oscillations and to track them as the system became superconducting.

These results can provide valuable insights into the physics of both pseudogap and superconducting states, and, thus, it is desirable to have a better theoretical understanding of the possible collective modes of these systems. One particularly interesting point is that the coexistence of charge order and superconductivity makes possible the direct observation of the superconducting Higgs mode, as first pointed out in the pioneering work of Littlewood and Varma [96].

In this chapter we present a theoretical study of the Higgs modes, [1] or oscillations of the amplitude[2], of the order parameters in underdoped cuprates. We consider both the pure BDW state, as well as the coexistent BDW-superconductivity phase. We use the so-called "hot-spot" model [36, 37, 53, 62, 67, 68, 70, 73] of the pseudogap phase, which is based on a picture of a metallic state close to a magnetic instability, and considers the physics of the special points on the Fermi surface connected by the magnetic ordering vector. Although relatively simple, this model has seen extensive

---

[1]Higgs modes have a long history in condensed matter physics, being first observed in ^{3}He: [97, 98]

[2]For a review of Higgs modes in condensed matter see e.g. Refs. [99, 100]

use recently, as it naturally leads to coexistence between BDW and superconductivity, and also correctly predicts the d-wave phase factor of the charge order [36, 37, 73].

Our results provide a general framework for identifying and understanding order-parameter collective modes of the system. In the single-order phase (i.e., only BDW or superconductivity) we find, as expected, a single amplitude mode, which is coupled with the quasiparticle continuum and is always damped. However, the coexistence regime is much more interesting – the fluctuations of the different order parameters become intertwined [96].

As a consequence, in this region we find two Higgs modes, which represent coupled oscillations of the order parameters. One of the modes is slow, with frequency well below the amplitude of the order parameters, but which is, nevertheless, weakly damped. The other mode is pushed inside the high-energy continuum, and quickly becomes overdamped. We follow the slow mode in the entire coexistence phase, and find its frequency to be a non-monotonic function of temperature. This mode is weakly damped through an unusual low-energy decay channel for the antinodal quasi-particles, caused by the coexistence of the two orders and the associated band reconstruction. Even more unusually, this damping initially increases with the decrease of temperature.

To account for the damping from the gapless degrees of freedom present at the nodal regions we develop a phenomenological time-dependent Ginzburg-Landau theory. We demonstrate that, by allowing for significant damping, the in-gap mode is strongly suppressed, while the frequency of the high-energy mode is brought down.

Our results provide a characterization of the amplitude modes of the coexistent superconductivity BDW system which can be compared with the experimental data and used to identify the appropriate Higgs modes of the system.

3.2 Microscopic calculation of collective modes frequencies

We will consider here the collective modes in a 2D "hot-spot" model described in Section 2.2. Such a model can be obtained as a low-energy theory from the 2D t-J-V model, [36, 37, 67, 73] which contains hoppings $t_{(1/2/3)}$ on a square lattice as well as nearest-neighbor exchange and Coulomb interactions J and V. Specifically, one projects the lattice theory onto regions in the vicinity of 8 "hot-spots" where the Fermi surface intersects the magnetic Brillouin zone boundary. In the vicinity of these hot-spots the nearest-neighbor interactions J and V can be approximated by constants. Time reversal symmetry allows the problem to be reduced to considering fermions near 4 inequivalent hot-spots where, in the channels of interest, the interactions take the form

$$\mathcal{H}_{\text{int}}^{\Delta} = \frac{g_s}{4} \sum_{k,p,q} \Psi_{k+q,a}^{\dagger} \check{V}_{\Delta} \Psi_{k,a} \Psi_{p-q,b}^{\dagger} \check{V}_{\Delta} \Psi_{p,b}, \tag{3.1}$$

$$\mathcal{H}_{\text{int}}^{\phi} = \frac{g_c}{4} \sum_{k,p,q} \Psi_{k+q,a}^{\dagger} \check{V}_{\phi} \Psi_{k,a} \Psi_{p-q,b}^{\dagger} \check{V}_{\phi} \Psi_{p,b}, \tag{3.2}$$

where $\Psi_{a,b}$ are Nambu spinors in pairs of hot-regions separated by the antiferromagnetic wave-vector $\mathbf{K} = (\pi, \pi)$ and g_s and g_c are the non-retarded components of the interaction in the superconducting and BDW channels, respectively. $\check{V}_{\Delta}$ and $\check{V}_{\phi}$ are the vertices for pairing in the superconducting and BDW channels. Their explicit forms for the system studied here are shown in Eq. (3.4).

Due to the d-wave symmetry of the order parameters one can further restrict attention to 2 of the 8 hot regions [37]. The interaction terms can be decoupled via a Hubbard-Stratonovich transformation. In the usual manner, the saddle point of the zero-frequency terms of the decoupling fields leads to a mean-field theory, which

in this case has mean-field Hamiltonian

$$\mathcal{H} = \sum_{\mathbf{k}} \Psi_{\mathbf{k}}^{\dagger} \check{H}_{\mathrm{MF}}(\mathbf{k}) \Psi_{\mathbf{k}} + \frac{2}{g_s}|\Delta|^2 + \frac{2}{g_c}|\phi|^2, \tag{3.3}$$

where now Ψ is a Nambu spinor $(c_{k1\uparrow}, c_{k2,\downarrow}, c_{-k2\downarrow}^{\dagger}, c_{-k1\uparrow}^{\dagger})^T$ describing one pair of hot-spots. The mean-field Hamiltonian describes two species (denoted 1 and 2) of spinful fermions which pair only with each other.

Specifically,

$$\check{H}_{\mathrm{MF}} = \check{H}_0 + \Delta \check{V}_{\Delta} + \phi \check{V}_{\phi},$$
$$\check{H}_0 = \mathrm{diag}(\xi_1, \xi_2) \otimes \hat{\tau}_z, \tag{3.4}$$
$$\check{V}_{\Delta} = \hat{\rho}_0 \otimes \hat{\tau}_1, \quad \check{V}_{\phi} = \hat{\rho}_1 \otimes \hat{\tau}_3,$$

where $\hat{\tau}_i$ and $\hat{\rho}_i$ are Pauli matrices acting in particle-hole space and species space, respectively, and Δ describes d-wave superconductivity while ϕ is the BDW order [37]. Here, and in what follows, $\check{M}$ denotes a matrix in the 4×4 Nambu-hot-spot space, and $\hat{M}$ a 2×2 matrix. The self-consistency equations associated with Eq. (3.4) are

$$\Delta = \frac{g_s}{4} T \sum_k \mathrm{tr}\, \check{V}_{\Delta} \check{G}_k,$$
$$\phi = \frac{g_c}{4} T \sum_k \mathrm{tr}\, \check{V}_{\phi} \check{G}_k, \tag{3.5}$$

where $\check{G}_k$ is the matrix Matsubara Green's function of the Hamiltonian in Eq. (3.3), which is described below, and $k = (i\epsilon_n, \mathbf{k})$, with ϵ_n being a fermionic Matsubara frequency. Here we have considered Δ and ϕ to be real and non-negative (they can always be brought to this form via a gauge transformation).

In the case of a hot-spot model of cuprates, the two species correspond to fermions within a vicinity of inequivalent "hot-spots" in the Brillouin zone. Close to the hot-spot points the electron dispersion can be modeled as $\xi_1(\mathbf{k}) = \xi_2(-\mathbf{k}) = v_F k_x + \gamma k_y^2$, where we include the curvature γ as it plays an important role in breaking the

degeneracy between the two orders and allowing coexistence [37, 79].

The matrix Matsubara Green's function of Eq. (3.3) can be obtained by two consecutive Bogoliubov transformations in subspaces of the Nambu-spinor matrix structure. Doing so allows for the Green's function to be written in terms of the eigenvalues of the Hamiltonian as

$$\check{G}_k = \check{U}_k \check{g}_k \check{U}_k^\dagger, \tag{3.6}$$

$$\check{g}_k^{-1} = i\epsilon_n \check{1} - \text{diag}\left(E_k^+, E_k^-, -E_k^+, -E_k^-\right), \tag{3.7}$$

where the energies of the Bogoliubov quasiparticles are given by

$$E^\pm = \sqrt{(\lambda^\pm)^2 + \Delta^2}, \qquad \lambda^\pm = \xi_+ \pm \sqrt{\xi_-^2 + \phi^2},$$
$$\xi_\pm = \frac{\xi_1 \pm \xi_2}{2}. \tag{3.8}$$

The diagonalization matrix can be written in terms of the matrices $\hat{A} = w\hat{\tau}_0 - i\hat{\rho}_2 z$, and $\hat{B}^\pm = u^\pm \hat{\tau}_0 - i\hat{\tau}_2 v^\pm$, as

$$\check{U} = \left(\hat{A} \otimes \hat{\tau}_0\right)\left(\sum_\pm \hat{P}^\pm \otimes \hat{B}^\pm\right), \tag{3.9}$$
$$\hat{P}^\pm = \frac{1}{2}(\hat{\rho}_0 \pm \hat{\rho}_3)$$

where

$$w = \sqrt{\frac{1}{2}\left[1 + \xi_-\left(\xi_-^2 + \phi^2\right)^{-1/2}\right]}, \qquad z = \sqrt{\frac{1}{2}\left[1 - \xi_-\left(\xi_-^2 + \phi^2\right)^{-1/2}\right]},$$
$$u^\pm = \sqrt{\frac{1}{2}\left(1 + \frac{\lambda^\pm}{E^\pm}\right)}, \qquad v^\pm = \sqrt{\frac{1}{2}\left(1 - \frac{\lambda^\pm}{E^\pm}\right)}. \tag{3.10}$$

We follow Ref. [37] by choosing units where $v_F = 1$, $\gamma = 1/\Lambda = \pi$, with Λ being the hot-spot cutoff, and parametrize $\{g_c, g_s\} = 3J \pm 4V$ with $J = 1.2$. Note that V strengthens the interaction in the charge channel, while decreasing the interaction

in the superconducting channel,[3] and thus can be used to tune the coexistence (as depicted in Fig. 3.1). We consider two qualitatively different cases of coexisting charge order and superconductivity corresponding to the two dashed lines in Fig. 3.1: one where charge order disappears for some finite temperature below the superconducting T_c ($V = 0.2$), and one where charge order survives all the way down to $T = 0$ ($V = 0.21$). In both of these cases, the BDW order will onset at a temperature $T_{\mathrm{BDW}} > T_c$. The competition between the two orders can be readily confirmed by a decrease in ϕ below the superconducting T_c.
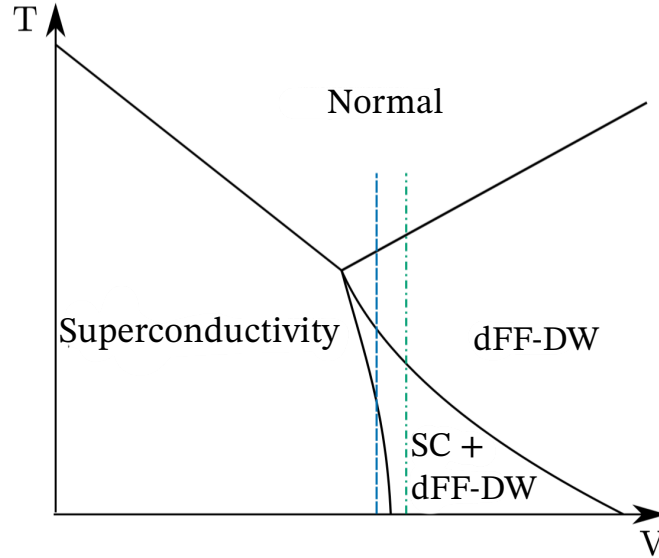
Figure 3.1: Schematic phase diagram of the hot-spot model, [37, 53] which illustrates the transition from superconductivity to charge order, tuned by V (nearest-neighbor Coulomb interaction). In this chapter we consider the transition from BDW to BDW-superconducting mixed state along the "trajectories" indicated by the dashed lines. Depending on the exact value of V the $T \to 0$ limit of the system could be either in a pure superconducting state (indicated by the blue dashed line), or in a mixed state (green dot-dashed line).

The ordering vector of the BDW is determined by the separation in the Brillouin zone of the hot-spots being paired. [36, 37, 62, 67, 68, 70] It is important to note that

---

[3]We note that previous works (such Refs. [67, 73]) have investigated an emergent SU(2) symmetry of the superconducting and charge order, associated with particle-hole transformation on one of the hot-spots. However, this emergent symmetry is explicitly broken by the curvature in the electron dispersion as well as the V term in the interaction Hamiltonian, so we do not consider its effects here.

we are considering a BDW with ordering vector (Q, Q), which is known to be the leading instability of this simple model. [36, 37, 62, 68, 70] This is different from the experimentally observed bond-oriented ordering directions $(Q, 0)$ and $(0, Q)$, which correspond to a different choice of hot-spots for the BDW pairing to occur between. It is possible to stabilize the $(Q, 0)$ and $(0, Q)$ orders, [61, 62, 70] but at the price of significantly complicating the model, and we will not pursue these modifications here.

We expect that most of our results and conclusions are applicable to the $(Q, 0)/(0, Q)$ orders as well.

3.2.1 Hybridized Higgs modes

The collective modes of coexisting charge-density-wave and superconducting states have been studied theoretically previously [96, 101–106], and we apply the methods developed in these earlier works. In general, the collective modes of the system are described by a 5×5 matrix, which includes the amplitude and the phase modes of each order parameter, as well as the density oscillations of the fermions. However, this matrix factorizes into two decoupled sectors, [102] with a 2×2 block describing the interacting amplitude modes, and the other $- 3 \times 3 -$ block describing the order parameters phases coupled to each other, as well as to the fermionic density.[4] This being the case, we devote our attention to the amplitude mode sector. In particular, we consider amplitude fluctuations of these order parameters with finite frequency ω, but zero wave-vector. Doing so allows us to calculate the mass of the collective modes: the minimum energy required to excite the collective modes of the ordered state.

---

[4]The oscillations of the phase of superconductor are usually pushed up to plasma frequencies by coupling with the Coulomb interaction. In contrast, the phase mode of an incommensurate charge order is theoretically a Goldstone mode of the system, but in real materials this degree of freedom is usually pinned by disorder.

Returning to the Hubbard-Stratonovich decoupling of the hot-spot model's inter-actions, inclusion of the finite-frequency components of the decoupling fields leads to the action

$$S = S_{\mathrm{MF}} + \sum_{k,\mathbf{q},\omega_m} \bar{\Psi}_{\mathbf{k}+\mathbf{q},\epsilon_n+\omega_m} \left(\Delta_{\mathbf{q},\omega_m} \check{V}_\Delta + \phi_{\mathbf{q},\omega_m} \check{V}_\phi \right) \Psi_{\mathbf{k},\epsilon_n}$$
$$+ \frac{2}{g_s} \sum_{\mathbf{q},\omega_m} |\Delta_{\mathbf{q},\omega_m}|^2 + \frac{2}{g_c} \sum_{\omega_m,\mathbf{q}} |\phi_{\mathbf{q},\omega_m}|^2, \quad (3.11)$$

where S_{MF} is the action corresponding to Eq. (3.3), which describes the mean-field state, and we are working in imaginary time. We have kept here the fluctuations $\Delta(\tau)$, $\phi(\tau)$ which are along the direction of Δ, ϕ in the complex plane,[5] corresponding to the amplitude modes,[6] which are described by the remaning terms in Eq. (3.11)

Particularly we will be interested in the 2×2 matrix collective mode propagator

$$D_{ij}(\omega_m, \mathbf{q}) = \langle O_{i,\omega_m,\mathbf{q}} O_{j,-\omega_m,-\mathbf{q}} \rangle, \quad (3.12)$$

where $O_{1,\omega_m,\mathbf{q}} = \Delta_{\omega_m,\mathbf{q}}$ and $O_{2,\omega_m,\mathbf{q}} = \phi_{\omega_m,\mathbf{q}}$, and the related object $D_{ij}^R(\omega, \mathbf{q}) = D_{ij}(i\omega_m \to \omega + i0^+, \mathbf{q})$, which can be obtained via analytic continuation. The off-diagonal elements of this matrix are in general non-zero and this is what leads to the hybridization of collective modes. The poles of the retarded propagator $\hat{D}^R$ will describe the on-shell collective mode energies.

After integrating out the fermionic degrees of freedom, $\hat{D}(\omega_m, \mathbf{q})$ can be expressed (at the quadratic level) as

$$\hat{D}^{-1}(\omega_m, \mathbf{q}) = (\hat{D}^0)^{-1} - \hat{Q}(\omega_m, \mathbf{q}), \quad (3.13)$$

---

[5]$\Delta(\tau)$ and $\phi(\tau)$ may be treated, then, as real fields since they may always be brought to lie along the real axis via a gauge transformation.

[6]This is a parametrization in terms of longitudinal and transverse modes such as considered in Refs. [101, 102] as opposed to radial and angular modes (c.f. Ref. [99]).

where we have defined

$$\hat{D}^0 \equiv \frac{1}{4} \begin{bmatrix} g_s & 0 \\ 0 & g_c \end{bmatrix}. \tag{3.14}$$

Here Q_{ij}, also a 2×2 matrix, is the self-energy of the collective modes due to the fermionic quasiparticles (this treatment is equivalent to obtaining the generalized susceptibilities of the order parameters within the random phase approximation (RPA)). Since, $\hat{D}^0$ is already known, $\hat{Q}$ is the object of interest.

Specifically, $\hat{Q}$ is given by

$$Q_{ij}(i\omega_m, \mathbf{q}) = -T \sum_{\mathbf{k}, \epsilon_n} \text{tr} \left[\check{G}(\mathbf{k}, \epsilon_n) \check{V}_i \check{G}(\mathbf{k} - \mathbf{q}, \epsilon_n - \omega_m) \check{V}_j \right], \tag{3.15}$$

where $i, j \in \{\Delta, \phi\}$.

After performing the fermionic Matsubara sums in Eq. (3.15) we analytically continue the bosonic frequency to the real axis, in order to obtain the finite-temperature, retarded self-energy $Q^R(\omega, \mathbf{q})$.[7]

The long-wavelength frequencies of the amplitude modes are given by the solutions of

$$\det \left[(\hat{D}^0)^{-1} - \hat{Q}^R(\omega_0 - i\Gamma_0, \mathbf{q} \to 0) \right] = 0, \tag{3.16}$$

where

$$\omega_0 \equiv \text{Re}[\omega(q \to 0)], \qquad \Gamma_0 \equiv -\text{Im}[\omega(q \to 0)], \tag{3.17}$$

are, respectively, the mass and the decay rate of the Higgs mode in the long wavelength limit. The in-gap collective modes, are those for which $\omega_0 < 2\min(\phi, \Delta)$.

One can explicitly show that the diagonal components of $\hat{Q}^R$ reproduce the usual $2\phi/2\Delta$ amplitude modes [96] in the limit where one of the order parameters vanishes. However, in our case, we focus our attention on the eigenmodes of the

---

[7]We have verified that Q^R satisfies the Kramers-Kronig relations, both exactly in its analytic form (in terms of integrals), and approximately in our numerics for the regions of interest to within the same degree of accuracy as that of Q^R itself.

response function, which describe hybridized modes of the system[8] and which cannot be obtained from purely considering the superconducting and BDW susceptibilities.

Because we are interested in weakly damped oscillations such that it makes sense to describe them as collective modes, we are able to employ a technique to determine the complex frequency of the oscillations from considerations of the response function on the real frequency line. In particular, we obtain the real part of the frequency as the solution to the equation $\mathrm{Re}[\lambda(\omega_0)] = 0$ where λ is a solution to the eigenvalue problem

$$\left[(\hat{D}^0)^{-1} - \hat{Q}^R(\omega) - \lambda(\omega)\hat{I}\right] \begin{pmatrix} \Delta_\omega \\ \phi_\omega \end{pmatrix} = 0. \tag{3.18}$$

The imaginary part of the frequency can then be calculated by expanding the eigenvalue as a function of complex ω about the real frequency. [101, 107] We defer analysis of the imaginary part (shown in Fig. 3.3) until Sec. 3.2.2 and focus now on the real part.

In order to track the temperature dependence of the collective modes, we explicitly solve the mean field equations for a range of temperatures and then calculate the collective mode frequencies at each temperature. Below T_{BDW}, in the pure BDW phase, we find an amplitude mode starting at frequency 2ϕ, as expected. [96] With the onset of superconductivity, another mode appears inside the gap. Physically, it represents coupled oscillations of the two order parameters, wherein pairs are excited in both the BDW and superconducting channels. The mixing of the two orders arises due to the off-diagonal elements of $\hat{Q}^R$, proportional to $\phi\Delta$. Intuitively, one might anticipate the presence of such an in-gap mode by arguing that one could convert one type of pairing into the other at a smaller energy than it would take to completely break a pair.

---

[8]A similar framework was recently used in Ref. [106]. However, the focus of that work was on the effects of the superconducting gap on the charge order, and the off-diagonal terms of $\hat{Q}^R$ (and thus the mixing) were assumed to be small.

The temperature dependence of the mode's frequency is non-trivial – initially it grows, but then reaches a maximum and goes down with the decrease of either ϕ or Δ. Depending on the shape of the coexistence region, this mode either survives all the way down to $T = 0$ or it vanishes at the second transition to a single-order-parameter phase. This behavior can be seen in Fig. 3.2. Note that near the phase transitions, this mode approaches the $2\phi/2\Delta$ amplitude mode of the order that vanishes at that temperature, which is the reason for the softening of the mode in the vicinity of these points.

At the onset of the coexistent phase, the other (2ϕ) mode is pushed to higher energies, enters the quasiparticle continuum, and quickly becomes overdamped. Thus, it is outside the region of validity of our method of finding ω, and so we do not track it.

3.2.2 Damping from antinodal quasiparticles

As explained in Sec. 3.2.1, the damping rate Γ_0, can be obtained by expanding the eigenvalues of Eq. (3.18) about the real part of the zero momentum dispersion ω_0. The temperature dependence of this damping rate is shown in Fig. 3.3. Although the in-gap mode stays below the $(2\Delta, 2\phi)$ threshold, its frequency has a finite damping rate, which, furthermore, initially *increases* as temperature goes down. This unusual behavior of the damping arises from the BDW bubble $Q_{\phi\phi}^R$; when just charge order is present, the only scattering which could lead to damping requires at least energy 2ϕ (as can be seen in Fig. 3.4(b)). All other types of scattering have zero matrix element, and thus there is no damping at $q = 0$ for $\omega_0 < 2\phi$. However, as soon as Δ becomes non-zero the bands are reconstructed due to hybridization of the BDW bands with their corresponding hole bands, and simultaneously scattering matrix elements between all bands become non-zero, allowing transitions between any two bands to contribute (c.f. Fig. 3.4(a)). As a result, there now exist transitions for
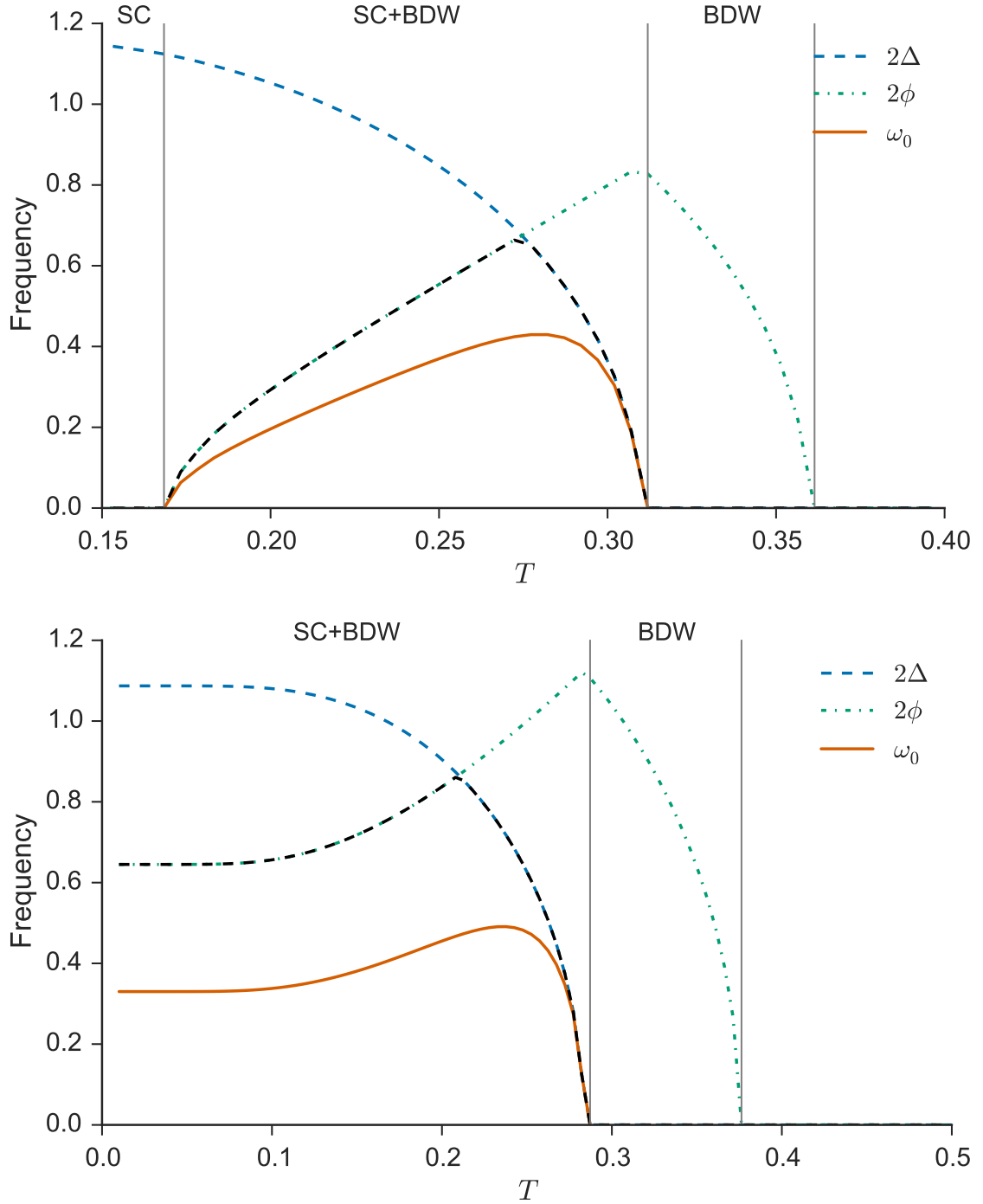
Figure 3.2: Mass of the in-gap hybrid Higgs mode $\omega_0 = \mathrm{Re}[\omega(q \to 0)]$ as obtained from Eq. (3.16). The frequency is plotted as a function of temperature for two different cases of $\phi(T \to 0)$ ($V = 0.2, 0.21$) as depicted by the dashed lines in Fig. 3.1, using the units of Ref. [37]. A soft mixed mode emerges in both cases below the superconducting T_c. For reference, twice the single-particle energy gap, which is determined by $2\min(\Delta, \phi)$, is plotted in the black dashed line. In proximity of a phase transition, the in-gap mode approaches the $2\Delta/2\phi$ Higgs mode of the vanishing order.
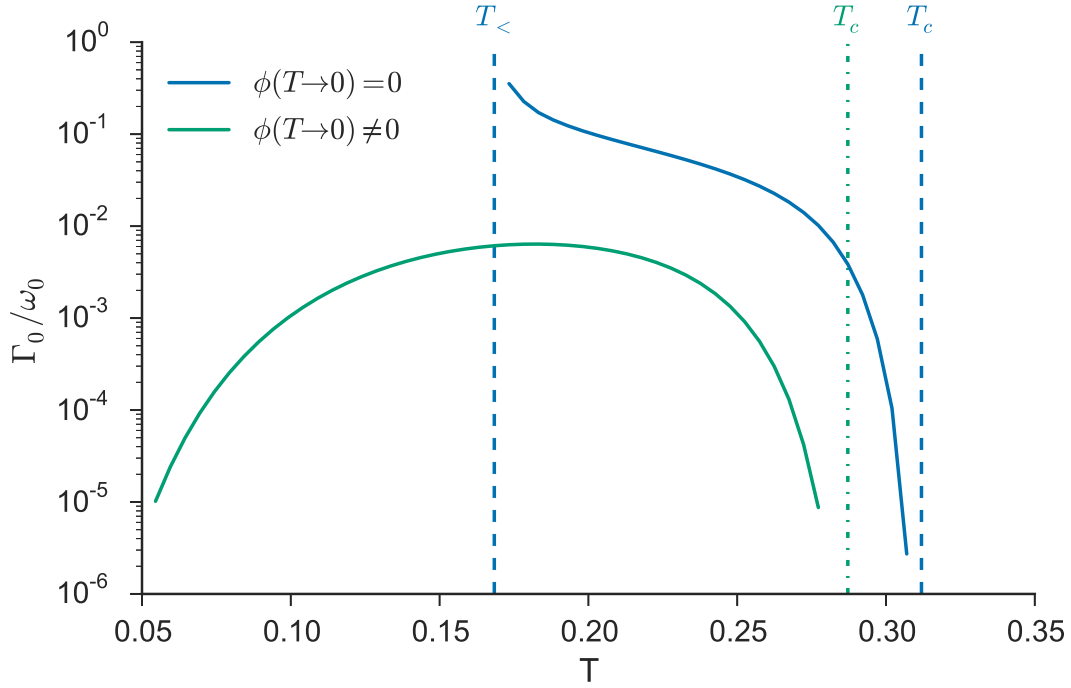
Figure 3.3: Damping rate Γ_0 of the in-gap collective mode in the long wavelength limit for two different values of V corresponding to the two trajectories depicted in Fig. 3.1. Damping is an order of magnitude smaller in the case where $\phi(T \to 0) \neq 0$ (lower line), and is exponentially suppressed at low temperature due a lack of thermally excited quasiparticles. In both cases, the decay rate is strongly suppressed in the vicinity of the superconducting T_c. The transition temperatures are marked for $\phi(T \to 0) = 0$ ($\phi(T \to 0) \neq 0$) by the dashed (dot-dashed) vertical lines. T_c denotes the onset temperature of superconductivity, while $T_<$ indicates the boundary between the coexistent and pure superconductivity phases for the case of the blue curve (c.f. the upper plot of Fig. 3.2).

arbitrarily small frequency (between the two particle/hole bands), giving rise to the damping of collective modes within the gap.

The specific temperature dependence of the damping results from a combination of two effects. Because we are considering energies $\omega_0 < 2\min(\phi, \Delta)$, we see that transitions from a particle to a hole band (or vice versa) cannot contribute as they will always have energy equal or greater than 2Δ. Thus, damping must be solely due to scattering between the hole or particle bands. As ϕ decreases, the two particle (and correspondingly the two hole) bands become more similar (in the limit $\phi \to 0$ they are degenerate), increasing the phase space for low energy transitions

and therefore leading to greater damping of the BDW amplitude mode. This in turn leads to an increased damping of the mixed mode, which is visible in Fig. 3.3. However, in opposition to this effect, as $\phi \to 0$, the matrix element for scattering between these bands will begin to vanish, as it is proportional to ϕ. At some point this second effect will overcome the increase due to the larger phase space, leading to a disappearance of the damping as we approach the critical point at which the charge order disappears.

The competition between scattering elements and band structure generically leads to a non-monotonic temperature dependence of the damping, which in turn means that there exists a region of maximal damping away from which the decay rate remains weak (within the gap). In the case with $\phi(T \to 0) \neq 0$, the BDW order remains sufficiently large that the system never approaches this region of larger damping and thus the decay rate is noticeably smaller than for $\phi(T \to 0) = 0$. In all cases where the mixed phase exists down to $T = 0$, this damping term will be exponentially suppressed at low temperatures as there are no thermally excited quasiparticles available to scatter.

3.3 Damping from nodal quasiparticles

The hot-spot model we have used so far is only defined in the antinodal regions, and thus completely ignores the gapless degrees of freedom existing close to the nodes. These can have a particularly strong effect on the damping of the collective modes by providing a low-energy decay channel. However, the contribution of these quasiparticles is different for the different orders.

We expect the charge order to couple only weakly to the nodal quasiparticles, due to the mismatch between its wavevector (Q, Q) and the wavevector separating the nodes [108] [note that the same argument applies to BDW with $(Q, 0)$ or $(0, Q)$
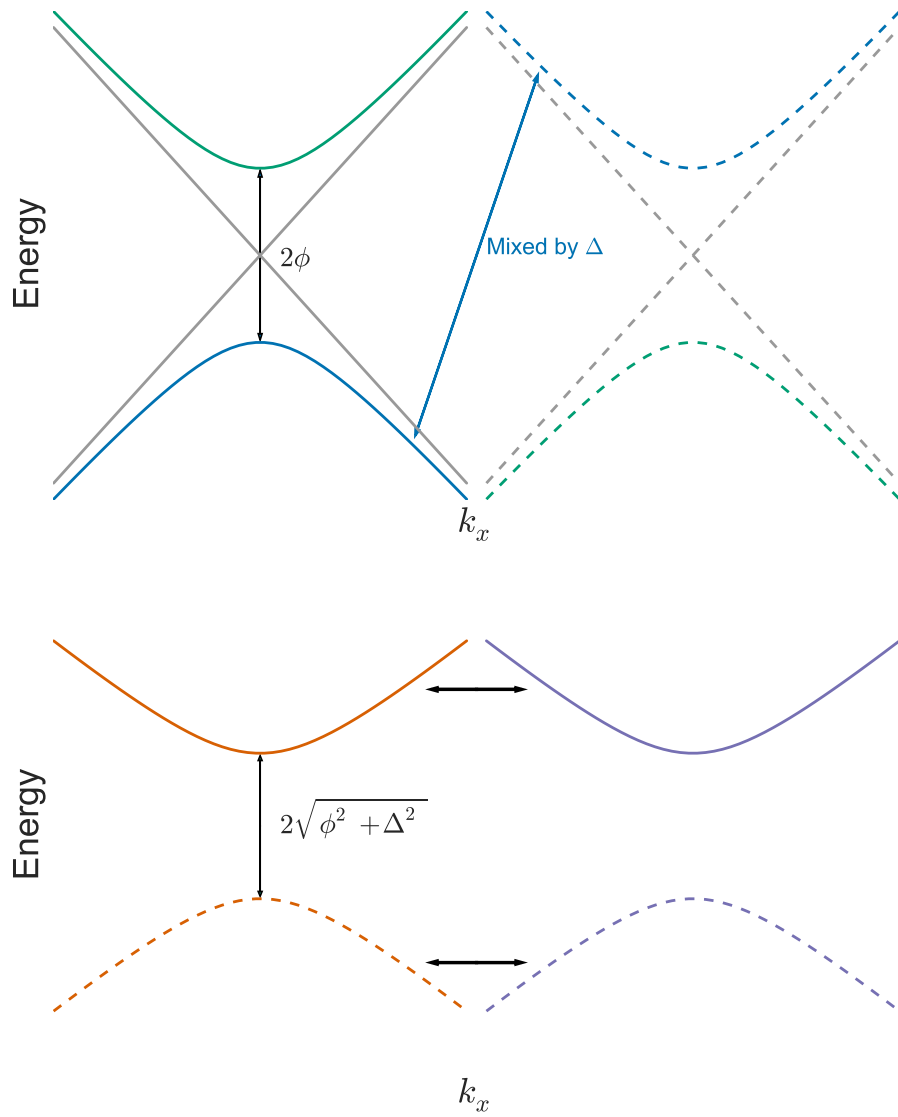
Figure 3.4: Slices of the quasiparticle band structure for $k_y = 0$. Dashed lines indicate the particle hole conjugate of the band of the same color. (a) The normal state (gray) and BDW state (green/blue) dispersions. Only transitions between the two solid/dashed bands contribute to $\mathrm{Im}Q_{\phi\phi}^R$. The onset of superconductivity hybridizes the green/blue bands with their particle-hole conjugates. (b) Bogoliubov band dispersions in the coexistent state. Transitions between all bands may contribute to $\mathrm{Im}Q_{\phi\phi}^R$ leading to damping of the Higgs modes (even for those with mass less than 2Δ.). Processes indicated by horizontal arrows are of particular importance as they occupy a finite phase space for arbitrary frequencies within the gap.

wavevector]. There is no such restriction for the superconductivity, however, and its amplitude fluctuations are unavoidably damped by the nodal excitations.

To include these effects and to study their consequences for the collective modes, we supplement the calculation from the previous section with a phenomenological time-dependent Ginzburg-Landau theory. In addition to the more familiar quadratic and quartic in the order parameters terms, this theory contains also first and second derivatives in (real) time. The time-dependent Ginsburg-Landau equations can be written in the following form:[9]

$$-\frac{\partial^2 \Delta}{\partial t^2} - \gamma_\Delta \frac{\partial \Delta}{\partial t} = \frac{\partial \mathcal{F}_{GL}}{\partial \Delta^*}, \qquad -\frac{\partial^2 \phi}{\partial t^2} - \gamma_\phi \frac{\partial \phi}{\partial t} = \frac{\partial \mathcal{F}_{GL}}{\partial \phi^*}, \qquad (3.19)$$

where the Ginsburg-Landau action is given by:

$$\mathcal{F}_{GL} = \alpha_\phi |\phi|^2 + \alpha_\Delta |\Delta|^2 + \beta_\phi |\phi|^4 + \beta_\Delta |\Delta|^4 + u|\phi|^2 |\Delta|^2.$$

The quadratic coefficients α have the usual linear-in-temperature dependence, whereas β and u (which parametrises the competition between the two orders) are temperature-independent.[10] Note that expressions for the coefficients in $\mathcal{F}_{GL}$ can be straightforwardly derived from the microscopic theory presented in the previous section [110] (spatial derivative terms are not included since we are considering only uniform states). Although the Ginzburg-Landau theory is strictly applicable only close to the critical region, it can be used beyond its region of validity as an effective model for the collective modes of the system. [99] For this reason we keep the second-order time derivative terms, which are usually omitted close to the critical temperature. [111]

---

[9]In general, there is no simple time-dependent extension of Ginzburg-Landau theory, precisely due to the presence of damping, which introduces non-analytic terms (see, for example, I. J. R. Aitchison, G. Metikas, and D. J. Lee, Phys. Rev. B 62, 6638 (2000), and references therein). We circumvent this difficulty by considering only the $q = 0$ limit.

[10]We can also add coupling to the lattice degrees of freedom, by including bi-linear terms like $g_{ep}\phi b$ and $g_\Delta \Delta b$, where b is a phonon mode, and g_{ep} and g_Δ are coupling constants. [109] However, the effects of these couplings appear modest (see Appendix B), so we will not include them.

The coefficients γ_ϕ and γ_Δ are responsible for the damping of the collective modes. It is important to note that despite the symmetric way these terms enter Eq. (3.19), they encode very different physics.

The γ_ϕ term is native to the hot-spot regions. At low energies it is proportional to Δ, since it is only allowed by the band reconstruction (see the discussion in the previous section), whereas above $2\min(\Delta, \phi)$ we can treat it as a constant, originating from the coupling of the fluctuations to the high-energy quasiparticle continuum. In contrast, the main contribution to the γ_Δ term originates from the nodal regions (and thus is completely absent in the hot-spot-only approach of the previous section). Close to T_c we can obtain its temperature dependence from the following qualitative considerations. This term is proportional to the number of available states at the oscillation frequency, given by $\sim \rho(\omega) \tanh(\omega/4T)$. [112] Linearizing the density of states close to the nodes $\rho(\omega) \sim \omega$, and approximating the frequency as $\omega \approx 2\Delta$ we finally get for the damping terms of the slow mode

$$\gamma_\Delta \approx \gamma_\Delta^0 \Delta^2 = \gamma_\Delta^0 (T_c - T), \ \ \gamma_\phi \approx \gamma_\phi^0 \Delta = \gamma_\phi^0 \sqrt{T_c - T}$$

(we have expanded in powers of Δ). Note that we have thus determined the temperature dependence of γ_ϕ and γ_Δ, but their relative strength at some fixed temperature depends on the parameters of the microscopic models (like V), which cannot be estimated within our phenomenological theory. However, given the general temperature dependence of γ_ϕ and γ_Δ, we expect the antinodal particles to dominate damping sufficiently close to T_c (Δ vs. Δ^2), whereas at low temperatures the nodal excitations take over – γ_Δ stays finite for $T \to 0$, while γ_ϕ goes to zero exponentially.

To obtain the frequencies and damping of the mixed modes we expand $\phi(t)$ and $\Delta(t)$ around the mean field values of the order parameters ϕ_0 and Δ_0: $\phi(t) = \phi_0 + \delta\phi(t)$ and $\Delta(t) = \Delta_0 + \delta\Delta(t)$. Assuming that $\delta\phi(t)$ and $\delta\Delta(t)$ are relatively

small we can simplify Eq. (3.19) by keeping only the terms linear in $\delta\phi$ and $\delta\Delta$. Since we are interested in the collective modes we write their time dependence as $e^{-i\omega t}$. Inserting this ansatz in the linearized equations, we can exclude $\delta\phi$ and $\delta\Delta$ altogether, and finally arrive at the following equation for ω:

$$\omega^2 + i\gamma_\phi\omega + 2(\alpha_\phi + u\Delta_0^2) - \frac{(2u\phi_0\Delta_0)^2}{2(\alpha_\Delta + u\phi_0^2) + i\gamma_\Delta\omega + \omega^2} = 0. \qquad (3.20)$$

We solve it numerically (with $\phi_0(T)$ and $\Delta_0(T)$ determined by the time-independent mean-field equations), and obtain both complex and purely imaginary solutions for ω. The former solutions are oscillatory (with $\text{Re}[\omega]$ giving the frequency of the uniform oscillations around the mean field values), while the latter represent exponential decay. We show the real and the imaginary parts of the two ω solutions as a function of temperature in Fig. 3.5. There we plot ω_0 and Γ_0 for two different strengths of γ_Δ^0, as a comparison between small and large contribution from the nodal quasiparticles, respectively. For small γ_Δ^0 we can see that both the real and imaginary parts of the frequency of the hybridized modes show behavior similar to that obtained in the previous section. However, when we increase γ_Δ^0 we see not only enhancement of the damping of both modes, but also decrease of their real frequencies (the top panel of Fig. 3.5). Although the effect is more dramatic for the in-gap mode, which now exists only in a narrow region below T_c, it is significant for the fast one as well. This is a consequence of one important feature of Eq. (3.20) – the coupling of the two channels mixes their real and imaginary parts. Thus, increase of the damping leads to the gradual suppression of the real part of both mixed modes. Note also that the disappearance of ω_0 of the in-gap mode corresponds to a peak in its Γ_0.
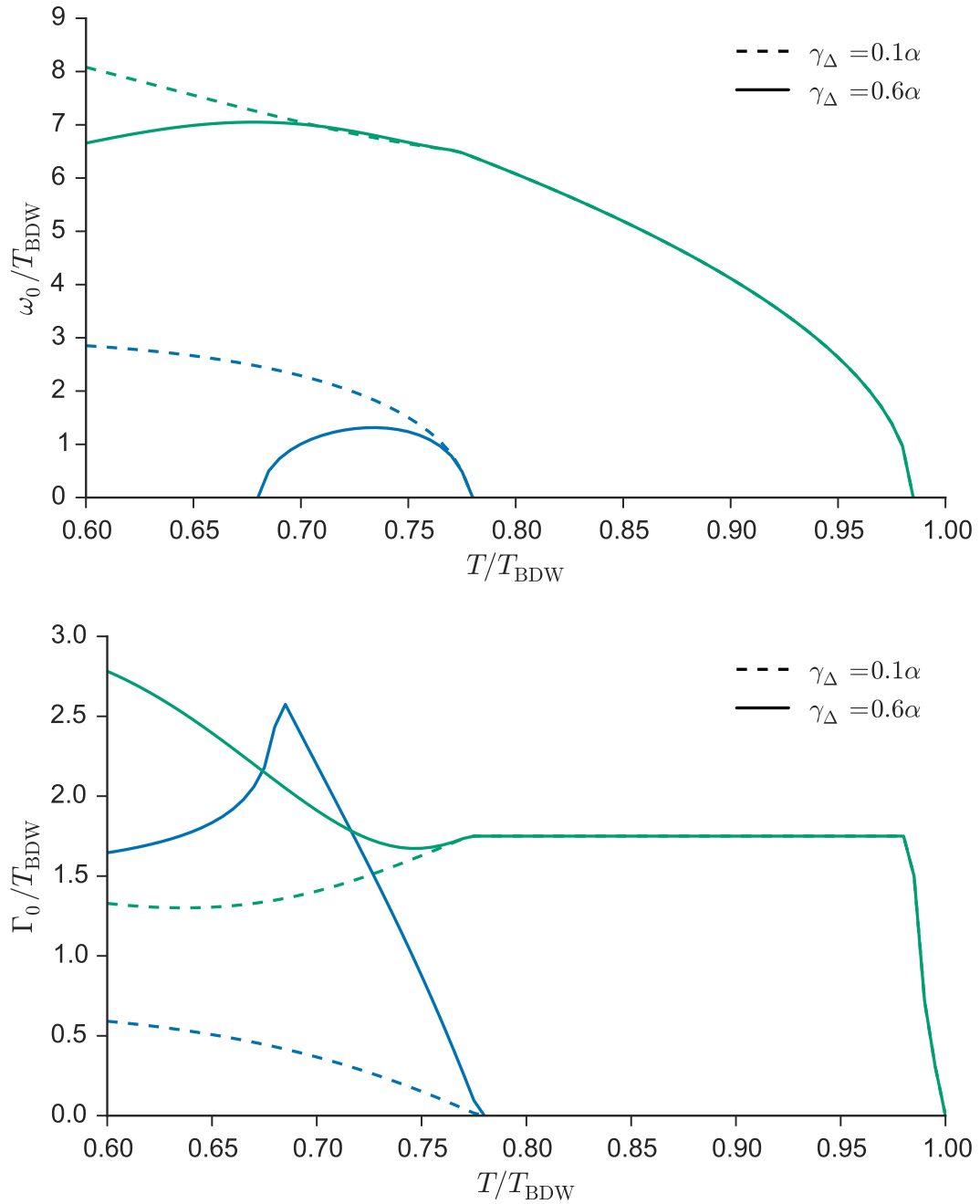
Figure 3.5: The evolution of ω_0 (top panel) and Γ_0 (bottom panel) of the two Higgs modes with temperature. For each mode the cases of weak and strong damping from the nodal regions are shown [$\gamma_\Delta = 0.1\alpha$ (dashed line) and $\gamma_\Delta = 0.6\alpha$ (solid line), respectively]. γ_ϕ, the damping from antinodal region, is the same on both plots.

3.4   Discussion and Conclusion

Note that our calculation is to some extent complementary to those in Refs. [79, 113]. These works studied the dynamics of the system after an external perturbation, and were done in the time domain, thus allowing direct comparison with the experimental data. The temperature dependence of the frequencies extracted in Ref. [113] appears consistent with our calculation, as it shows a low-frequency mode appearing below the superconducting transition.

The experiments [93–95] have not observed a soft mode close to either charge or superconducting transition temperatures. Instead, Refs. [93, 94] identify a single amplitude mode, with intensity that goes down with temperature, but whose frequency stays almost constant, with only a small decrease at the superconducting T_c observed in Ref. [93], and no clear change seen in Ref. [94].[11] In contrast to these, Ref. [95] reported two collective modes at the wavevector corresponding to the charge order, with one of them disappearing close to the superconducting transition (the other – higher-frequency – one follows behavior similar to that observed in Refs. [93, 94]). This seems to be a direct confirmation of the coupling between the charge order and superconductivity, and in agreement with our theory. However, the frequency of this mode remains constant with temperature, without any signs of softening. The absence of softening close to either T_c or T_{BDW} appears incompatible with our calculation, and requires alternative explanations (such as optical phonons). [93]

There remains an important point regarding the experimental signatures of the amplitude modes. Since the superconducting Higgs mode does not directly couple to the electromagnetic field (although it could be detected by indirect methods [114]), the mixing provides a convenient way of observing it. However, it can be easily shown

---

[11]This is consistent with the behavior of the high-energy mode in the case of strong damping from the nodal regions (see section 3.3). This damping could lead to a decrease of the frequency of the fast mode, observed in Ref. [93] (note that a different phenomenological explanation for this decrease, based on time-independent Ginzburg-Landau theory, was given in Ref. [93]).

that the soft mode's coupling to reflectivity is proportional to Δ_0, and is thus small just below the superconducting transition. Combined with the fact that damping from the nodal regions can restrict this mode to a small region in the vicinity of the superconducting transition (as explored in Sec. 3.3), this might explain why some groups [93, 94] have not observed a low-frequency mode at temperatures below the superconducting T_c.

In conclusion, we have studied the collective modes for the BDW and superconducting order parameters expected to exist in the pseudogap state of cuprates. In the pure BDW phase we observed the conventional amplitude mode with frequency starting at 2ϕ. In the coexistent phase two collective modes representing the coupled oscillations of the amplitudes of the order parameters are present. One of them is soft at the superconducting critical temperature, and despite having frequency $\omega_0 < 2\min(\phi, \Delta)$ is (weakly) damped, due to band-structure reconstruction caused by superconductivity. The other mixed mode is continuously connected to the pure BDW mode, with frequency pushed up in the coexisting regime. To study the effects of damping originating from the nodal regions, we developed a phenomenological time-dependent Ginzburg-Landau theory. We demonstrated that strong damping can have significant effect on the real frequency of the modes.

Chapter 4: Cavity Quantum Eliashberg Enhancement of Superconductivity

This work is based on Curtis, Raines, Allocca, Hafezi, and Galitski [115, ©
American Physical Society], published in Physical Review Letters.

4.1 Overview

It has been known since the late 1960's that subjecting a superconductor to strong
microwave radiation can lead to an enhancement of superconductivity [12, 13]. The
explanation of this was first provided by Eliashberg *et. al.* [14, 15, 17], who showed
that the irradiation yields a non-thermal distribution of the Bogoliubov excitations
with an effectively colder band edge. The degree of enhancement can be obtained by
using standard BCS theory with a non-thermal quasi-particle distribution function.
In the subsequent decades, Eliashberg's theoretical explanation for this effect has
been extended and applied to a variety of other systems [19, 56, 85, 116–119].

In recent years there has been a renewed interest in non-equilibrium supercon-
ductivity motivated in-part the pump-probe experiments, discussed in Chapter 2,
which have found that materials subjected to intense Terrahertz (THz) pulses ex-
hibit transient superconducting properties up to very high sample temperatures [22,
26, 120]. Understanding these transient states has led to a variety of theoretical
models which go beyond the quasi-particle redistribution effect [58, 121–125].

All of these systems concern the interaction between quantum matter and a
classical external field. Particularly interesting and novel however, is the effect that
a fluctuating *quantum* gauge field has on quantum matter. Indeed, it has been a
long-standing focus in the field of cavity-quantum-electrodynamics to realize the
dynamical quantum nature of the electromagnetic field through the use of resonant

electromagnetic cavities [126–130]. Recently there have been many advances in this area including the realization of exciton-polariton condensates [131, 132], states formed from hybridizing cavity photons and semiconductor excitons.

This chapter extends some of these concepts to superconducting systems with an eye on cavity-induced Eliashberg-type enhancement of superconductivity. The central observation is that even in a non-equilibrium steady-state the BCS self-consistency equation

$$\frac{1}{g\nu} = \int_0^\infty \frac{d\epsilon}{\epsilon} \rho_{\text{BQP}}(\epsilon) \left[1 - 2n(\epsilon)\right] \tag{4.1}$$

can be solved for a non-thermal quasi-particle distribution function $n(\epsilon)$, where $\rho_{\text{BQP}} = |\epsilon|/\sqrt{\epsilon^2 - \Delta^2}$ is the quasi-particle density of states. The solution of this equation – the BCS superconducting gap Δ – is therefore a functional of the distribution function $n(\epsilon)$ as well as the BCS coupling constant g. Of particular interest are cases where the gap exceeds its equilibrium thermal value, $\delta\Delta = \Delta[n_F + \delta n] - \Delta[n_F] > 0$. In the classical Eliashberg effect, this is achieved via irradiation with a coherent microwave field. For frequencies smaller than 2Δ, pair breaking is suppressed and existing thermal quasi-particles are scattered up to higher energies, where their debilitating effect is lessened by the reduced relative density of states. This emptying of states near the band edge increases Δ above its equilibrium value. In this chapter we generalize this idea to include the dynamical fluctuations of the electromagnetic field in a microwave cavity, depicted in the inset of Fig. 4.1(b). Our main result is that, by appropriately tuning the parameters of the cavity environment (e.g. resonance, line-width, temperature, etc), an enhancement in the BCS gap strength may be obtained, now in the absence of coherent electromagnetic radiation. This gap enhancement is shown in Fig. 4.1(a), which illustrates the change in the BCS gap strength $\delta\Delta$ as a function of the cavity resonant frequency ω_0. The rest of the
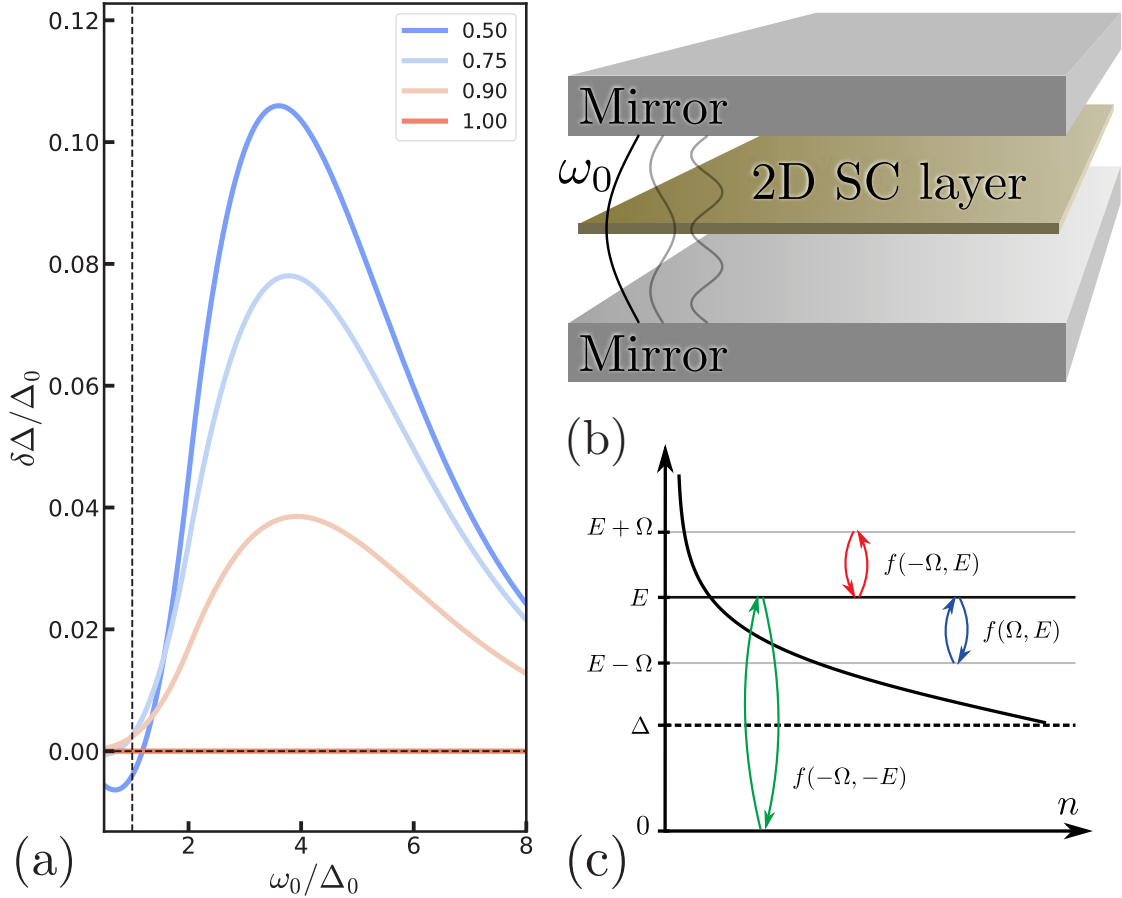
Figure 4.1: (a) Relative enhancement of the gap function as a function of cavity frequency ω_0 for a particular value of the overall scaling constant $\pi \alpha X D \tau_{\mathrm{in}}/c^2$ (we take $X = 133$ and $\pi \alpha D \tau_{\mathrm{in}} T_c^2/c^2 = 9.17 \times 10^{-5}$ with T_c set to unity). Curves are colored and labeled according to the ratio $T_{\mathrm{cav}}/T_{\mathrm{qp}}$, comparing the photon and quasi-particle temperatures. The enhancement is seen set in after the cavity frequency surpasses the pair-breaking energy $2\Delta_0$. (b) Schematic picture of the system used for calculation. The lowest cavity resonator mode with cutoff frequency ω_0 is shown. (c) Depiction of the various processes which contribute to the quasi-particle collision integral, plotted against the equilibrium $n(E)$. The blue arrows depict the down-scattering terms captured by $f(\Omega, E)$, the red arrows depict the up-scattering terms captured by $f(-\Omega, E)$ and the green arrows represent the pair-processes captured by $f(-\Omega, -E)$, where f is defined in Eq. (4.34).

chapter is devoted to deriving this result.

4.2 Types of Processes

In order to better understand the types of processes that occur when coupling a superconductor to cavity photons, we begin with a model of an s-wave superconductor described by the BCS Hamiltonian (setting $\hbar = k_B = 1$)

$$H = \int d^2 r \left[\psi_\sigma^\dagger \left(-\frac{\mathbf{D}^2}{2m} - \mu \right) \psi_\sigma - g \psi_\uparrow^\dagger \psi_\downarrow^\dagger \psi_\downarrow \psi_\uparrow \right], \qquad (4.2)$$

where ψ_σ is the electron field operator, which is minimally coupled to the electromagnetic vector potential $\mathbf{A}$ through the gauge covariant derivative $\mathbf{D} = \boldsymbol{\nabla} - i(e/c)\mathbf{A}$. Throughout we will employ the radiation gauge $\nabla \cdot \mathbf{A} = 0$. The interaction is decoupled via standard mean-field theory, and the resulting Hamiltonian is diagonalized with a Bogoliubov transformation

$$\begin{pmatrix} \psi_{\mathbf{p},\uparrow} \\ \psi_{-\mathbf{p},\downarrow}^\dagger \end{pmatrix} = \begin{pmatrix} u_{\mathbf{p}} & -v_{\mathbf{p}} \\ v_{\mathbf{p}} & u_{\mathbf{p}} \end{pmatrix} \begin{pmatrix} \gamma_{\mathbf{p},+} \\ \gamma_{-\mathbf{p},-}^\dagger \end{pmatrix}, \quad u,v = \sqrt{\frac{1}{2}\left(1 \pm \frac{\xi}{E}\right)}, \qquad (4.3)$$

where $\gamma_{\mathbf{p}\pm}$ are the Bogoliubov quasi-particle annihilation operators, $E_{\mathbf{p}} = \sqrt{\xi_{\mathbf{p}}^2 + \Delta^2}$ is the quasi-particle dispersion, and $\xi_{\mathbf{p}} = \mathbf{p}^2/2m - \mu$. The electromagnetic field $\mathbf{A}$ is subject to cavity quantization of the transverse-momentum, leading to a dispersion relation for in-plane momentum $\mathbf{q}$ of

$$\omega_{n,\mathbf{q}} = \sqrt{\left(\frac{n\pi c}{L}\right)^2 + c^2 \mathbf{q}^2} \equiv \sqrt{n^2 \omega_0^2 + c^2 \mathbf{q}^2} \qquad (4.4)$$

where $n = 1, 2, 3, \ldots$ indexes the harmonic of the confined mode. For simplicity, we will only consider the fundamental $n = 1$ harmonic and place the superconducting

sample at the anti-node where the coupling to the field is strongest, as depicted in Fig. 4.1(b).

To leading order, the interaction between photons and quasi-particles obtained from Eq. (4.2) occurs through the coupling of the vector potential to the electronic current via

$$H^{\text{int}} = -\frac{e}{c} \int d^d r \mathbf{j} \cdot \mathbf{A}. \tag{4.5}$$

Applying the Bogoliubov transformation and Fourier transforming to momentum space this becomes

$$\mathbf{j_q} = \int \frac{\mathrm{d}p}{(2\pi)^2} \frac{\mathbf{p}}{m} \left[\left(u_{\mathbf{p}_-} u_{\mathbf{p}_+} + v_{\mathbf{p}_-} v_{\mathbf{p}_+} \right) \gamma^{\dagger}_{\mathbf{p}_-,\sigma} \gamma_{\mathbf{p}_+,\sigma} \right.$$
$$\left. + \left(u_{\mathbf{p}_-} v_{\mathbf{p}_+} - v_{\mathbf{p}_-} u_{\mathbf{p}_+} \right) \left(\gamma^{\dagger}_{\mathbf{p}_-,+} \gamma^{\dagger}_{-\mathbf{p}_+,-} - \gamma_{\mathbf{p}_+,+} \gamma_{-(\mathbf{p}_-,-)} \right) \right], \tag{4.6}$$

where we use the shorthand $\mathbf{p}_{\pm} = \mathbf{p} \pm \mathbf{q}/2$. There are three types of matrix element appearing in Eq. (4.6), corresponding to scattering (by both emission and absorption of photons), pair-breaking, and pair-recombination respectively. Through these processes, the fluctuating cavity photon field will induce transitions amongst the quasi-particle eigenstates, resulting in a redistribution of the quasi-particle occupations. This is described by a kinetic equation

$$\frac{\partial n_{\mathbf{p}}}{\partial t} = \mathcal{I}_{\text{cav}}[n] - \frac{n_{\mathbf{p}} - n_F \left(E_{\mathbf{p}}, T_{\text{qp}} \right)}{\tau_{\text{in}}}. \tag{4.7}$$

The first term on the right hand side describes the photon-induced pairing/de-pairing and scattering of quasi-particles while the second term describes a generic inelastic relaxation mechanism which describes the coupling to a phonon bath at temperature T_{qp}. The approximation here is that the inelastic relaxation rate τ_{in}^{-1} is small compared to other energy scales, as was assumed in the original work of Eliashberg [15, 116, 117].

In this limit we can perturbatively solve for the steady-state of the kinetic equation Eq. (4.7) by expanding in small deviations $\delta n = n - n_F$ from equilibrium. To lowest order, the correction is $\delta n = \tau_{\rm in} \mathcal{J}_{\rm cav}[n_F]$. Utilizing the detailed balance properties of thermal equilibrium, this will end up depending on the photon occupation function $N(\omega)$ through its deviation from equilibrium:

$$\delta N_{\rm cav}(\omega) \equiv N(\omega) - n_B\left(\omega, T_{\rm qp}\right), \tag{4.8}$$

where $n_B(z)$ is the Bose occupation function.

4.3   Cavity Enhancement of Superconductivity

To derive the correction to the distribution function we employ the KNLσM of a disordered superconductor as introduced in Section 1.4.1.[1]   We begin with Eq. (1.32) which we briefly recap here

$$iS = -\frac{\pi\nu}{8}\,{\rm Tr}\left[D\left(\partial\check{Q}\right)^2 + 4i\left(i\hat{\tau}_3\partial_t\check{Q} + i\frac{\gamma}{2}\check{Q}_{\rm rel}\check{Q} + \check{\Delta}\check{Q}\right)\right] - i\frac{\nu}{2\lambda}\,{\rm Tr}\,\check{\Delta}^\dagger\hat{\gamma}^q\check{\Delta} \tag{4.9}$$

where $D = v_F\tau_{\rm imp}^2/2$ is the diffusion constant, $\nu = \nu_\uparrow + \nu_\downarrow$ is the total electronic density of states at the Fermi surface, λ is the strength of the BCS type coupling, and $\mathbf{A}$ couples to the model through the covariant derivative $\partial\check{X} = \nabla\check{X} - i(e/c)[\check{\mathbf{A}}, \check{X}]$. The variables of the model are the vector potential $\mathbf{A}$, the BCS gap Δ, and the quasi-classical Green's function $\check{Q}$ which obeys the non-linear constraint $\check{Q}\circ\check{Q} = \check{1}$. The relaxation approximation is included through coupling to a bath

$$\check{Q}_{\rm rel}(\epsilon) = \begin{pmatrix} 1 & 2\tanh\left(\frac{\epsilon}{2T_{\rm QP}}\right) \\ 0 & -1 \end{pmatrix}_K \tag{4.10}$$

[1]The results obtained below can be found through general, although non-rigorous arguments using the Boltzmann equation and Fermi's Golden rule. For more details see Curtis, Raines, Allocca, Hafezi, and Galitski [115].

via $\gamma = 1/\tau_{\text{in}}$ is the inelastic scattering rate.

Our general strategy follows that employed by Tikhonov, Skvortsov, and Klapwijk [19]. We recall that the BCS gap equation is the saddle-point of iS with respect to the quantum component of the gap Δ_q (c.f. Section 1.4.1). We may thus directly obtain the correction due to cavity photons by deriving the linear-in-Δ_q term arising from the coupling to photons.

To begin, we employ the exponential parameterization Eq. (1.36) to expand Eq. (1.32) to quadratic order in the diffuson and cooperon fields as described in Section 1.4.1 leading to the quadratic diffusive action Eq. (1.39), which we repeat here for reference

$$iS_{cd} = \frac{\pi\nu}{4} \int \frac{d\epsilon}{2\pi} \int \frac{d\epsilon'}{2\pi} \, \text{tr} \left[\vec{d}_{\epsilon'\epsilon} \hat{\mathcal{D}}^{-1}_{\epsilon\epsilon'} \vec{d}_{\epsilon\epsilon'} + \vec{c}_{\epsilon'\epsilon} \hat{\mathcal{C}}^{-1}_{\epsilon\epsilon'} \vec{c}_{\epsilon\epsilon'} \right] \tag{4.11}$$

with

$$\hat{\mathcal{D}}^{-1}_{\epsilon\epsilon'} = \mathcal{D}^{-1}_{\epsilon'\epsilon} \sigma_1, \qquad \hat{\mathcal{C}}^{-1}_{\epsilon\epsilon'} = \text{diag} \left([\mathcal{C}^R_{\epsilon\epsilon'}]^{-1}, [\mathcal{C}^A_{\epsilon\epsilon'}]^{-1} \right), \tag{4.12}$$

and the diffuson and cooperon propagators

$$\mathcal{D}^{-1}_{\epsilon\epsilon'} = \mathcal{E}^R(\epsilon) + \mathcal{E}^A(\epsilon'), \qquad [\mathcal{C}^{R/A}]^{-1}_{\epsilon\epsilon'} = \mathcal{E}^{R/A}(\epsilon) + \mathcal{E}^{R/A}(\epsilon')$$

$$\mathcal{E}^R(\epsilon) = i \left(\epsilon + i\frac{\gamma}{2} \right) \cosh\theta_\epsilon - i\Delta \sinh\theta_\epsilon \tag{4.13}$$

$$\mathcal{E}^A(\epsilon) = \left(\mathcal{E}^R(\epsilon) \right)^*.$$

Additionally, at linear order we have a coupling between diffusive modes and the gap

$$iS_{\Delta-cd} = \pi\nu \int \frac{d\epsilon}{2\pi} \left[\vec{c}_{\epsilon\epsilon} \cdot \vec{s}^c_\epsilon + \vec{d}_{\epsilon\epsilon} \hat{\sigma}_1 \vec{s}^d_\epsilon \right] \tag{4.14}$$

where we have taken Δ_q to be homogeneous and real, and a coupling of the diffusons and cooperons to the photon field

$$iS_{A-cd} = \pi\nu D \int \frac{d\omega}{2\pi} \mathbf{A}^{\alpha}_{-\omega,-\mathbf{q}} \cdot \mathbf{A}^{\beta}_{\omega,\mathbf{q}} \int \frac{d\epsilon}{2\pi} \int \frac{d\mathbf{q}}{(2\pi)^2} \left[\vec{c}_{\epsilon\epsilon} \cdot \vec{r}^{\,c;\alpha\beta}_{\epsilon} + \vec{d}_{\epsilon\epsilon} \hat{\sigma}_1 \vec{r}^{\,d;\alpha\beta}_{\epsilon} \right] \quad (4.15)$$

where for now we have absorbed the paramagnetic coupling strength into the definition of the $\mathbf{A}$ field. We will restore it at the end of the calculation.

The $\vec{r}^{\,i;\alpha\beta}$ are matrices in the photon Keldysh space and vectors in the sense induced by Eq. (1.40). They are determined by the structure of the saddle-point solution and arise from expanding to covariant derivative term in Eq. (1.32) to lowest order in the W matrix fields.

The coupling to the diffusive modes may be removed by making a shift of the fields

$$\vec{c}_{\epsilon\epsilon} \to \vec{c}_{\epsilon\epsilon} - 2\Delta^q \hat{\mathcal{C}}_{\epsilon\epsilon} \vec{s}^{\,c}_{\epsilon} - 2D \int \frac{d\omega}{2\pi} \int \frac{d\mathbf{q}}{(2\pi)^2} \mathbf{A}^{\alpha}_{-\omega,-\mathbf{q}} \mathbf{A}^{\beta}_{\omega,\mathbf{q}} \hat{\mathcal{C}}_{\epsilon\epsilon} \vec{r}^{\,c;\alpha\beta}_{\epsilon} \quad (4.16)$$

$$\vec{d}_{\epsilon\epsilon} \to \vec{d}_{\epsilon\epsilon} - 2\Delta^q \hat{\mathcal{D}}_{\epsilon\epsilon} \hat{\sigma}_1 \vec{s}^{\,d}_{\epsilon} - 2D \int \frac{d\omega}{2\pi} \int \frac{d\mathbf{q}}{(2\pi)^2} \mathbf{A}^{\alpha}_{-\omega,-\mathbf{q}} \mathbf{A}^{\beta}_{\omega,\mathbf{q}} \hat{\mathcal{D}}_{\epsilon\epsilon} \hat{\sigma}_1 \vec{r}^{\,d;\alpha\beta}_{\epsilon}. \quad (4.17)$$

This shift has three effects: The first two are to create a nonlinear term in the photon action, which we will ignore as we are not considering non-linear effects, and to create a term at second order in Δ_q which we can ignore as Δ_q will be taken to 0 at the end. The important effect is that a coupling between photons and Δ_q is induced

$$iS_{\Delta-A} = 2\pi\nu D\Delta^q \int \frac{d\omega}{2\pi} \int \frac{d\mathbf{q}}{(2\pi)^2} \mathbf{A}^{\alpha}_{-\omega,-\mathbf{q}} \cdot \mathbf{A}^{\beta}_{\omega,\mathbf{q}} \int \frac{d\epsilon}{2\pi} \left[\vec{s}^{\,c}_{\epsilon} \hat{\mathcal{C}}_{\epsilon\epsilon} \vec{r}^{\,c;\alpha\beta}_{\epsilon} + \vec{s}^{\,d}_{\epsilon} \hat{\sigma}_1 \hat{\mathcal{D}}_{\epsilon\epsilon} \hat{\sigma}_1 \vec{r}^{\,d;\alpha\beta}_{\epsilon} \right].$$
$$(4.18)$$

At this point we may safely integrate out the d modes and henceforth ignore them.[2] Making the definition

$$-i\Pi^{\alpha\beta} = 2\pi\nu D\Delta^q \int \frac{d\epsilon}{2\pi} \left[\vec{s}^c_\epsilon \hat{\mathcal{C}}_{\epsilon\epsilon} \vec{r}^{c;\alpha\beta}_\epsilon + \vec{s}^d_\epsilon \hat{\mathcal{D}}_{\epsilon\epsilon} \vec{r}^{d;\alpha\beta}_\epsilon \right] \tag{4.19}$$

we can write the photon action as

$$iS_A = i \int \frac{d\omega}{2\pi} \int \frac{d\mathbf{q}}{(2\pi)^2} \mathbf{A}^\alpha_{-\omega,-\mathbf{q}} \left(\check{S}^{-1}_0(\omega,\mathbf{q}) - \check{\Pi}(\omega,\mathbf{q}) \right) \mathbf{A}^\beta_{\omega,\mathbf{q}}. \tag{4.20}$$

Integrating out $\mathbf{A}$ we obtain

$$iS = -\frac{1}{2} \operatorname{Tr} \ln \left[-i \left(\check{S}^{-1}_0 - \check{\Pi} \right) \right] \approx \frac{1}{2} \operatorname{Tr} \left[\check{S}_0 \check{\Pi} \right] \tag{4.21}$$

where we have expanded to linear order in Δ_q. Since the momentum $\mathbf{q}$ appears only in $\check{S}$ we can immediately integrate over it. Similarly we can trace over the in-plane components of A. We thus define

$$\hat{D}(\omega) = \sum_{i\in\{x,y\}} \int \frac{d\mathbf{q}}{(2\pi)^2} \hat{S}^{ii}(\omega,\mathbf{q}). \tag{4.22}$$

We assume the photon modes to be governed by a density matrix which is diagonal in energy. $\hat{D}$ can then be written in the usual fluctuation-dissipation form

$$\hat{D}(\omega) = \begin{pmatrix} F_B(\omega)(D^R(\omega) - D^A(\omega)) & D^R(\omega) \\ D^A(\omega) & 0 \end{pmatrix} \tag{4.23}$$

where F_B is the generalized occupation function, related to the Bose occupation function by $F_B = 1 + 2N$. Defining $-2\pi i J(\omega) = D^R(\omega) - D^A(\omega)$ and, using the

---

[2]We are free to ignore the residual coupling to Δ as the saddle-point equation guarantees that it vanishes.

analytic properties of $\hat{D}$, Eq. (4.21) can be written

$$iS = -\frac{i}{2} \int d\omega J(\omega) \left[F_B(\omega)\Pi_{0,0}(\omega) - (\Pi^R(\omega) - \Pi^A(\omega)) \right] \qquad (4.24)$$

where we have defined $\Pi^{R/A}$ as the retarded/advanced part of $\Pi^{01/10}$. We now decompose the self-energy into rescaled cooperon and diffuson terms $P^{(c/d)}$

$$\nu\Delta^q \left(P^c_{\alpha\beta}(\omega) + P^d_{\alpha\beta}(\omega) \right) = -i\Pi^{\alpha\beta} \qquad (4.25)$$

$$B(\omega) = \frac{P^d_R(\omega) - P^d_A(\omega)}{P^d_0(\omega)} \qquad (4.26)$$

with $P^0 = P_{00}$ and $P^{R/A}$ defined analogously to $\Pi^{R/A}$ as the retarded (advanced) part of $P^{01/10}$. The correction to the gap equation can then be separated into two contributions. The first is the equilibrium self-energy correction to the cavity photons

$$iS^c_{\mathrm{eq}} = \frac{\nu\Delta^q}{2} \int d\omega J(\omega) \left[B(\omega)P^c_0(\omega) - (P^c_R(\omega) - P^c_A(\omega)) \right]. \qquad (4.27)$$

This term should be included in the bare equilibrium result as it is a property of the equilibrium cavity-superconductor system and we therefore subtract it off henceforth. The other term

$$iS_{\mathrm{fluc}} = \frac{\nu\Delta^q}{2} \int d\omega J(\omega)(F_B(\omega) - B(\omega))(P^c_0(\omega) + P^d_0(\omega)) \qquad (4.28)$$

is the fluctuation induced enhancement to superconductivity. This is to be compared with the correction term due to a classical monochromatic field (i.e. the original Eliashberg effect)

$$iS = (-i\Pi_{0,0}(\omega) - i\Pi_{0,0}(-\omega))|\mathbf{A}_\omega|^2 = \nu\Delta^q(P_0(\omega) + P_0(-\omega))|\mathbf{A}_\omega|^2 \equiv \nu\Delta^q Y(\omega)|\mathbf{A}_\omega|^2. \qquad (4.29)$$

Using the functional dependence of the classical Eliashberg effect on frequency $Y(\omega)$ the quantum Eliashberg effect can be written in a fluctuation-dissipation-like form

$$iS_{\text{fluc}} = \frac{\nu \Delta^q}{2} \int_0^\infty d\omega J(\omega)(F_B(\omega) - B(\omega))Y(\omega). \tag{4.30}$$

It should be noted that in the linearized regime P_0^d goes as γ^{-1} while P_0^c goes as γ^0. Thus, in the limit of $\gamma \to 0$ we expect the diffuson contribution to be dominant.

4.3.1 Gap Equation

As mentioned previously, the BCS gap equation is the saddle-point equation of our action with respect to the source field Δ_q. Including the correction term Eq. (4.30) the gap equation then becomes

$$0 = \left. \frac{\delta iS}{\delta \Delta_q} \right|_{\Delta_q=0} = -4i\frac{\nu}{\lambda}\Delta + \frac{\pi\nu}{2}\operatorname{Tr}\hat{Q}^K\hat{\tau}_2 + \frac{\nu}{2}\int_0^\infty d\omega J(\omega)(F_B(\omega) - B(\omega))Y(\omega) \tag{4.31}$$

We therefore define

$$F_{\text{BCS}} = \frac{1}{\lambda} + \frac{i\pi}{8\Delta}\operatorname{Tr}\hat{Q}^K\hat{\tau}_2, \qquad F_{\text{phot}} = \frac{i\nu}{8\Delta}\int_0^\infty d\omega J(\omega)(F_B(\omega) - B(\omega))Y(\omega) \tag{4.32}$$

Which allows us to write the gap equation as $F_{\text{BCS}} = -F_{\text{phot}}$. Furthermore, F_{phot} can be broken up into a kinetic contribution F^{kin} arising from modification of the quasiparticle occupation function and a spectral contribution F^{spec} due to modification of the density of states from self-energy effects, as discussed above. Most notably, because the gap equation is linearly related to the action, the corrections to the gap equation are related to the conventional Eliashberg effect via the same fluctuation-dissipation-like relation.

4.4 Corrections to the distribution function

Using the correspondence in Eq. (4.30) we find that the correction to the distribution function is

$$\delta n(E) = \tau_{\text{in}} \frac{\alpha D}{c} \int_{-\infty}^{\infty} d\Omega J_{\text{cav}}(\Omega) \delta N_{\text{cav}}(\Omega) K(\Omega, E), \qquad (4.33)$$

where δN_{cav} is as in Eq. (4.8) and $K(\Omega, E) = f(\Omega, E) + f(-\Omega, E) - f(-\Omega, -E)$, with

$$f(\Omega, \epsilon) = \Theta(\epsilon - \Omega - \Delta)\rho_{\text{BQP}}(\epsilon - \Omega)\left(1 + \frac{\Delta^2}{\epsilon(\epsilon - \Omega)}\right)\left[n_F\left(\epsilon - \Omega, T_{\text{qp}}\right) - n_F\left(\epsilon, T_{\text{qp}}\right)\right]. \qquad (4.34)$$

Here $\Theta(x)$ is the Heaviside function. The three f terms appearing in $K(\Omega, E)$ are depicted schematically in Fig. 4.1(c), alongside the various processes they describe. The coupling to the cavity is effectively characterized by the coupling function $J(\Omega)$. In particular, the derivation above is valid for any photonic spectral function and generalized occupation.

For a BCS gap of order $\Delta = 10\,\text{K}$ we find a corresponding resonance frequency $\omega_0 \sim 1.3\,\text{THz}$. Recently, a number of advances have lead to large enhancements in the strength and tunability of the light-matter coupling strength in this frequency regime, such that $J_{\text{cav}}(\Omega)$ may potentially exceed what is expected from our simple planar cavity model by many orders of magnitude [133–136]. We incorporate this fact by rescaling the spectral function J by a phenomenological factor X, so that $J(\Omega) \to \tilde{J}(\Omega) = X J_{\text{cav}}(\Omega)$.

In order to simplify the calculation, we will study the system in the Ginzburg-Landau (GL) regime $(T_{\text{qp}} \lesssim T_c)$, which allows us to expand the gap equation in powers of Δ. Including the non-equilibrium distribution function contribution, this
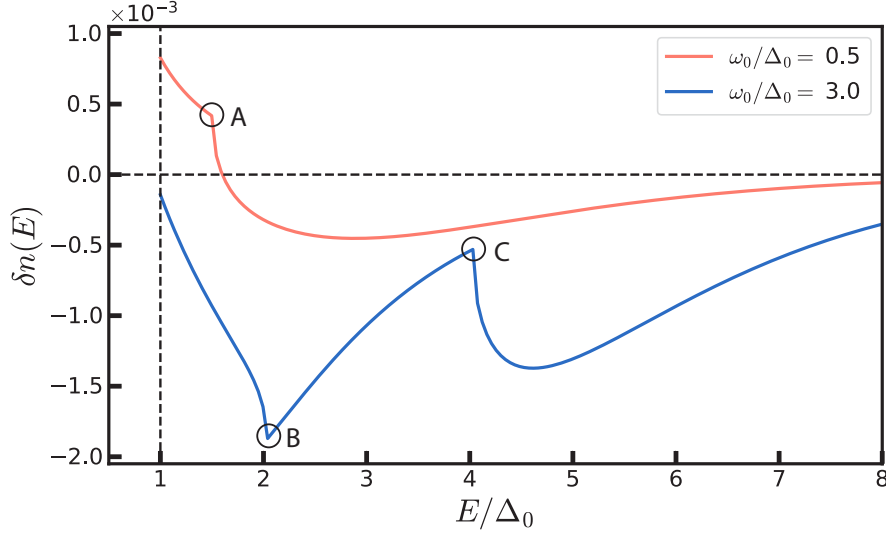
Figure 4.2: Change in quasi-particle distribution function due to cavity photons. The two curves are at the same temperature $(T_{\text{cav}}/T_{\text{qp}} = 0.5)$ but different cavity frequencies ω_0/Δ_0. For low cavity frequency (orange), the gap Δ is diminished due to an accumulation of cooler quasi-particles near the gap-edge, due to a down-scattering of particles. For higher cavity frequency (blue), the recombination processes are more dominant and lead to a net reduction in quasi-particles, enhancing the gap Δ. The kink-features labeled A and C reflect the onset of the term $f(\Omega, E)$ in Eq. (4.33), which is only non-zero for $E > \omega_0 + \Delta_0$. At higher cavity frequencies $(\omega_0 > 2\Delta_0)$ an additional kink-feature (located at B) emerges at $E = \omega_0 - \Delta_0$. For $E < \omega_0 - \Delta_0$, the term $f(-\Omega, E)$ (which represents the pair-processes) contributes over the entire integration region of $\Omega > \omega_0$, while for $E > \omega_0 - \Delta_0$ the integral only captures some of the frequencies where this term contributes.

results in

$$\left(\frac{T_c - T_{\mathrm{qp}}}{T_c} - \frac{7\zeta(3)}{8\pi^2} \frac{\Delta^2}{T_c^2} - 2 \int_\Delta^\infty \frac{d\epsilon}{\epsilon} \rho_{\mathrm{BQP}}(\epsilon)\delta n(\epsilon) \right) \Delta = 0. \qquad (4.35)$$

To leading order in the gap change, we obtain the correction to the BCS gap

$$\frac{\delta\Delta}{\Delta_0} = -\frac{T_c}{T_c - T_{\mathrm{qp}}} \int_{\Delta_0}^\infty \frac{d\epsilon}{\epsilon} \rho_{\mathrm{BQP}}(\epsilon)\delta n(\epsilon). \qquad (4.36)$$

This is plotted in Fig. 4.1(a) as a function of the cavity frequency ω_0 for different photon temperatures relative to the quasi-particle temperature T_{qp}. The enhancement is ultimately driven by the enhanced quasi-particle recombination rate which, for a cold photon reservoir serves to remove detrimental quasi-particles.

This can be seen explicitly in Fig. 4.2, which shows the change in the distribution function δn for two different cavity frequencies. When the cavity frequency is too low, scattering-processes dominate and the photons cool the existing quasi-particles, leading to a build-up of particles near the gap edge. At higher cavity frequencies the pair-processes dominate, leading to an enhancement as photons now cool the system by reducing the total number of harmful quasi-particles.

While the effect we predict here essentially relies on the cooling ability of the cold photon reservoir, we also remark that our formula for $\delta n(E)$, presented in Eq. (4.33), is valid for a wide-variety of photon spectral functions. In particular, switching from a multi-mode planar cavity, where $J_{\mathrm{cav}}(\Omega) \sim \omega_0(1 + \omega_0^2/\Omega^2)\Theta(\Omega - \omega_0)$ is roughly constant for $\Omega > \omega_0$, to a simpler single-mode cavity, where $J_{\mathrm{cav}} \sim \omega_0^2 \frac{2\kappa}{(\Omega-\omega_0)^2+\kappa^2}$ is peaked at the resonant frequency, will allow for an enhancement in $\delta\Delta$ even when the photon reservoir is hotter than the sample.[3] This is explicitly demonstrated in Fig. 4.3, where we plot $\delta\Delta$ against ω_0 for the case of a single-mode $J_{\mathrm{cav}}(\Omega)$. The

---

[3]Calculation of the coupling function for the planar and single-mode cavities are performed in Appendix C.

enhancement in $\delta\Delta$ due to hot photons is now qualitatively similar to the classical Eliashberg effect, albeit with a narrow spectral broadening applied to the driving and supplied power related to the energy density of the bath. For cold photons, the enhancement is similar to that seen in the multi-mode system and results from the photons cooling the sample via enhanced quasi-particle recombination.
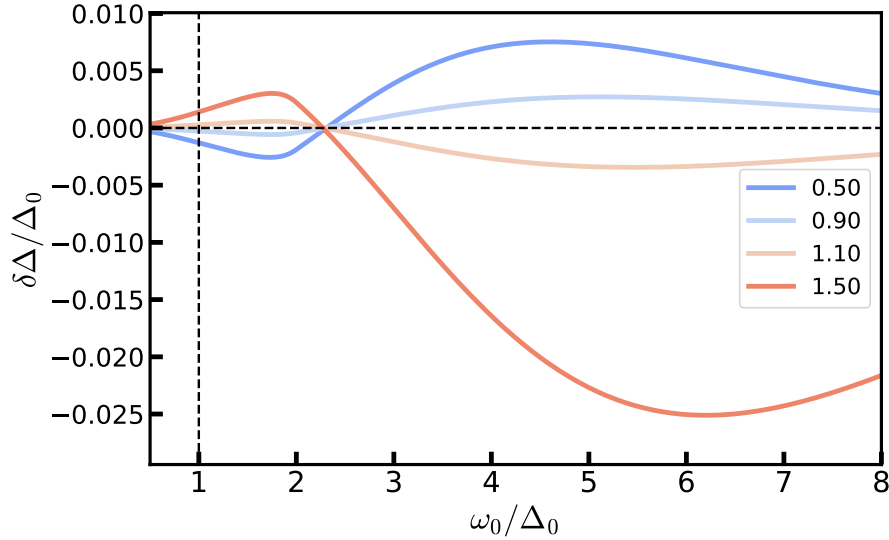
Figure 4.3: Gap enhancement $\delta\Delta_0$ for a single-mode cavity, for both cold and hot photons. The y-axis is determined by the overall scale $4\pi\alpha D\tau_{\text{in}}T_c^2/((\pi\sqrt{3})^3 c^2)X$; with the same values chosen for X and $\tau_{\text{in}},\tau_{\text{el}},v_F/c$ as in Fig. 4.1. Curves are colored and labeled according to the ratio $T_{\text{cav}}/T_{\text{qp}}$, comparing the photon and quasi-particle temperatures. Here the cavity width is held fixed at $1/2\tau_{\text{cav}} = 10\omega_0$.

4.5 Conclusion

In conclusion, we have generalized the classical Eliashberg effect to include both quantum and thermal fluctuations, as realized by a thermal microwave resonator cavity. In the appropriate parameter regime, we show that the photonic reservoir can be used to drive the quasi-particles into a non-equilibrium state which enhances the superconducting gap Δ. In our calculation, we assumed that the cavity relaxation rate τ_{cav}^{-1} was fast, allowing us to essentially ignore the dynamics and kinetics of

the photons themselves. We should not expect this to remain the case when we go to the limit of a high-quality cavity, in which the relaxation rate τ_{cav}^{-1} is no longer small compared to all the other energy scales in the problem. In the high-quality limit, a more elaborate treatment which treats the joint evolution of fermion-photon system is required. Though potentially much more complicated, the inclusion of photons as a participating dynamical degree of freedom may unveil many new and interesting phenomena. These range from the formation of new collective modes (including polaritons) [137, 138], superradiant phases [128, 139], and potentially photon-mediated superconductivity [140]. The prospect of exploring the full breadth of these joint matter-gauge systems is an exciting development in the fields of quantum optics and condensed matter physics.

Chapter 5: Cavity Superconductor-Polaritons

This chapter is based upon Allocca, Raines, Curtis, and Galitski [138, © American Physical Society] and Raines, Allocca, and Galitski [141].

5.1 Overview

A prototypical example of strong light-matter coupling is the exciton-polariton [38], a superposition of photon states and exciton states in condensed matter systems [43]. These objects have drawn much attention due to their experimentally observed Bose condensation at temperatures up to and above room temperature [45, 47, 142, 143]. Furthermore, there has been a recent surge in interest in the physics of superconductors coupled to cavity

acqed systems. A number of schemes for realizing superconductivity with novel pairing mechanisms [140, 144, 145] and for enhancing the strength of the superconducting state [115, 137] have been proposed using these types of systems. This provides an opportunity for marrying developments in the coupling of cavity photons to matter with the advances in accessing the collective modes of superconductors. Particularly of interest in this context are two collective modes which are particularly difficult to couple to with light: the Bardasis-Schrieffer mode, and the Higgs mode. Some schemes are known for accessing these states electromagnetically, through e.g. intense laser pulses [146–148] or Raman spectroscopy [106, 149–151]. These schemes rely on couplings in the non-linear regime since these modes do not couple to light at the linear response level [99, 152]. However, it has recently been understood that a linear coupling between photons and typically inactive modes of a superconductor can be induced with the addition of a uniform supercurrent [138, 153]. Indeed, such

a supercurrent-mediated linear coupling has recently been implemented successfully in NbN [154], allowing for observation of the Higgs mode in optical measurements.

In this chapter we demonstrate two examples of polaritons formed from cavity photons and the collective modes of a quasi-2D superconductor using the supercurrent induced coupling construction. Our primary results, presented in Figs. 5.1 and 5.4, the existence of Bardasis-Schrieffer- and Higgs-polaritons, respectively. The degree of hybridization is dependent on the strength of the externally imposed supercurrent allowing for the nature of the modes to be tuned in situ. Motivated by the condensation of cavity exciton-polaritons seen in experiments, we speculate on the implications of forming a finite coherent density of these polaritons.

5.2 Bardasis-Schrieffer Polaritons

Not long after the advent of BCS theory, Bardasis and Schrieffer [155] showed the existence of exciton-like excitations in superconductors with pairing potentials in competing channels.

We consider a setup consisting of a two-dimensional electron system at the center of a perfectly reflecting parallel mirror
acqed cavity, as shown in the inset of Fig. 5.1. The 2D electron system is described by a single-band fermion action with a BCS interaction decomposed into angular momentum channels. With $\hbar = 1$ it is

$$S_\psi = \sum_{k,\sigma} \bar{\psi}_{k,\sigma} \left(-i\epsilon_n + \xi_k \right) \psi_{k,\sigma} - \frac{1}{\beta} \sum_q \sum_{\ell=s,d} g_\ell \bar{\varphi}_q^\ell \varphi_q^\ell, \tag{5.1}$$

with $\xi_k = k^2/2m^* - \mu$ the energy measured from the Fermi surface, σ labeling spin, k and q each representing momentum and Matsubara frequency, g_ℓ the interaction
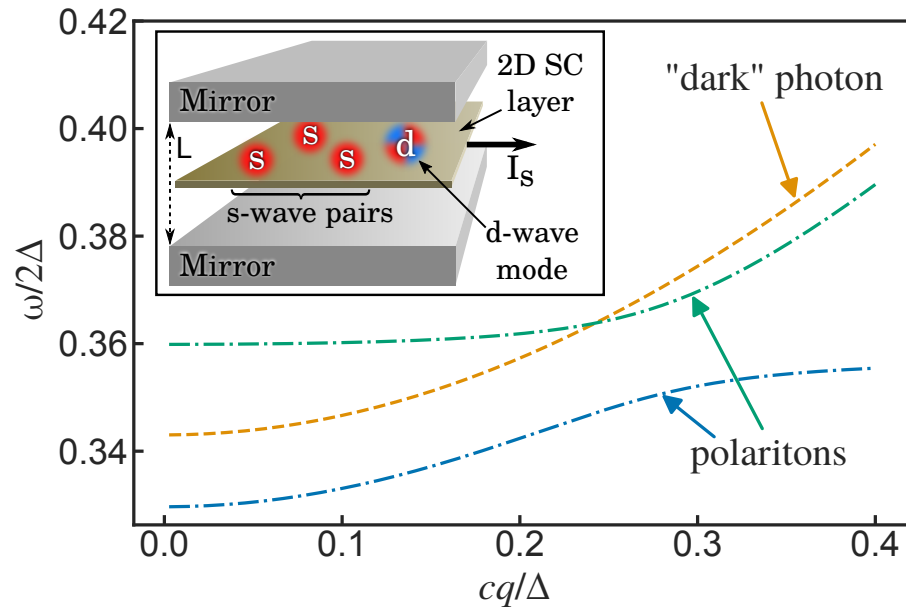
Figure 5.1: The dispersion of the Bardasis-Schrieffer-polariton modes (dot-dashed). An external supercurrent causes the BS mode and cavity photons to hybridize, and the polariton states have significant overlap with each. The "dark" photon mode (dashed) remains decoupled. The splitting of otherwise degenerate photon modes is a result of a supercurrent-induced self-energy contribution. Temperature and supercurrent angle are chosen to maximize hybridization (see Fig. 5.2). *Inset* — schematic of the system: a 2-dimensional superconductor with an applied supercurrent I_S at the center of a planar cavity.

strength in the ℓ-channel, and the interaction written in terms of bilinears,

$$\varphi_q^\ell = \sum_k f_\ell(\phi_k)\psi_{-k+\frac{q}{2},\downarrow}\psi_{k+\frac{q}{2},\uparrow}. \tag{5.2}$$

Importantly, following Bardasis and Schrieffer [155] we assume the interaction is sizable in both s-wave and d-wave channels, but a stronger s-wave component, $g_s > g_d$, leads to a purely s-wave superconducting ground state. The form factors are taken to be $f_s(\phi_k) = 1$ and $f_d(\phi_k) = \sqrt{2}\cos(2\phi_k)$. This choice of f_d breaks the model's full rotational symmetry by choosing an explicit reference axis from which the angle of $\mathbf{k}$, here called ϕ_k, is measured, which we expect to be chosen by the underlying crystal structure of the system — not explicitly present in our continuum model. The interaction can be decoupled in both angular momentum channels simultaneously with a Hubbard-Stratonovich transformation

$$S = \sum_k \bar{\Psi}_k\left(-i\epsilon_n\hat{\tau}_0 + \xi_k\hat{\tau}_3\right)\Psi_k + \frac{1}{\beta}\sum_{q,\ell}\frac{1}{g_\ell}|\Delta_q^\ell|^2$$
$$- \frac{1}{\beta}\sum_{k,q}\bar{\Psi}_{k+\frac{q}{2}}\sum_\ell f_\ell(\phi_k)\left(\Delta_q^\ell\hat{\tau}_+ + \bar{\Delta}_{-q}^\ell\hat{\tau}_-\right)\Psi_{k-\frac{q}{2}}, \tag{5.3}$$

where $\Psi_k = (\psi_{k,\uparrow}, \bar{\psi}_{-k,\downarrow})$ are Nambu spinors, $\hat{\tau}_i$ are the Pauli matrices in Nambu space with $\hat{\tau}_0$ the identity, and Δ_q^ℓ are the complex Hubbard-Stratonovich decoupling fields labeled by angular momentum channel.

The model of the photonic sector used in this chapter is that of a parallel mirror cavity consisting of two conducting plates of infinite extent in the $x - y$ plane and separated by a distance L along the z axis. The action for photons inside the empty cavity is (with $c = 1$)

$$S_{\text{cav}} = -\frac{1}{2\beta}\sum_{q,n,\alpha} A_{\alpha,n,-q}\left[(i\Omega_m)^2 - \omega_{n,q}^2\right]A_{\alpha,n,q}. \tag{5.4}$$

Here α indexes the two cavity polarizations, n labels the quantized modes resulting from the confinement in z, and $\omega_{n,q}^2 = n^2\omega_0^2 + q^2$, with $\omega_{n,0} = n\pi/L$, is the dispersion of photons inside the cavity. We consider just the $n = 1$ mode and drop the index; all other modes are higher in energy and far from the resonance we tune to later. The vector potential is written in terms of polarizations as $\mathbf{A}_q(z) = \sum_\alpha \boldsymbol{\epsilon}_{\alpha,\mathbf{q}}(z)A_{\alpha,q}$, with $\boldsymbol{\epsilon}_{\alpha,\mathbf{q}}(z)$ the polarization vectors inside the cavity. In particular, we have chosen to work with the $n = 1$ transverse electric and transverse magnetic solutions, which in the Coulomb gauge have polarization vectors

$$\boldsymbol{\epsilon}_1(\mathbf{q}, z) = i\sqrt{\frac{2}{L}}\sin\left(\frac{\pi z}{L}\right)\hat{\mathbf{z}} \times \hat{\mathbf{q}}$$

$$\boldsymbol{\epsilon}_2(\mathbf{q}, z) = \sqrt{\frac{2}{L}}\frac{1}{\omega_\mathbf{q}}\left(cq\cos\left(\frac{\pi z}{L}\right)\hat{\mathbf{z}} - i\omega_0\sin\left(\frac{\pi z}{L}\right)\hat{\mathbf{q}}\right),$$

(5.5)

where the z axis is perpendicular to the plane of the superconductor and the momentum $\mathbf{q}$ is in the plane, $\hat{\mathbf{z}}$ and $\hat{\mathbf{q}}$ are the unit vectors along $\mathbf{z}$ and $\mathbf{q}$, and photon dispersion $\omega_\mathbf{q}$ as above. The electron system is located in the middle of the cavity, so only $z = L/2$ must be considered

$$\boldsymbol{\epsilon}_1(\mathbf{q}, L/2) = i\sqrt{\frac{2}{L}}\hat{\mathbf{z}} \times \hat{\mathbf{q}}, \qquad \boldsymbol{\epsilon}_2(\mathbf{q}, L/2) = -i\sqrt{\frac{2}{L}}\frac{\omega_0}{\omega_\mathbf{q}}\hat{\mathbf{q}},$$

(5.6)

Note that in the limit of small $\mathbf{q}$ these eigenvectors form an approximately orthonormal basis.[1]

Minimal coupling between the cavity photon and the electron system generates a paramagnetic term proportional to $e\mathbf{v_k} \cdot \mathbf{A}_q$, with the electron velocity operator $\mathbf{v_k} = \mathbf{k}/m^*$, and a diamagnetic term proportional to $e^2 A_q^2$. We drop the diamagnetic term since it is unimportant both in the weak-field regime [134] and for the cavity

---

[1]In the basis of the components of $\mathbf{A}$ the diagonal components of the vector potential action go as $1 + \left(\omega_\mathbf{q}/\omega_0\right)^2$, while the off diagonal components go as $1 - \left(\omega_\mathbf{q}/\omega_0\right)^2$. Thus, as long as $1 + 2(\omega_0/cq)^2 \gg 1$, we can treat the vector potential action as approximately diagonal.

photon self-energy in the presence of disorder, which is ubiquitous in 2D [49, 50].

Note that our cavity geometry is chosen for calculation simplicity, but in real microwave cavities the transverse nature of the of photon amplitude envelope is more complicated. The effect of this is to increase the strength of the paramagnetic coupling, which we include via a phenomenological enhancement in the light-matter coupling term [134, 136, 140].

We now consider externally driving a homogeneous supercurrent through the system. A supercurrent can be understood as the superconducting condensate moving at constant uniform velocity with respect to the lab frame, with Bogoliubov quasi-particles being defined in the comoving frame, i.e. the supercurrent can be included via a simple Galilean transformation. Calling the condensate superfluid velocity $\mathbf{v}_S$, we have $\mathbf{v_k} \to \mathbf{v_k} + \mathbf{v}_S$. The angle of $\mathbf{v}_S$ with respect to the axis defined by $f_d(\phi_k)$, as depicted in the inset in Fig. 5.2, is denoted θ_S. This modifies the quasi-particle dispersion in the lab frame

$$\xi_k \to \xi_k + \mathbf{k} \cdot \mathbf{v}_S + \frac{1}{2} m v_S^2 \equiv \xi_k^S + \mathbf{k} \cdot \mathbf{v}_S. \tag{5.7}$$

The term linear in $\mathbf{k}$ is a Doppler shift in the energy while the v_S^2 term can be absorbed into a (negligible) redefinition of the chemical potential. The velocity shift also affects the paramagnetic coupling,

$$S_{\psi-A} \to \frac{X}{\beta} \sum_{k,q} \bar{\Psi}_{k+\frac{q}{2}} \underbrace{(-e\mathbf{v_k}\hat{\tau}_0 - e\mathbf{v}_S\hat{\tau}_3) \cdot \mathbf{A}_q}_{\equiv \hat{\chi}_{k,q}[A]} \Psi_{k-\frac{q}{2}}. \tag{5.8}$$

Here X denotes the phenomenological coupling enhancement described above [134, 136, 140], which we absorb into a redefinition of the charge. Crucially the Nambu structure for the paramagnetic and supercurrent-induced terms are different, since particle and hole velocities are shifted in opposite senses, ultimately allowing the

coupling of the BS mode to light. The supercurrent can equivalently be included as a uniform phase winding of Δ^s which, upon appropriate gauge transformation, reproduces these results while maintaining explicit gauge invariance.

We make the mean-field approximation on the s-wave gap function

$$S = S_{\Delta,s} + S_{\Delta,d} + S_{\text{cav}} - \sum_k \bar{\Psi}_k \hat{G}_k^{-1} \Psi_k + \frac{1}{\beta} \sum_{k,q} \bar{\Psi}_{k+\frac{q}{2}} \left(\hat{\chi}_{k,q}[A] - \hat{\Delta}^d_{k,q} \right) \Psi_{k-\frac{q}{2}}, \quad (5.9)$$

with $S_{\Delta,s} = \beta|\Delta|^2/g_s$ describing the static, homogeneous s-wave component Δ, $S_{\Delta,d} = \beta^{-1} \sum_q |\Delta^d_q|^2/g_d$ describing the d-wave fluctuations, $\hat{G}_k^{-1} = (i\epsilon_n - \mathbf{k} \cdot \mathbf{v}_S)\hat{\tau}_0 - \xi_k^S \hat{\tau}_3 + \Delta \hat{\tau}_1$ the inverse Nambu Green's function, and

$$\hat{\Delta}^d_{k,q} = f_d(\phi_k) \begin{pmatrix} 0 & \Delta^d_q \\ \bar{\Delta}^d_{-q} & 0 \end{pmatrix}. \quad (5.10)$$

The mean field value of Δ is obtained as the saddle point solution in the absence of $\mathbf{A}$ and Δ^d but in the presence of the supercurrent, in keeping with the approximation that Δ is unaffected by d-wave fluctuations and photons.

We now integrate out the fermions and expand to second order in $\hat{\Delta}^d$ and $\hat{\chi}$, giving

$$S_{\text{eff}} = S_d + S_A + S_{d-A}. \quad (5.11)$$

These three terms are defined as the parts of the action describing free d-wave fluctuations, cavity photons in the presence of the superconducting system, and the supercurrent-generated coupling between them, respectively.

Since the d-wave fluctuations have much greater kinetic mass than photons, we approximate them with a flat dispersion: their energy in the limit $\mathbf{q} \to 0$. Additionally, we drop all terms which vanish in the quasi-classical ξ-approximation. Writing Δ^d in terms of its real and imaginary components, S_d decouples into an action for each. The real mode is within the Bogoliubov quasi-particle continuum,

and is therefore over-damped [152, 155]. It also remains decoupled from photons despite the supercurrent so we do not consider it further. The imaginary mode is the in-gap Bardasis-Schrieffer mode. Naming this mode d_q, the BS mode action is

$$S_d = \frac{1}{\beta} \sum_q d_{-q} \left[\frac{1}{g_d} + \sum_{\mathbf{k}} f_d(\phi_k)^2 \frac{2\lambda_k \left(n_F(E_{\mathbf{k}}^-) - n_F(E_{\mathbf{k}}^+)\right)}{(i\Omega_m)^2 - (2\lambda_k)^2} \right] d_q, \qquad (5.12)$$

where $\bar{d}_q = d_{-q}$, $\lambda_k = \sqrt{\left(\xi_k^S\right)^2 + \Delta^2}$ is the quasi-particle energy in the comoving frame, n_F is the Fermi function, and $E_{\mathbf{k}}^{\pm} = \pm\lambda_k + \mathbf{k} \cdot \mathbf{v}_S$ is the Doppler-shifted energy.

The photon sector of the action consists of the empty cavity action S_{cav} plus a self-energy term due to the superconductor,

$$S_A = -\frac{1}{2\beta} \sum_{q,\alpha,\beta} A_{\alpha,-q} \left[\left((i\Omega_m)^2 - \omega_q^2\right) \delta_{\alpha\beta} - \Pi_{\alpha\beta,q} \right] A_{\beta,q}. \qquad (5.13)$$

The matrix $\Pi_{\alpha\beta,q}$ is the electromagnetic linear response function of the superconducting system written in the cavity polarization basis.

Within the approximations discussed above the coupling between photons and the BS mode arises *entirely* through the supercurrent-induced term,

$$S_{d-A} = -\frac{ie\Delta}{\beta} \sum_{\mathbf{k},q,\alpha} f_d(\phi_k) \frac{i\Omega_m \left(n_F(E_{\mathbf{k}}^-) - n_F(E_{\mathbf{k}}^+)\right)}{(i\Omega_m)^2 - (2\lambda_k)^2} \frac{\mathbf{v}_S \cdot \boldsymbol{\epsilon}_{\alpha,q}}{\lambda_k} \left(A_{\alpha,q} d_{-q} - A_{\alpha,-q} d_q \right), \qquad (5.14)$$

consistent with the known result that the BS mode does not normally couple linearly to light. As a consequence, the BS mode only couples to the component of the vector potential parallel to the supercurrent.

The action is then straightforwardly written in terms of a hybrid inverse Green's function

$$S_{\mathrm{eff}} = \frac{1}{2\beta} \sum_q (d_{-q}, A_{\alpha,-q}) \begin{pmatrix} D_{\mathrm{BS},q}^{-1} & g_{\beta,q} \\ g_{\alpha,q}^* & D_{\alpha\beta,q}^{-1} \end{pmatrix} \begin{pmatrix} d_q \\ A_{\beta,q} \end{pmatrix}, \qquad (5.15)$$

with sums over repeated indices and with $D_{\mathrm{BS},q}^{-1}$, $D_{\alpha\beta,q}^{-1}$, and $g_{\alpha,q}$ defined implicitly through Eq. (5.12)–(5.14). A more intuitive description can be obtained by first making a harmonic approximation to the BS action: continue D_{BS}^{-1} to complex frequency, expand around the saddle point solution Ω_{BS}, then restrict back to imaginary frequency. In our clean model Ω_{BS} is purely real, so the BS mode is undamped. We then expand in terms of BS and photon mode operators, $d_q = (b_q + \bar{b}_{-q})/\sqrt{2K\Omega_{\mathrm{BS}}}$ and $A_{\alpha,q} = (a_{\alpha,q} + \bar{a}_{\alpha,-q})/\sqrt{2\omega_q}$, where K is a constant coming from the harmonic expansion. We make the standard approximation of dropping the counter-rotating terms $(aa, \bar{a}\bar{a})$ – an approximation we verify post-hoc – and perform a change of basis from photon polarizations to components parallel and perpendicular to the supercurrent. Inside the coupling and photon terms, we analytically continue to real frequency $i\Omega_m \to \Omega + i0$, then expand around relevant frequencies. The imaginary parts exactly vanish, and the action becomes

$$S_{\mathrm{eff}} \approx \frac{1}{\beta} \sum_q \left(\bar{b}_q, \bar{a}_q^{\parallel}, \bar{a}_q^{\perp} \right) \left(-i\Omega_m \check{\mathbb{1}} + \check{H}_{\mathbf{q}}^{\mathrm{eff}} \right) \begin{pmatrix} b_q \\ a_q^{\parallel} \\ a_q^{\perp} \end{pmatrix}, \qquad (5.16)$$

now written in terms of an effective Hamiltonian[2]

$$\check{H}_q^{\mathrm{eff}} = \begin{pmatrix} \Omega_{\mathrm{BS}} & g_q & 0 \\ g_q & \omega_q + \Pi_q^S & 0 \\ 0 & 0 & \omega_q \end{pmatrix}, \qquad (5.17)$$

---

[2]The parameters of the Hamiltonian can be obtained via an analytic method under suitable approximation. A complete derivation of the Hamiltonian was performed by Andrew Allocca. For details see the supplement of Ref. [138].

where $q = |\mathbf{q}|$, Π_q^S is a self-energy shift in the photon mode polarized parallel to the supercurrent, coming from a supercurrent-dependent term in $\Pi_{\alpha\beta,q}$, and

$$g_q = ev_S\Delta\sqrt{\frac{2\,\Omega_{\mathrm{BS}}}{L\,K\omega_q}}\sum_{\mathbf{k}}\frac{f_d(\phi_k)}{\lambda_k}\frac{n_F(E_{\mathbf{k}}^-) - n_F(E_{\mathbf{k}}^+)}{\Omega_{\mathrm{BS}}^2 - (2\lambda_k)^2}. \qquad (5.18)$$

For small $\mathbf{q}$, only one photon mode hybridizes with the BS mode in the Hamiltonian approximation. This photon mode and the BS mode can be made resonant by tuning parameters of the system, most straightfowardly the cavity size L, allowing them to strongly hybridize.

For numerical calculations we use material parameters motivated by iron-based superconductors [156–159], where BS modes have been experimentally detected. We set the Fermi energy $\epsilon_F = 100\,\mathrm{meV}$, the effective mass $m^* = 4m_e$ [3], where m_e is the electron mass, and critical temperature $T_c = 35$ K. We put $1/g_d - 1/g_s = 0.1\nu$, where $\nu = m^*/2\pi$ is the density of states, and tune the size of the cavity L so that $\omega_0 = \pi/L = 0.96\,\Omega_{\mathrm{BS}}(\theta_S = 0)$, putting photons and the BS mode very near resonance. Finally, we set the phenomenological coupling enhancement to $X = 10$, although enhancements of $X = 10^2$ or greater have been predicted in similar cavity systems [134, 136, 140].

First consider the dependence of coupling strength g_q on temperature, superfluid velocity v_S, and supercurrent angle θ_S, as shown in Fig. 5.2. The coupling is mediated by thermally excited quasi-particles and so vanishes for $T \to 0$. It also vanishes for $T \to T_c$ since $\Delta \to 0$. The result is a unique maximum of $g(T)$ at an intermediate temperature, $T_{\max} \approx 0.42T_c$, which we use for all other computations. Similarly, g vanishes for small v_S — this can be verified by expansion of the Fermi functions — and also as v_S approaches a value corresponding to the critical current,

---

[3]In the quasi-classical approximation the value of the effective mass cancels everywhere, since only $v_S \propto 1/k_F \propto 1/\sqrt{m^*}$, $K \propto \nu = m^*/2\pi$, and $\sum_{\mathbf{k}} \sim \nu \int d\xi$ depend on it. Therefore, the choice of effective mass is mostly unimportant.
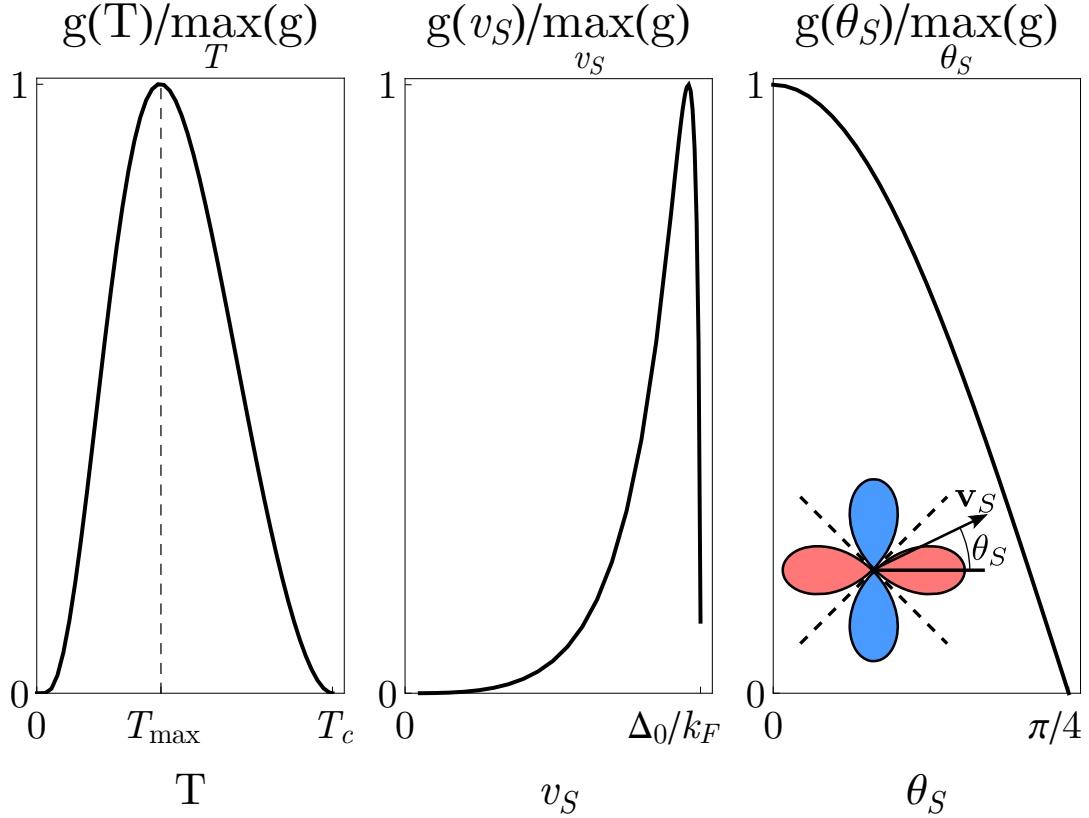
Figure 5.2: The hybridization matrix element g in the effective Hamiltonian as a function of temperature, superfluid velocity, and θ_S, the angle between the direction of the supercurrent and the axis defined implicitly by the d-wave form factor $f_d(\phi_k)$, all scaled by their respective maxima. (Left) $g(T)$ is maximized for a temperature $T_{\max} \approx 0.42 T_c$. (Center) $g(v_S)$ is sharply peaked for large superfluid velocity around $v_S \approx 0.96 \Delta(v_S = 0)/k_F$. (Note, $\Delta_0 \equiv \Delta(v_S = 0)$.) (Right) $g(\theta_S)$ is maximal for $\theta_S = m\pi/2$, $m \in \mathbb{Z}$, and vanishes when the supercurrent runs along a node of f_d, $\theta_S = (2m + 1)\pi/4$. *Inset* — the orientation of the supercurrent with respect to the d-wave form factor. The color of the lobes gives the relative sign of f_d for different angles, and the dashed lines are the nodes where $f_d = 0$. The plots use $T = T_{\max}$, $v_S = 0.9\Delta(v_S = 0)/k_F$, and $\theta_S = 0$ where applicable, and fixed detuning $\omega_0 = 0.96\Omega_{\text{BS}}$.

where the superconducting state vanishes. We set $v_S = 0.9\Delta(v_S = 0)/k_F$ in our calculations, near the value giving the maximum coupling but not too near the critical value [4]. Dependence on the supercurrent angle θ_S comes through the d-wave form factor. The coupling is strongest when the supercurrent is along an anti-node of the form factor – $\theta_S = m\pi/2$, $m \in \mathbb{Z}$ – and vanishes when the supercurrent is along a node – $\theta_S = (2m + 1)\pi/4$. We use $\theta_S = 0$ for all other calculations.

To obtain the polariton modes we both directly solve for the poles of the hybridized Green's function (5.15) and calculate the eigenvalues of the effective Hamiltonian (5.17), which can be diagonalized analytically. The results of both approaches are in excellent agreement; the dispersions are plotted for both methods in Fig. 5.1. One of the photon modes can be made to strongly hybridize with the BS mode, while the other "dark" photon remains distinct. This is made especially clear by examining the BS component of the eigenvectors of the effective Hamiltonian, as shown in Fig. 5.3. Because the strength of the hybridization is controlled exclusively by g, any of the parameters on which it depends, namely T, v_S, or θ_S, can be used to directly control the strength of the effect.

5.3   Higgs Polaritons

We now investigate coupling to a mode which is a little further from the analogous exciton-polariton case: the Higgs or amplitude mode. As with the Bardasis-Schrieffer mode there is no linear coupling between the Higgs mode and light in the absence of a supercurrent. However, as shown by Moor, Volkov, and Efetov [153], in the presence of a supercurrent *and* disorder, the linear coupling is finite.

---

[4]The value $\Delta(v_S = 0)/k_F$ yields an approximate critical current consistent with values measured in iron-based systems, though in type II materials the current is limited by vortex pinning rather than condensate depletion [160, 161].
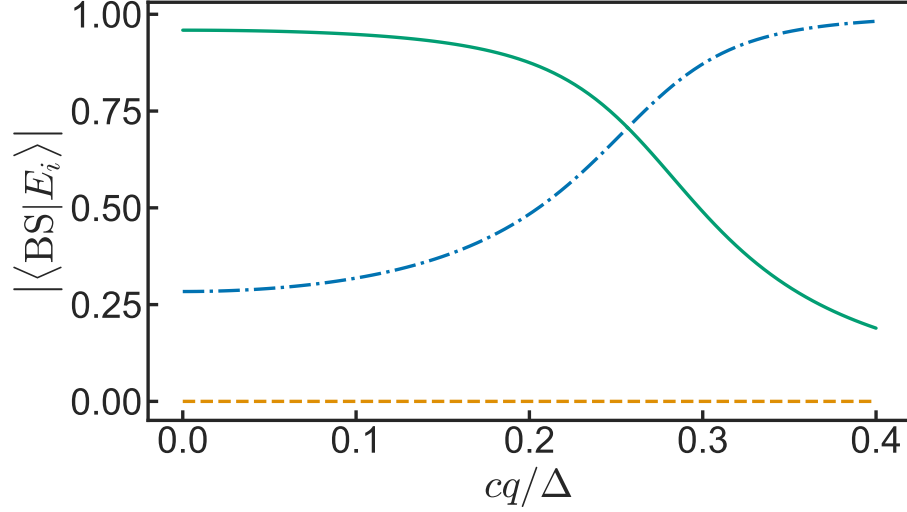
Figure 5.3: The Bardasis-Schrieffer component of the eigenvectors of the effective Hamiltonian, Eq. (5.17). The upper (solid) and lower (dot-dashed) polaritons have significant photon and Bardasis-Schrieffer character, indicating strong hybridization between the systems. One can also clearly see the "dark" photon mode (dashed) which does not hybridize with the superconductor's collective mode.

Our goal will be to obtain a coupled bosonic action

$$S = \frac{1}{2} \int_{\omega,\mathbf{q}} \begin{pmatrix} \vec{h}(-q) & \vec{\mathbf{A}}(-q) \end{pmatrix} \check{G}^{-1}(\omega, \mathbf{q}) \begin{pmatrix} \vec{h}(q) \\ \vec{\mathbf{A}}(q) \end{pmatrix} \tag{5.19}$$

describing the coupled evolution of the Higgs mode and cavity photons. From this we will extract the spectral function $-2\pi i \mathcal{A} = G^R(\omega, \mathbf{q}) - G^A(\omega, \mathbf{q})$ shown in Fig. 5.4.

To this end we will employ the following procedure. We consider a quasi-2D disordered superconductor within a planar photonic cavity. We expand the action of the coupled system about the saddle-point solution corresponding to the BCS ground state, including Gaussian amplitude fluctuations (the Higgs mode) and the hydrodynamic diffusive modes of the electron fluid (cooperons and diffusons). Upon integrating out the electronic modes, a linear coupling is generated between the Higgs and the photons, as well as self-energy terms for both bosonic fields, leading to Eq. (5.19).
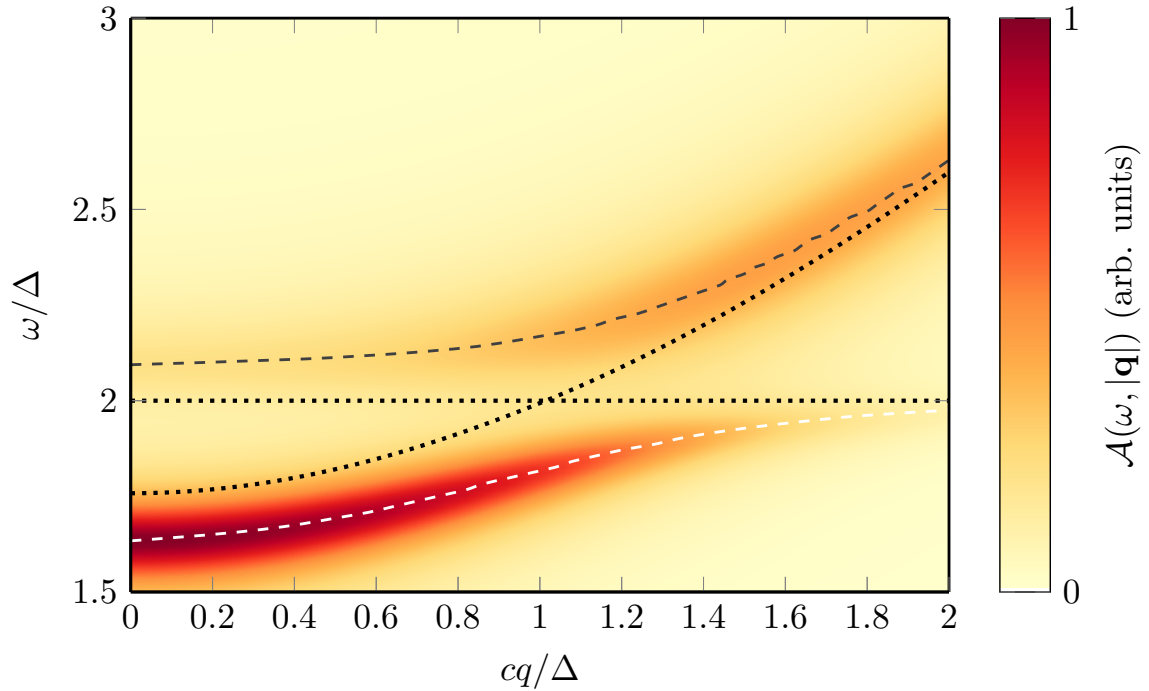
Figure 5.4: (Color Online) The Higgs-polariton spectral function as a function momentum q and frequency ω. All quantities are given in units of the superconducting gap Δ. The uncoupled Higgs and photon dispersions are plotted as dotted lines. Gray dashed lines indicate the local maxima of the spectral function. A well defined lower polariton exists below the quasi-particle continuum as well as a broadened upper polariton above 2Δ. Of note is that the lower polariton mode is clearly distinct from the original photon branch, indicating the hybridized character of the excitation.

5.3.1 Cavity Photons

The photon sector is described by the Keldysh action

$$S_{\text{cav}}[a, \bar{a}] = \int_{\omega, \mathbf{q}} \bar{a}_{\omega, \mathbf{q}, \alpha} \begin{pmatrix} 0 & \omega - i\kappa - \omega_{\mathbf{q}} \\ \omega + i\kappa - \omega_{\mathbf{q}} & 2i\kappa N(\omega) \end{pmatrix}_K a_{\omega, \mathbf{q}, \alpha} \qquad (5.20)$$

with equilibrium distribution $N(\omega) = \coth(\omega/2T)$. We consider a dispersion $\omega_{\mathbf{q}} = \sqrt{\omega_0^2 + c^2 q^2}$, due to quantization resulting from confinement perpendicular to the plane. The subscript K denotes that the matrix is in Keldysh space. The frequency $\omega_0 = \pi c / L$, where L is the size of the cavity, is chosen to be near the bare Higgs frequency $\Omega_{\text{Higgs}} \sim 2\Delta$. The cavity confinement naturally leads to a quantization of the photon field into discrete modes and we consider just the lowest of these, with all higher modes at an energy far from resonance with the Higgs frequency. The decay of photons in the cavity is described by the constant κ.

The action for the photon mode operators is supplemented by the polarization vectors for the corresponding modes: Eq. (5.6). The vector potential is expressed in terms of mode operators a as

$$\mathbf{A}_{\omega, \mathbf{q}} = \sqrt{\frac{2\pi c^2}{\omega_{\mathbf{q}}}} \left(\boldsymbol{\epsilon}_\alpha(\mathbf{q}) a_{\omega, \mathbf{q}, \alpha} + \boldsymbol{\epsilon}_\alpha^*(-\mathbf{q}) \bar{a}_{-\omega, -\mathbf{q}, \alpha} \right) \qquad (5.21)$$

where $\epsilon_i(\mathbf{q})$ are the two polarization vectors of the photon mode and we take the photon field to be in the radiation gauge $\nabla \cdot \mathbf{A} = 0$.

5.3.2 Superconductor

The superconductor is described by a Keldysh Non-Linear σ Model (KNLσM) [18, 52], as discussed in Section 1.4.1 and Chapter 4,

$$
iS_{\mathrm{NL\sigma M}} = -i\frac{\nu}{4\lambda}\,\mathrm{Tr}\,\check{\Delta}^{\dagger}(\hat{\gamma}^{q}\otimes\hat{\tau}_{0})\check{\Delta}
$$
$$
-\frac{\pi\nu}{8}\,\mathrm{Tr}\left[D\left(\partial\check{Q}\right)^{2} + 4i\left(i(\hat{\sigma}_{0}\otimes\hat{\tau}_{3})\partial_{t} + i\gamma\check{Q}_{\mathrm{bath}} + \check{\Delta}\right)\check{Q}\right], \quad (5.22)
$$

where D, ν are respectively the diffusion constant and density of states of the fermionic normal state, λ is the BCS interaction strength, and γ is a relaxation rate describing coupling to a bath.

All objects with a check $(\check{X})$ are 4×4 matrices in the product of Nambu and Keldysh spaces, with $\hat{\tau}_{i}$ and $\hat{\sigma}_{i}$ representing Pauli matrices in the Nambu and Keldysh spaces respectively. Tr is used to represent a trace over all matrix and space-time indices, i.e. $\mathrm{Tr}(\cdots) = \int dt\,dt'\,d\mathbf{r}\,\mathrm{tr}(\cdots)$ and $\check{A}\circ\check{B}$ indicates a matrix multiplication over all relevant indices (including convolutions over time indices). $\partial\check{X} = \nabla\check{X} - i(e/c)\big[\check{\mathbf{A}},\check{X}\big]$ denotes a matrix covariant derivative, the means by which the photonic sector couples to the electronic degrees of freedom. The bath is modeled in the relaxation approximation by

$$
\check{Q}_{\mathrm{bath}}(\epsilon) = \begin{pmatrix} 1 & 2F(\epsilon) \\ 0 & -1 \end{pmatrix}_{K} \otimes \hat{\tau}_{0}. \tag{5.23}
$$

The degrees of freedom of the model are the quasi-classical Green's function $\check{Q}_{tt'}(\mathbf{r})$ – which is subject to the non-linear constraint $\check{Q}\circ\check{Q} = \check{1}$, the vector potential $\check{\mathbf{A}} = \sum_{\alpha}\mathbf{A}_{\alpha}\hat{\gamma}^{\alpha}\otimes\hat{\tau}_{3}$, and the BCS pair field $\check{\Delta} = \sum_{\alpha}\left(\Delta_{\alpha}\hat{\gamma}^{\alpha}\otimes\hat{\tau}_{+} - \Delta_{\alpha}^{*}\hat{\gamma}^{\alpha}\otimes\hat{\tau}_{-}\right)$, where $\gamma^{\mathrm{cl}} = \hat{\sigma}_{0}, \gamma^{\mathrm{q}} = \hat{\sigma}_{1}$ are the Keldysh space vertices for the classical and quantum fields.

5.3.3   Saddle-point

The saddle-point equations for Eq. (5.22) are the Usadel equation[16]

$$\partial\left(D\check{Q}_{\mathrm{sp}}\partial\check{Q}_{\mathrm{sp}}\right) + i\left\{i\hat{\tau}_3\partial_t, \check{Q}_{\mathrm{sp}}\right\} + i\left[\check{\Delta} + i\gamma\check{Q}_{\mathrm{bath}}, \check{Q}_{\mathrm{sp}}\right] = 0 \qquad (5.24)$$

and BCS gap equation

$$\frac{1}{\lambda} = \frac{1}{4\Delta}\int_{-\infty}^{\infty} d\epsilon\,\mathrm{tr}\left[\hat{\tau}_-\hat{Q}_{\mathrm{sp}}^K(\epsilon)\right] \qquad (5.25)$$

which together determine the mean field state. At the saddle-point level, the quasi-classical Greens' function has the structure

$$\check{Q}_{\mathrm{sp}} = \begin{pmatrix} \hat{Q}_{\mathrm{sp}}^R & \hat{Q}_{\mathrm{sp}}^K \\ 0 & \hat{Q}_{\mathrm{sp}}^A \end{pmatrix}, \qquad (5.26)$$

with the relation $Q_{\mathrm{sp}}^A = -\hat{\tau}_3[Q_{\mathrm{sp}}^R]^\dagger\hat{\tau}_3$ due to causality and in equilibrium $\hat{Q}_{\mathrm{sp}}^K(\epsilon) = F_{\mathrm{eq}}(\epsilon)\left(\hat{Q}_{\mathrm{sp}}^R(\epsilon) - \hat{Q}_{\mathrm{sp}}^A(\epsilon)\right)$ where $F_{\mathrm{eq}}(\epsilon) = \tanh\left(\epsilon/2T\right)$ – a manifestation of the fluctuation-dissipation relation.

In what follows we define the global $U(1)$ phase of the order parameter such that the mean-field value is real. All electromagnetic quantities use Gaussian units.

It is well established that the Higgs mode of a superconductor does not couple linearly to light due to the absence of electromagnetic moments [99]. One may readily verify that for a uniform BCS state there is no linear coupling of the photons to diffusion modes in Eq. (5.22), and therefore no linear coupling between the Higgs mode and photons is possible. However, as was pointed out recently [153], in the presence of a uniform supercurrent[5] there is an allowed coupling at linear order. The supercurrent can be included into the KNLσM by the addition of a constant vector

---

[5]Disorder is also required. One can verify that in the clean limit the coupling between Higgs mode and photon is still 0 in the limit of $\mathbf{q} \to 0$.

potential term $\mathbf{A}(\mathbf{r}, t) \rightarrow \mathbf{A}(\mathbf{r}, t) - (c/e)\mathbf{p}_S$ where $\mathbf{p}_S$ is the associated superfluid momentum [19].

We now derive the action of Gaussian fluctuations about the BCS saddle point, describing amplitude mode fluctuations, the low-energy excitations of a disordered superconductor (diffusons and cooperons), and cavity photons. We first rotate our global phase so that the bulk order parameter is real. Due to the causality structure it is sufficient to solve for the retarded component of the quasi-classical Green's function

$$\hat{Q}_{\text{sp}}^R(\epsilon) = \cosh(\theta_\epsilon)\hat{\tau}_3 + i\sinh(\theta_\epsilon)\hat{\tau}_2, \qquad (5.27)$$

where θ_ϵ is a complex angle parameterizing the solution of the retarded Usadel equation

$$\Delta \cosh\theta_\epsilon - (\epsilon + i\gamma)\sinh\theta_\epsilon = i\frac{\Gamma}{2}\sinh 2\theta_\epsilon, \qquad (5.28)$$

and $\Gamma = 2D|\mathbf{p}_s|^2$ is the depairing energy associated with the supercurrent. Conjugating Eq. (5.28) and taking $\epsilon \rightarrow -\epsilon$ establishes the useful relation $-\theta_{-\epsilon}^* = \theta_\epsilon$. In the absence of supercurrent the Usadel equation is solved by

$$\cosh\theta_\epsilon^0 = \frac{\epsilon}{\zeta_R(\epsilon)}, \qquad \sinh\theta_\epsilon^0 = \frac{\Delta}{\zeta_R(\epsilon)}, \qquad (5.29)$$

where we have defined $\zeta_{R/A}(\epsilon) = \pm\operatorname{sgn}\epsilon\sqrt{(\epsilon \pm i\gamma)^2 - \Delta^2}$.[6] We provide an exact solution of Eq. (5.28) in the presence of finite supercurrent in Appendix E.1.

The Usadel equation is supplemented by the BCS gap equation Eq. (5.25) to form a closed, self-consistent system of equations for the saddle-point.

---

[6]This differs from the definition given in Ref. [153] due a choice of branch cuts. We take the branch cut of the square root to go between $-\Delta$ and Δ.

5.3.4 Gaussian fluctuations

Now we parameterize fluctuations of $\check{Q}$ about the saddle point solution as in Section 1.4.1

$$\check{Q} = \check{R}^{-1} \circ e^{-\check{W}/2} \hat{\sigma}_3 \hat{\tau}_3 \circ e^{\check{W}/2} \circ \check{R}. \tag{5.30}$$

similar to Refs. [19, 52], where in frequency space

$$\check{R}(\epsilon) = \begin{pmatrix} e^{\hat{\tau}_1 \theta_\epsilon / 2} & 0 \\ 0 & e^{\hat{\tau}_1 \theta_\epsilon^* / 2} \end{pmatrix}_K \begin{pmatrix} \hat{\tau}_0 & F_{\mathrm{eq}}(\epsilon) \hat{\tau}_0 \\ 0 & -\hat{\tau}_0 \end{pmatrix}_K. \tag{5.31}$$

In this parameterization the first matrix describes the spectral structure of the saddle point, while the second enforces the fluctuation-dissipation structure on the matrix $\check{Q}$. One can verify that for $\check{W} = 0$, Eq. (5.31) reproduces Eq. (5.27).

The matrix $\check{W}$ anticommutes with $\hat{\sigma}_3 \otimes \hat{\tau}_3$ and describes fluctuations on the soft manifold $\check{Q} \circ \check{Q} = \check{1}$. There are in total 8 independent components of $\check{W}$ but only 4 of these couple to the amplitude mode or photon. We therefore write the matrix $\check{W}$

$$\check{W}_{\epsilon\epsilon'}(\mathbf{q}) = i \begin{pmatrix} c^R \hat{\tau}_1 & d^{\mathrm{cl}} \\ d^{\mathrm{q}} & c^A \hat{\tau}_1 \end{pmatrix}_K \tag{5.32}$$

in terms of the cooperon $c^{R/A}$ and diffuson d^α fields.

The Higgs mode is introduced by the substitution $\check{\Delta} \to (\Delta_0 \hat{\tau}_0 + h_\alpha \hat{\gamma}^\alpha) \otimes i\hat{\tau}_2$, with Δ_0 a real constant. Having made these substitutions, we again expand the action to second order in the fields c, d, h, and $\mathbf{A}$. Only the second order terms are of significance as the 0-th order terms do not include the fluctuation fields and the first order terms vanish due to the saddle point equation and gauge condition. We

are left with

$$iS = \pi\nu \int_{\epsilon,\epsilon',\mathbf{q}} \left(\frac{1}{4} \left[\vec{d}_{\epsilon'\epsilon} \hat{\mathcal{D}}_{\epsilon\epsilon'}^{-1} \vec{d}_{\epsilon\epsilon'} + \vec{c}_{\epsilon'\epsilon} \hat{\mathcal{C}}_{\epsilon\epsilon'}^{-1} \vec{c}_{\epsilon\epsilon'} \right] + \left[\vec{c}_{\epsilon'\epsilon} \hat{s}_{\epsilon\epsilon'}^c + \vec{d}_{\epsilon'\epsilon} \hat{\sigma}_1 \hat{s}_{\epsilon\epsilon'}^d \right] \vec{h}(\epsilon - \epsilon') \right.$$

$$\left. + \frac{e}{c} D \left[\vec{c}_{\epsilon'\epsilon} \hat{r}_{\epsilon\epsilon'}^c + \vec{d}_{\epsilon'\epsilon} \hat{\sigma}_1 \hat{r}_{\epsilon\epsilon'}^d \right] \mathbf{p}_s \cdot \vec{\mathbf{A}}(\epsilon - \epsilon') \right) \quad (5.33)$$

where the dependence on the momentum $\mathbf{q}$ has been suppressed, $\vec{c} = \left(c^R, c^A \right)$, for the fields d, h, and $\mathbf{A}$ we use the notation $\vec{X} = \left(X^{\mathrm{cl}}, X^{\mathrm{q}} \right)$, and

$$\hat{\mathcal{D}}_{\epsilon\epsilon'}^{-1} = \mathcal{D}_{\epsilon'\epsilon}^{-1} \hat{\sigma}_+ + \mathcal{D}_{\epsilon\epsilon'}^{-1} \hat{\sigma}_-, \qquad \hat{\mathcal{C}}_{\epsilon\epsilon'}^{-1} = \mathrm{diag}\left(\mathcal{C}_{\epsilon\epsilon'}^R, \mathcal{C}_{\epsilon\epsilon'}^A \right)^{-1} \quad (5.34)$$

The fluctuation propagators can be expressed in terms of the function θ_ϵ,

$$\mathcal{D}_{\epsilon\epsilon'} = \left(-Dq^2 + \mathcal{E}^R(\epsilon) + \mathcal{E}^A(\epsilon') \right.$$

$$+ \Gamma \left[1 - \cosh\left(\theta_\epsilon - \theta_{\epsilon'}^* \right) \right] \cosh\left(\theta_\epsilon + \theta_{\epsilon'}^* \right) \right)^{-1}$$

$$\mathcal{C}_{\epsilon\epsilon'}^{(R/A)} = \left(-Dq^2 + \mathcal{E}^{(R/A)}(\epsilon) + \mathcal{E}^{(R/A)}(\epsilon') \right. \quad (5.35)$$

$$- \Gamma \left[1 + \cosh\left(\theta_\epsilon - \theta_{\epsilon'} \right) \right] \cosh\left(\theta_\epsilon + \theta_{\epsilon'} \right) \right)^{-1}$$

$$\mathcal{E}^R(\epsilon) = (\mathcal{E}^A)^* = i\epsilon \cosh\theta_\epsilon - i\Delta_0 \sinh\theta_\epsilon.$$

The latter two terms of Eq. (5.33) constitute a linear coupling between diffusons/cooperons and both the photons and Higgs mode.

5.3.5 Hybrid Bosonic Action

Upon integrating out the diffusion modes c and d this generates a linear coupling between the Higgs mode and photon field as well as additional terms in the action for each individually

$$S = \frac{1}{2} \int_{\omega,\mathbf{q}} \left(\vec{h}(-q) \quad \vec{\mathbf{A}}(-q) \right) \check{G}^{-1}(\omega, \mathbf{q}) \begin{pmatrix} \vec{h}(q) \\ \vec{\mathbf{A}}(q) \end{pmatrix} \quad (5.36)$$

with[7]

$$\check{G}^{-1}(\omega, \mathbf{q}) = \begin{pmatrix} -\frac{2\nu}{\lambda}\hat{\sigma}_1 - \hat{\Pi}^h(\omega) & \hat{\mathbf{g}}(\omega) \\ \hat{\mathbf{g}}(-\omega)^T & \hat{D}^{-1}(\omega, \mathbf{q}) - \hat{\Pi}^A(\omega) \end{pmatrix}.$$ (5.37)

$D(\omega, \mathbf{q})$ is the correlators of the vector potential and can be obtained from the action for the photon mode operators Eq. (5.20) and the relation Eq. (5.21). Equation (5.37), along with the explicit expressions for its elements, Eqs. (5.40), (5.42) and (5.43), constitute one of the main results of this work.

The generated terms g and Π are then expressed in terms of the couplings s and r and the diffuson and cooperon propagators $\mathcal{D}$ and $\mathcal{C}^{(R/A)}$. Explicitly, defining

$$\mathcal{F}[\omega, \hat{x}, \hat{y}] = -i\nu \int d\epsilon \left(\left[\hat{x}^c_{\epsilon_-\epsilon_+}\right]^T \hat{\mathcal{C}}_{\epsilon_+\epsilon_-} \hat{y}^c_{\epsilon_+\epsilon_-} + \left[\hat{x}^d_{\epsilon_-\epsilon_+}\right]^T \hat{\sigma}_1 \hat{\mathcal{D}}_{\epsilon_+\epsilon_-} \hat{\sigma}_1 \hat{y}^d_{\epsilon_+\epsilon_-} \right),$$ (5.38)

we have

$$\hat{\Pi}^h(\omega) = \hat{\mathcal{F}}(\omega, \hat{s}, \hat{s})$$

$$\hat{\Pi}^A_{ij}(\omega) = \frac{e^2}{c^2} D^2 p^i_S p^j_S \hat{\mathcal{F}}(\omega, \hat{r}, \hat{r}) + \hat{\Pi}_{\text{MB};ij}$$ (5.39)

$$\hat{\mathbf{g}}(\omega) = \frac{e}{c} D\mathbf{p}_S \hat{\mathcal{F}}(\omega, \hat{s}, \hat{r}),$$

where Π_{MB} is the photon polarization operator arising from the saddle point – the Mattis-Bardeen[162] result – and $\epsilon_{\pm} = \epsilon \pm \omega/2$. We will be particularly interested in the retarded Green's function which is the $q - cl$ component of Eq. (5.37) in Keldysh space and as such below we give the explicit forms for the elements of the retarded Green's function.

In evaluating these terms we set $\mathbf{q} \to 0$ in the fermionic bubbles since any finite $\mathbf{q}$ terms are an extra factor of v_F/c smaller. In the absence of a supercurrent, the action for the Higgs mode gives the well known result $\text{Re}\,\Omega_{\text{Higgs}} = 2\Delta_0 + O(\gamma^2)$, with finite imaginary part arising only from quasi-particle damping. Nonetheless, the Higgs mode is still damped due to branch cuts in the complex plane. It is this

---

[7]One can use the gap equation to rewrite the the Higgs sector of the Green's function in a more useful form as a single integral over ϵ.

analytic structure that gives rise to the asymptotic decay $h(t \to \infty) \propto \cos(2\Delta t)/\sqrt{t}$ derived by Volkov and Kogan [163].

While the calculation for the elements of the Green's function can performed for arbitrary supercurrent (c.f. Appendices E.1 and E.3) the results can be understood by considering the behavior at small supercurrent. Working to lowest order in $\mathbf{p}_s$ we can drop the supercurrent dependence everywhere but the prefactor to $\hat{\mathbf{g}}(\omega)$ in Eq. (5.39). Using the gap equation the Higgs component of the retarded propagator takes the form

$$
[G_h^R(\omega)]^{-1} = \nu \int_0^\infty d\epsilon \left(\frac{2\Delta_0^2 - \omega z_+}{\zeta_R(\epsilon_+)\zeta_R(\epsilon_-)\left(\zeta_R(\epsilon_+) + \zeta_R(\epsilon_-)\right)} F(\epsilon_-) \right.
$$
$$
- \frac{2\Delta_0^2 + \omega z_-^*}{\zeta_A(\epsilon_+)\zeta_A(\epsilon_-)\left(\zeta_A(\epsilon_+) + \zeta_A(\epsilon_-)\right)} F(\epsilon_+)
$$
$$
\left. + \frac{z_+ z_-^* + \Delta_0^2 + \zeta_R(\epsilon_+)\zeta_A(\epsilon_-)}{\zeta_R(\epsilon_+)\zeta_A(\epsilon_-)\left(\zeta_R(\epsilon_+) + \zeta_A(\epsilon_-)\right)} (F(\epsilon_+) - F(\epsilon_-)) \right). \quad (5.40)
$$

In the limit of infinitesimal damping this is

$$
[G_h^R(\omega)]^{-1} = 2\nu \int_{\Delta_0}^\infty d\epsilon \, \frac{F(\epsilon)}{\zeta_R(\epsilon)} \frac{\omega^2 - 4\Delta_0^2}{(\omega + i0)^2 - 4\epsilon^2}. \quad (5.41)
$$

Substituting in the expressions for s and r allows us to write

$$
\mathbf{g}^R(\omega) = 4\frac{e}{c} D\mathbf{p}_S i\Delta_0 \nu \int_0^\infty d\epsilon
$$
$$
\times \left(z \frac{\zeta_R(\epsilon_+)z_- + \zeta_R(\epsilon_-)z_+}{\zeta_R^2(\epsilon_+)\zeta_R^2(\epsilon_-)\left(\zeta_R(\epsilon_+) + \zeta_R(\epsilon_-)\right)} F(\epsilon_-) \right.
$$
$$
- z^* \frac{\zeta_A(\epsilon_+)z_-^* + \zeta_A(\epsilon_-)z_+^*}{\zeta_A^2(\epsilon_+)\zeta_A^2(\epsilon_-)\left(\zeta_A(\epsilon_+) + \zeta_A(\epsilon_-)\right)} F(\epsilon_+)
$$
$$
\left. + \epsilon \frac{\zeta_R(\epsilon_+)z_-^* + \zeta_A(\epsilon_-)z_+}{\zeta_R^2(\epsilon_+)\zeta_A^2(\epsilon_-)\left(\zeta_R(\epsilon_+) + \zeta_A(\epsilon_-)\right)} \left[F(\epsilon_+) - F(\epsilon_-)\right] \right), \quad (5.42)
$$

where $\epsilon_\pm = \epsilon \pm \omega/2$, $z_\pm = \epsilon_\pm + i\gamma$ in agreement with Ref. [153], and $\zeta_{R/A}$ is as in

Eq. (5.29).[8] Additionally, we can see that Higgs mode couples only to the component **A** along $\mathbf{p}_s$. As discussed in Section 5.3, for small enough **q** the photon polarizations, Eq. (5.6), form an orthonormal basis in the plane and we can rotate into a frame where one photon mode is polarized along $\mathbf{p}_s$ and one is polarized perpendicular. We may then focus our attention on the former for the consideration of polariton formation as this is the only component for which Eq. (5.42) is non-zero in this basis.

Finally, the contribution to the photonic self-energy is exactly the current-current correlators responsible for the Mattis-Bardeen optical conductivity [162]. Explicit calculation gives

$$\Pi_{\text{MB}}^R = iD\frac{e^2}{c^2}\nu \int_0^\infty d\epsilon \left(\frac{z_+ z_-^* + \Delta_0^2}{\zeta_R(\epsilon_+)\zeta_A(\epsilon_-)} \left[F(\epsilon_+) - F(\epsilon_-) \right] \right.$$
$$\left. + \frac{z_+ z_- + \Delta_0^2}{\zeta_R(\epsilon_+)\zeta_R(\epsilon_-)} F(\epsilon_-) - \frac{z_+^* z_-^* + \Delta_0^2}{\zeta_A(\epsilon_+)\zeta_A(\epsilon_-)} F(\epsilon_+) \right). \quad (5.43)$$

We are then left with a 2×2 bosonic retarded Green's function in Higgs-photon space. From this we can obtain the spectral function $-2\pi i\mathcal{A} = G_R(\omega, \mathbf{q}) - G_R^\dagger(\omega, \mathbf{q})$. The dispersions of the eigenmodes can be observed by considering $\text{tr}\,\mathcal{A}(\omega, |\mathbf{q}|)$, shown in Fig. 5.4. For our numerical calculations, we used $T_c = 9.5\,\text{K}$, $\nu = 1.6 m_e/(2\pi)$, and $D = 9.4\,\text{cm}^2/\text{s}$, $T = T_c/2$. The depairing energy Γ was taken to be 0.1Δ. Cavity parameters were $\omega_0 = 1.5\Delta$ and $\kappa = 0.1\Delta$. As expected, the upper polariton branch is in the continuum and over-damped. The lower polariton branch, however, is below the two particle-gap, and well defined. This can be clearly seen by looking at cuts of the spectral function for fixed $|\mathbf{q}|$ as shown in Fig. 5.5.

In contrast to the BS-polaritons, the analytic structure of $\left[G_h^R\right]^{-1}$ precludes a Hamiltonian description of the coupled bosonic sector. This is due to a branch point

---

[8]The notation $z^* = \epsilon - i\gamma$ is chosen for compactness, but in the case where one wants to analytically continue to complex frequency $\epsilon \to w \in \mathbb{C}$, '$z^*$' should be analytically continued to $w - i\gamma$ *not* $w^* - i\gamma$.
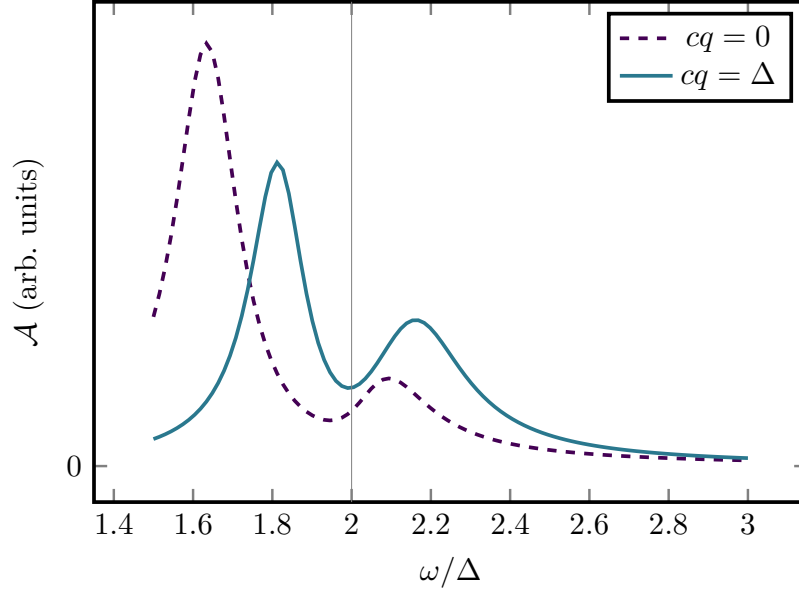
Figure 5.5: (Color online) Cut of the polariton spectral function $\mathcal{A}$ at $q = 0$ (dashed line) and $q = \Delta$ (solid line). The upper polariton is a broad feature as a function of frequency and is over-damped, but the lower polariton lies below the particle-hole continuum and appears as a sharp peak.

at $\omega \simeq 2\Delta_0 - 2i\gamma$ which forbids the usual Taylor expansion of the action about the mass-shell[106, 163]. Indeed, the momentum and frequency dependence of the action cannot be separated in the way required to construct the usual mode operators.

5.4 Discussion and Conclusion

In this chapter we have shown that driving a supercurrent through a superconductor in a planar microcavity leads to hybridization of cavity photons with collective modes of the superconductor i.e. the Bardasis-Schrieffer and Higgs modes. Which modes will hybridize is a function of the disorder strength, strength of instabilities, and resonant frequency of the gap.

In both case two polariton bands form which have significantly mixed character. This provides a means for observation and control of the Bardasis-Schrieffer and Higgs modes, and, as for exciton-polaritons, these dispersions could in principle be measured with k-space imaging of the photonic component of the polariton

states [46]. In the case of the BS-polariton, the nature of the construction allows for tuning of the hybridization strength, and therefore the polariton states, *in situ* through the externally applied supercurrent.

The condensation observed in exciton-polariton systems [45, 47, 143] suggests proper driving of these superconductor-polariton modes could lead to their condensation. In the BS case this would correspond to the formation of a non-equilibrium $s \pm id$ superconducting state; finite polariton density with coherence imposed externally, e.g. from a coherent drive, would produce a non-equilibrium state with $s \pm id$ character, which one would expect to be distinct in nature from a thermodynamic $s \pm id$ state. This is not, in principle, an unreasonable possibility. Polariton-polariton interactions, which are needed for thermalization of a driven population, naturally arise from the quartic terms in the action describing the superconducting modes themselves. For the BS case the polariton lifetime is set by the cavity photon lifetime — the BS mode is in-gap and therefore undamped in this clean model.

In the Higgs case, if the bottom of the photon dispersion is detuned below the Higgs energy, then the energy of lower polariton branch is seen to be pushed below the quasi-particle continuum and becomes under-damped. The question of what this state would be is complicated by the need to maintain self-consistency.

In either case it is in principle possible for polaritons to thermalize before decaying, allowing for a transient quasi-thermal ensemble. More work must be done, however, before definitive statements can be made about a condensed state, especially regarding spontaneous coherence of the condensate.

Chapter 6: Conclusion

In this dissertation we have been concerned with two classes of behavior in quasi-two dimensional superconductors: photo-induced enhancement and hybridization of collective modes.

In Chapter 2 we considered a theoretical model of the photo-induced enhancement of superconductivity seen in cuprates via pump-probe techniques. Therein we established that enhancement of superconductivity can be obtained due to a melting of competing charge order driven by an increase in interlayer coupling secondary to the pump pulse. Importantly, the existence of this effect is dependent on phase pinning of the charge order.

Chapter 3 considered a similar system, focusing on the behavior of collective modes within the quasi-two dimensional copper oxide planes. Motivated by time-domain reflectivity experiments we considered the interplay between amplitude (or Higgs) modes of competing superconductivity and charge order. We found that in general, the hybridization process leads to an in-gap, under-damped mode, with the characteristic frequency evolving as a function of temperature and softening as the boundaries of the coexistent phase.

In Chapter 4, we considered a different mechanism of photo-induced enhancement of superconductivity. There we proposed a model of a thin-film superconductor coupled to cavity photons and investigated the effect of the photon distribution on superconductivity. Specifically, we derived a general expression for the enhancement or suppression of superconductivity due to coupling to photons with a particular distribution and cavity spectral function. Using a proof-of-principle two-temperature model we demonstrated that depending on the nature of the cavity both a hotter and colder photon reservoir are capable of enhancing superconductivity in the thin

film.

In Chapter 5 we turned our attention back to hybridization of collective modes, this time in a photonic cavity. We showed two particular examples of polariton formation from the hybridization of a superconductor's collective mode with cavity photons. Additionaly, we characterized the parametric dependence of the hybridization strength. Finally, we discussed the possible implications of achieving condensation of the polariton modes.

Appendix A: Microscopic evaluation of the coefficients in Ginzburg-Landau theory

A.1 Low energy model away from $k_z = 0$
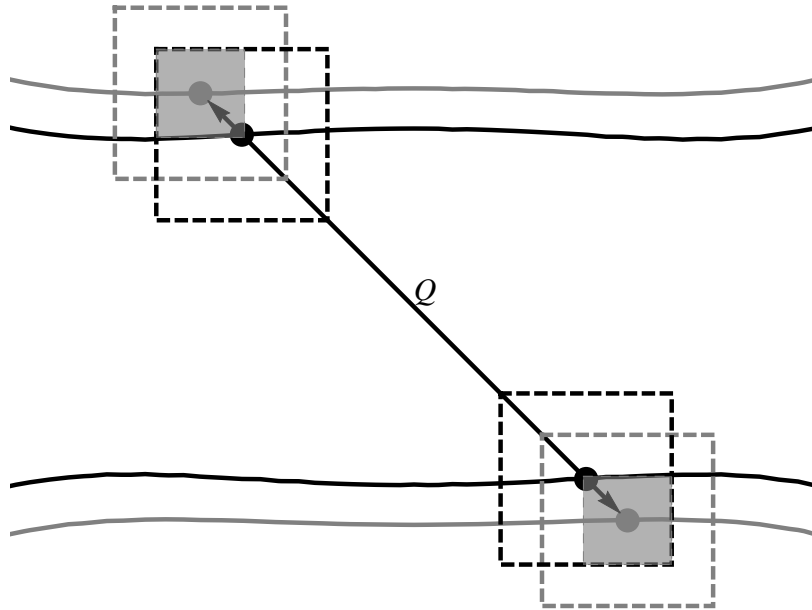
Figure A.1: Different choices of hot regions for charge integrals. The gray dashed lines denotes the *unmoving* hot regions. The black dashed lines represent the *moving* hot regions, where one must be careful to avoid double counting. Finally the gray-filled areas represent the *truncated* hot regions.

As discussed in Section 2.4 there are subtleties associated with defining the hotspot model for stacked planes with inter-plane hopping. Specifically, one has to define the integrals involving charge order such that the separation between paired particles remains constant with k_z, despite the fact that the Fermi surface changes shape. We considered three different methods of handling this issue. Each

is depicted in Fig. A.1. In all cases the coefficients Π_{SC} and u_{SC} are unchanged, so we only need to decide how to implement the other three: Π_{BDW}, u_{BDW} and w.
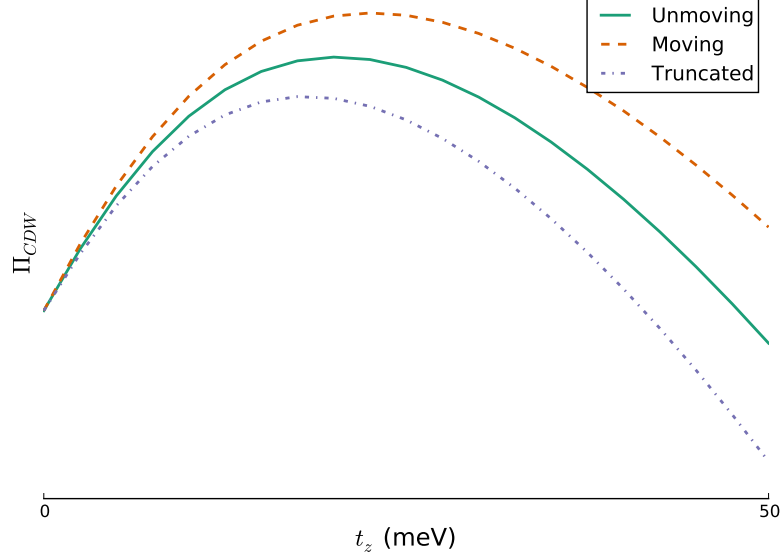
Figure A.2: Quadratic susceptibilities as a function of c-axis hopping for different choices of integration region in integrals involving charge order. The qualitative behavior is the same for all three schemes.

The first is to define two different hot regions: one remains bound to the Fermi surface and is associated with superconductivity, the other corresponds to the $k_z = 0$ hot regions for all k_z and is associated with charge order. All integrals involving charge order are done over the unmoving hotspots. We label this procedure the *unmoving* approximation.

Another approach is to perform the charge order integrations over the same hot regions as the superconducting terms, but enforce that pairing occur between particles separated by the fixed ordering vector $\vec{Q}$. We label this the *moving* approximation.

A final approach, and the one we used in this work, is to take a similar tact as the moving approximation, but to further restrict the integration such that both of the paired particles lie in a hot region. We will call this the *truncated* approximation. If we are committed to the notion that only fermions near the hotspots are important,

this seems the most natural of the approximations, as we are then only counting the fermions that live within the true hot regions. The coefficients Π_{BDW}, u_{BDW}, and w are shown for a range of t_z in Fig. A.2. As can be seen, while the results differ numerically, the qualitative behavior is the same. Since the hotspot model is itself a qualitative model, we chose to adopt the *truncated* approximation as it seemed the most in line with the spirit of the model.

While these issues make the 3D model slightly more complicated, the qualitative behavior of the system appears to be fairly robust to their method of resolution. This suggests that the extended model, like its simpler progenitor, can be used as a tool to uncover general physical mechanisms underlying the complicated behavior of various lattice models.

A.2   Microscopic expressions for Landau coefficients

As discussed in Section 2.5, the Landau theory for competing orders in this model takes the form

$$\mathcal{F}_O[\theta] = \alpha_\Delta |\Delta|^2 + \beta_\Delta |\Delta|^4 + \alpha_{\phi,O}[\theta]|\phi|^2 + \beta_{\phi,O}[\theta]|\phi|^4 + \gamma_O[\theta]|\phi|^2|\Delta|^2, \quad (A.1)$$

The quadratic Landau coefficients are simply related to the susceptibilities in the corresponding channels

$$\alpha_\Delta = \frac{1}{g_\Delta} - \Pi_\Delta, \qquad \alpha_\phi = \frac{1}{g_\phi} - \Pi_\phi \qquad (A.2)$$

The superconducting terms are simplest, with

$$\Pi_\Delta = \sum_{\mathbf{k}} f^1(\mathbf{k})^2 \sum_{\pm} \frac{\tanh \frac{\epsilon_{\mathbf{k},\pm}}{2T}}{2\epsilon_{\mathbf{k},\pm}} \qquad (A.3)$$

and

$$\beta_\Delta = \sum_{\mathbf{k}} f^1(\mathbf{k})^2 \sum_\pm \frac{1}{2\epsilon_{\mathbf{k},\pm}} \left[\frac{\tanh \frac{\epsilon_{\mathbf{k},\pm}}{2T}}{2\epsilon_{\mathbf{k},\pm}} + n'_f(\epsilon_{\mathbf{k},\pm}) \right], \tag{A.4}$$

where $\epsilon_{\mathbf{k},\pm} = \xi_{\mathbf{k}} \pm t_{\mathbf{k}}$ are the eigenvalues of the free Hamiltonian.

As mentioned above the terms involving ϕ can be broken into coefficients of $\cos^n \theta$. Beginning with the dFF-DW susceptibility

$$\Pi_\phi^{(n)} = \sum_{\mathbf{k}} f^1(\mathbf{k})^2 \sum_{\lambda\lambda'} (-1)^{n(\lambda-\lambda')} \Pi(\epsilon_{\mathbf{k},\lambda}, \epsilon_{\mathbf{k},\lambda'}) \tag{A.5}$$

where

$$\Pi(\epsilon_1, \epsilon_2) = \frac{n_f(\epsilon_2) - n_f(\epsilon_1)}{\epsilon_1 - \epsilon_2}. \tag{A.6}$$

The quartic dFF-DW terms are

$$\beta_\phi^{(1)} = \sum_{\mathbf{k}} \sum_{\lambda\lambda'} (-1)^{\lambda-\lambda'} \left[\frac{1}{2} f^1(\mathbf{k})^4 M_{\beta,1}(\epsilon_\lambda(\mathbf{k}+\mathbf{Q}2), \epsilon_{\lambda'}(\mathbf{k}-\mathbf{Q}2)) \right.$$
$$\left. + f^1(\mathbf{k}+\mathbf{Q})^2 f^1(\mathbf{k}-\mathbf{Q})^2 M_{\beta,2}(\epsilon_\lambda(\mathbf{k}), \epsilon_{\lambda'}(\mathbf{k}-\mathbf{Q}), \epsilon_{\lambda'}(\mathbf{k}+\mathbf{Q})) \right] \tag{A.7}$$

and

$$\beta_\phi^{(0,2)} = \sum_{\mathbf{k}} \left\{ f^1(\mathbf{k})^4 \left[\frac{1}{4} \sum_{\lambda\lambda'} M_{\beta,1}(\epsilon_\lambda(\mathbf{k}+\mathbf{Q}2), \epsilon_{\lambda'}(\mathbf{k}-\mathbf{Q}2)) \right. \right.$$
$$\left. \mp M_{\beta,3}(\{\epsilon_\lambda(\mathbf{k}+\zeta\mathbf{Q})\}_{\lambda,\zeta}) \pm \sum_\lambda M_{\beta,2}(\epsilon_\lambda(\mathbf{k}-\mathbf{Q}/2), \epsilon_{\lambda'}(\mathbf{k}+\mathbf{Q}/2), \epsilon_{-\lambda}(\mathbf{k}+\mathbf{Q}/2)) \right]$$
$$+ f^1(\mathbf{k}+\mathbf{Q})^2 f^1(\mathbf{k}-\mathbf{Q})^2 \left[\frac{1}{2} \sum_{\lambda_1,\lambda_2,\lambda_3} (\pm 1)^{\lambda_2-\lambda_3} M_{\beta,2}(\epsilon_{\lambda_1}(\mathbf{k}), \epsilon_{\lambda_2}(\mathbf{k}-\mathbf{Q}), \epsilon_{\lambda_3}(\mathbf{k}+\mathbf{Q})) \right.$$
$$\left. \left. \mp \sum_{\lambda\lambda'} (-1)^{\lambda-\lambda'} M_{\beta,3}(\{\epsilon_+(\mathbf{k}), \epsilon_-(\mathbf{k}), \epsilon_\lambda(\mathbf{k}+\mathbf{Q}), \epsilon_{\lambda'}(\mathbf{k}-\mathbf{Q})\}) \right] \right\}, \tag{A.8}$$

where we have defined

$$M_{\beta,1}(x,y) = \frac{1}{(x-y)^2}\left(\frac{\tanh\frac{x}{2T} - \tanh\frac{y}{2T}}{x-y} + n_f'(x) + n_f'(y)\right)$$

$$M_{\beta,2}(x,y,z) = \frac{1}{z-y}\left(\frac{n_f(z)}{(x-z)^2} - \frac{n_f(y)}{(x-y)^2}\right)$$

$$+ \frac{1}{(x-z)(x-y)}\left[n_f'(x) - n_f(x)\left(\frac{1}{x-z} + \frac{1}{x-y}\right)\right]$$

$$M_{\beta,3}(\{x_i\}) = \sum_i \prod_{j\neq i} \frac{n_f(x_i)}{x_i - x_j}.$$

(A.9)

Finally for the competition term

$$\gamma^{(n)} = \sum_{\mathbf{k}} f^1(\mathbf{k})^2 f^1(\mathbf{k}_+) \sum_{\lambda\lambda'}$$

$$\times (-1)^{n(\lambda-\lambda')}\left[f^1(\mathbf{k}_+)M_{\gamma,2}(\epsilon_\lambda(\mathbf{k}_+), \epsilon_\lambda(\mathbf{k}_-))\right.$$

$$\left. - f^1(\mathbf{k}_-)M_{\gamma,1}(\epsilon_\lambda(\mathbf{k}_+), \epsilon_\lambda(\mathbf{k}_-))\right] \quad \text{(A.10)}$$

where $\mathbf{k}_\pm = \mathbf{k} \pm \mathbf{Q}/2$ and we have defined

$$M_{\gamma,1}(x,y) = \frac{1}{(x)^2 - (y)^2}\left(\frac{\tanh\frac{y}{2T}}{2y} - \frac{\tanh\frac{x}{2T}}{2x}\right)$$

$$M_{\gamma,2}(x,y) = \frac{1}{2x}\left[\frac{n_f'(x)}{x-y} - \frac{\tanh\left(\frac{x}{2T}\right)}{2x(x+y)}\right] + (x \leftrightarrow y).$$

(A.11)

Appendix B: Effect of phonons on hybridization of Higgs modes

Beyond just the non-retarded interaction considered above, one can also consider the effect of phonons on the collective modes. Here we will take this into account by considering the contribution of the frequency dependent phonon-mediated interaction between electrons to the collective mode propagators. In particular, we will project this interaction onto a hot-spot model by taking the phonon momentum to be the fixed wavevector $\mathbf{Q}$ separating the hot-spots which are being paired – this is the same approximation that one uses on the non-retarded interaction in deriving the hot-spot model.

A simple A_{1g} symmetry phonon has no effect on the collective modes due to the pure d-wave symmetry of the order parameters. However, in reality we expect some direct order parameter-phonon coupling, either because there is a phonon mode with the correct symmetry (B_{1g}), or because in real systems the order parameter would not necessarily have a pure d-wave symmetry, but could have an s-wave component admixed. Regardless of the exact nature of the coupling, it gives rise to a term in the mean field theory which includes the phonon-mediated interaction as

$$H_{ph} = f \sum_{k,\epsilon_n,\omega_m} U(\omega_m) \left(\phi(\omega_m) c_{1\sigma}^\dagger(k, \epsilon_n - \omega_m) c_{2\sigma}(k, \epsilon_n) + h.c. \right) \tag{B.1}$$

where

$$U(\omega_m) = \frac{g_{\text{ep}}^2}{2} \frac{\Omega_Q}{\omega_m^2 + \Omega_Q^2}$$

is an Einstein phonon type propagator and f is a constant of order one arising from the form factor of the electron-phonon vertex.

If we consider the effect of this term on the charge collective mode, we find
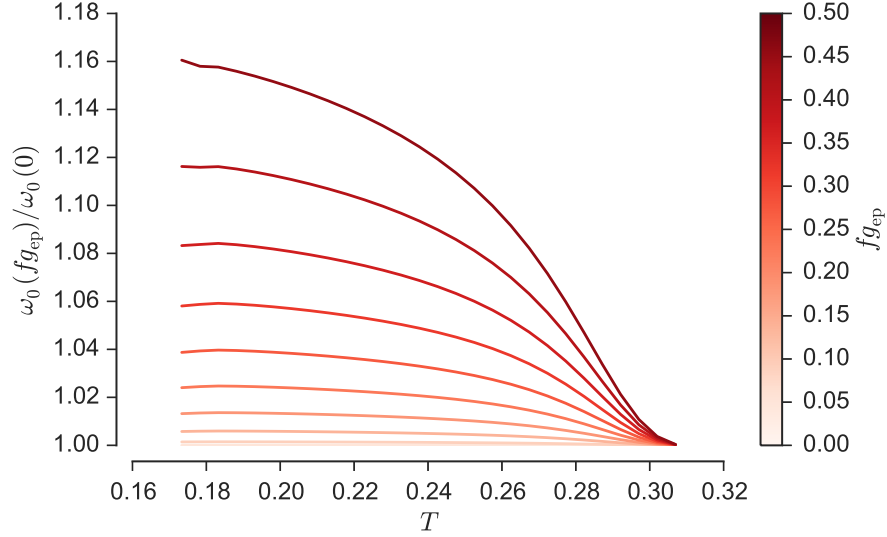
Figure B.1: The in-gap collective mode mass ω_0 (relative to the $g_{ep} = 0$ case) as a function of the electron phonon coupling g_{ep}, for $\Omega_Q = 1$. The $g_{ep} = 0$ line corresponds to the behavior shown in Fig. 3.2.

that it can be captured by the replacement $g_c \to \tilde{g}_c(i\omega_m)$. We absorb the $\omega = 0$ component into the definition of g_c (as that is what determines the static mean-field solution) and include the remaining frequency dependent part in our calculation of the collective modes. Upon analytic continuation to real frequency, this amounts to the substitution

$$g_c \to \tilde{g}_c(\omega) = g_c - \frac{fg_{ep}^2}{\Omega} - fg_{ep}^2 \frac{\Omega}{\omega^2 - \Omega^2} \tag{B.2}$$

in the collective mode equations (the additive constant is chosen so that we recover $\tilde{g}_c(\omega = 0) = g_c$). The previous analysis can now be repeated for a range of electron phonon couplings. As can be seen in Fig. B.1, the coupling to phonons tends to push the collective mode mass slightly upward, while leaving the softening at the phase transitions unmodified. Overall, the qualitative behavior of the mode is not markedly different.

Appendix C: Effective photonic spectral function

The function $J(\omega)$ which appears in Eq. (4.33) can be calculated by relating the field $\mathbf{A}$ to the cavity mode operators $a, \bar{a}$. The details of this depend on the nature of the cavity but the procedure is general. Here we demonstrate how to obtain $J(\omega)$ for the two types of cavity considered in Chapter 4.

C.1   Multimode Cavity

As an example of a multimode cavity we take the cavity mode Keldysh action to be given by

$$iS = i \int \frac{d\omega}{2\pi} \int \frac{d\mathbf{q}}{(2\pi)^2} \bar{a}_{q;\alpha} \underbrace{\begin{pmatrix} 0 & \omega - i\kappa - \omega_q \\ \omega + i\kappa - \omega_q & 2i\kappa N(\omega) \end{pmatrix}}_{\hat{G}^{-1}(\omega, \mathbf{q})} a_{q;\alpha}. \qquad \text{(C.1)}$$

to describe a cavity coupled to the environment [164]. Using the fact that we can expression $\mathbf{A}$ in terms of a and $\bar{a}$ (in Gaussian units) as

$$\mathbf{A}_q(z) = \sqrt{\frac{2\pi c^2}{\omega_q}} \left(a_{q;\alpha} \epsilon_{\mathbf{q};\alpha}(z) + \bar{a}_{-q;\alpha} \epsilon^*_{-\mathbf{q};\alpha}(z) \right) \qquad \text{(C.2)}$$

we can relate the Keldysh component of S and G

$$2S^K_{\omega,\mathbf{q};ii}(L/2, L/2) = \frac{2\pi c^2}{\omega_q} \sum_\alpha |\epsilon^i_{\mathbf{q};\alpha}(L/2)|^2 \left(G^K_{-q} + G^K_q \right) \qquad \text{(C.3)}$$

After some calculation we therefore find

$$J_{\text{MM}}(\omega) = \int \frac{d\mathbf{q}}{(2\pi)^2} \frac{\kappa c^2}{\omega_q} \sum_\alpha \left| \epsilon_{\mathbf{q};\alpha} \left(\frac{L}{2} \right) \right|^2 \left(\frac{1}{(\omega - \omega_q)^2 + \kappa^2} - \frac{1}{(\omega + \omega_q)^2 + \kappa^2} \right) \qquad \text{(C.4)}$$

where we have used the fact that $\epsilon(L/2)$ is in plane. Now with the explicit forms of ϵ_i from the main text

$$
\hat{\epsilon}_{1,\mathbf{q}}(L/2) = -i\sqrt{\frac{2}{L}\frac{\omega_0}{\omega_\mathbf{q}}}\frac{\mathbf{q}}{|\mathbf{q}|}
$$
$$
\hat{\epsilon}_{2,\mathbf{q}}(L/2) = \sqrt{\frac{2}{L}}\mathbf{e}_3 \times \frac{\mathbf{q}}{|\mathbf{q}|}
$$

(C.5)

we can immediately evaluate the angular integral

$$
\int \frac{d\theta}{2\pi}\sum_{i\in x,y,\alpha}|\epsilon^i_{\theta,\alpha}(L/2)|^2 = \frac{2}{L}\left(1 + \frac{\omega_0^2}{\omega_\mathbf{q}^2}\right).
$$

(C.6)

We now make a change of variables from $|\mathbf{q}| \to \omega' = \omega_\mathbf{q}$. The dispersion relation $\omega_q^2 = \omega_0^2 + c^2 q^2$ implies

$$
\frac{qdq}{2\pi\omega'} = \frac{d\omega'}{2\pi c^2}.
$$

(C.7)

This allows us to write J as

$$
J_{\mathrm{MM}}(\omega) = \frac{2\kappa}{L}\int_{\omega_0}^{\infty} d\omega'\left(\frac{1}{(\omega - \omega')^2 + \kappa^2} - \frac{1}{(\omega + \omega')^2 + \kappa^2}\right)\left(1 + \frac{\omega_0^2}{\omega'^2}\right).
$$

(C.8)

This integral may be performed exactly to find

$$
J_{\mathrm{MM}}(\omega) = \frac{2}{L}\left[\left(1 + \omega_0^2\frac{\omega^2 - \kappa^2}{(\omega^2 + \kappa^2)^2}\right)\left(\tan^{-1}\frac{\omega - \omega_0}{\kappa} + \tan^{-1}\frac{\omega + \omega_0}{\kappa}\right)\right.
$$
$$
\left. + \frac{\kappa\omega\omega_0^2}{(\omega^2 + \kappa^2)^2}\log\left(\frac{\left((\omega - \omega_0)^2 + \kappa^2\right)\left((\omega + \omega_0)^2 + \kappa^2\right)}{\omega_0^4}\right)\right].
$$

(C.9)

We will, however, introduce a factor X into J which describes enhancement of the electron-photon coupling due to e.g. squeezing of mode volume, one factor of $\sqrt{X}$ coming from the enhancement of each vertex. In principle this enhancement should come from a detailed study of the structure of the photon modes. However, this physics is not captured within our simple parallel plate model and so we include the

coupling enhancement phenomenonlogically via the factor X

$$J_{\text{eff}}(\omega) = X J(\omega). \tag{C.10}$$

C.2   Single mode cavity

We can also consider the effective photonic spectral function for a single mode cavity

$$iS = i \int \frac{d\omega}{2\pi} \bar{a}_\alpha(\omega) \underbrace{\begin{pmatrix} 0 & \omega - i\kappa - \omega_0 \\ \omega + i\kappa - \omega_0 & 2i\kappa N(\omega) \end{pmatrix}}_{\hat{G}^{-1}(\omega)} a_\alpha(\omega). \tag{C.11}$$

Following the steps outlined above we find that

$$J_{\text{eff;SM}}(\omega) = \frac{\kappa c^2 X}{\omega_0} \sum_\alpha \left| \epsilon_\alpha\left(\frac{L}{2}\right) \right|^2 \left(\frac{1}{(\omega - \omega_0)^2 + \kappa^2} - \frac{1}{(\omega + \omega_0)^2 + \kappa^2} \right). \tag{C.12}$$

Appendix D: Numerical solution for modes

The numerical method begins a with the effective Gaussian Matsubara action describing the coupled Bardasis-Schrieffer cavity-photon system. Schematically this is

$$S = -\frac{1}{2\beta} \sum_q \begin{pmatrix} d_{-q} & \mathbf{A}_{-q} \end{pmatrix} \begin{pmatrix} D_{\mathrm{BS}}(q)^{-1} & \mathbf{g}(i\Omega_m) \\ \mathbf{g}(-i\Omega_m) & \hat{D}_{\mathrm{phot}}^{-1} \end{pmatrix} \begin{pmatrix} d_q \\ \mathbf{A}_q \end{pmatrix}, \qquad (\mathrm{D.1})$$

where the cavity propagator $\hat{D}_{phot}^{-1} = \hat{D}_0^{-1} - \hat{\Pi}$ includes the self-energy due to the superconductor. At this stage the polariton modes can be found by solving for the frequency $z = i\Omega_m$ at which the inverse of the Green's function matrix vanishes. To do so, we numerically solve for the roots of the determinant of the inverse Green's function $\det \hat{D}^{-1}(\Omega_{\mathbf{q}i}, \mathbf{q}) = 0$. In particular the following algorithm was employed at each $\mathbf{q}$: noting that there are three roots that we are searching for

1. An interval $[\omega_l, \omega_u]$ is chosen within which to search for solutions.

2. An extremum f of $\det \hat{D}^{-1}(\Omega, \mathbf{q})$ with respect to Ω is located by finding the roots of the first derivative with respect to Ω using the Newton-Raphson method in the vicinity of the Bardasis-Schrieffer frequency Ω_{BS}.

3. The other extremum is found by searching for the root of the first derivative in the interval (ω_l, f) or (f, ω_u) as determined by the sign of the function at the endpoints. This gives us two extrema $\{f_0, f_1\}$.

4. Roots of $\det \hat{D}^{-1}(\Omega, \mathbf{q})$ are searched for using the Brent-Dekker method in the intervals (ω_l, f_0), (f_0, f_1), and (f_1, ω_u)

Numerical integration and root-finding were performed using the GSL Scientific Library [165].

Appendix E: Non-linear σ model in the case of finite supercurrent

E.1 Solution of the bulk Usadel equation with a uniform supercurrent

Writing the retarded quasi-classical Green's function as

$$\hat{Q}_{\mathrm{sp}}^{R}(\epsilon) = \cosh\theta_{\epsilon}\,\hat{\tau}_{3} + i\sinh\theta_{\epsilon}\,\hat{\tau}_{2} \tag{E.1}$$

one obtains the retarded Usadel equation in the form

$$\Delta\cosh\theta_{\epsilon} - \epsilon\sinh\theta_{\epsilon} = i\frac{\Gamma}{2}\sinh 2\theta_{\epsilon}. \tag{E.2}$$

In the absence of a supercurrent it is straightforward to solve the Usadel equation for a bulk superconductor

$$\tanh\theta_{\epsilon} = \frac{\Delta}{\epsilon}. \tag{E.3}$$

For a finite supercurrent the solution is not so simple. It is convenient to reparametrize the problem using the Ricatti parametrization

$$\begin{aligned}
\cosh\theta_{\epsilon} &= \frac{1 + \xi_{\epsilon}^{2}}{1 - \xi_{\epsilon}^{2}} \\
\sinh\theta_{\epsilon} &= \frac{2\xi_{\epsilon}}{1 - \xi_{\epsilon}^{2}}.
\end{aligned} \tag{E.4}$$

In terms of the Ricatti parameter ξ the Usadel equation can be rewritten

$$\xi^{4} + 2(\tilde{\epsilon} + i\tilde{\Gamma})\xi^{3} - 2(\tilde{\epsilon} - i\tilde{\Gamma})\xi - 1 = 0 \tag{E.5}$$

where we have defined $\tilde{\epsilon} = \epsilon/\Delta$ and $\tilde{\Gamma} = \Gamma/\Delta$. This rewriting introduces two extraneous roots of complex magnitude 1, with the remaining two roots describing the advanced and retarded solutions of the Usadel equation. Being a quartic equation, there a closed form solutions. The difficulty arises in uniquely determining the root corresponding to the retarded solution for every ϵ. Here we may use our knowledge of the structure of the solution and the limiting cases to simplify things.

First, we note that Eq. (E.5) is a self-inversive polynomial. In this case, this implies that for any root x, $-1/x^*$ is also a root. We also know that there are always at least to uni-modular roots. This means that there are two possible cases, either there are four unimodular roots are there are two unimodular extraneous roots and two distinct physical roots $x, -1/x^*$.

Eq. (E.5) can be rewritten

$$\left(e^{-i\phi}\xi^2 - 2\xi\rho + e^{i\phi}\right)\left(e^{i\phi}\xi^2 + 2i\xi\mu - e^{-i\phi}\right) = 0, \tag{E.6}$$

with μ, ρ, and ϕ currently undetermined. By matching the coefficients of the linear and cubic terms and comparing with the original equation we obtain a system of equations which be solved for the relations

$$\begin{aligned}
\rho &= \sec 2\phi \left(\tilde{\epsilon}\cos\phi + \tilde{\Gamma}\sin\phi\right) \\
\mu &= -\sec 2\phi \left(\tilde{\Gamma}\cos\phi + \tilde{\epsilon}\sin\phi\right).
\end{aligned} \tag{E.7}$$

The remaining non-trivial equation comes from the quadratic term and gives us the depressed cubic equation

$$y^3 + (\tilde{\Gamma}^2 + \tilde{\epsilon}^2 - 1)y + 2\tilde{\epsilon}\tilde{\Gamma} = 0 \tag{E.8}$$

for $y = \sin 2\phi$. Defining the quantities

$$p = \tilde{\Gamma}^2 + \tilde{\epsilon}^2 - \Delta^2$$
$$q = 2\tilde{\epsilon}\tilde{\Gamma}$$

(E.9)

the nature of the solutions is different depending on the sign of $4p^3 + 27q^2$. This is the position of the branch point. For $4p^3 + 27q^2 > 0$ there is only one real solution to Eq. (E.8). For the other case we must however choose the correct root. We do so by choosing the solution that is continuously connected to the real solution for $4p^3 + 27q^2 > 0$. In this way we arrive at

$$
y = \begin{cases}
-2\sqrt{\frac{-p}{3}}\,\mathrm{sgn}\,q\cosh\left(\frac{1}{3}\cosh^{-1}\left(\frac{-3|q|}{2p}\sqrt{\frac{-p}{3}}\right)\right), & 4p^3 + 27q^2 > 0 \cap p < 0 \\
2\sqrt{\frac{p}{3}}\sinh\left(\frac{1}{3}\sinh^{-1}\left(\frac{3q}{2p}\sqrt{\frac{p}{3}}\right)\right), & 4p^3 + 27q^2 > 0 \cap p > 0 \\
2\sqrt{\frac{-p}{3}}\cos\left(\frac{1}{3}\cos^{-1}\left(\frac{3q}{2p}\sqrt{\frac{-p}{3}}\right) - \frac{4\pi}{3}\right), & 4p^3 + 27q^2 \le 0.
\end{cases}
$$

(E.10)

We must now choose the correct angle ϕ. The four possible choices of ϕ correspond to a permutation of the form of the roots. In general, we can choose a prescription for ϕ such that the full solution can then be written in the form

$$\xi_\epsilon = e^{i\phi_\epsilon}\left(\rho_\epsilon - \sqrt{(\rho_\epsilon + i0^+)^2 - 1}\right),$$

(E.11)

which is to be compared with the supercurrent-free result

$$\xi_\epsilon^0 = \tilde{\epsilon} - \sqrt{(\tilde{\epsilon} + i0^+)^2 - 1}.$$

(E.12)

The correct prescription is

$$\sin^{-1}(\cdots) \in [-\pi, \pi]$$

$$\phi = \begin{cases} \frac{1}{2} \sin^{-1} y, & |\epsilon| > \Gamma \\ \\ -\frac{\pi}{2} - \frac{1}{2} \sin^{-1} y & |\epsilon| < \Gamma. \end{cases} \tag{E.13}$$

All the above is done for the case of infinitessimal damping. The finite damping case can be solved by analytically continuing the above solution from $\epsilon + i0^+ \to \epsilon + i\gamma$.

E.2   Evaluation of the diffusive mode vertices

The vertices $\hat{r}_{\epsilon\epsilon'}$ and $\hat{s}_{\epsilon\epsilon'}$ appearing in Eq. (5.33) can be expressed in terms of the parametrization, Eq. (5.31), of the saddle-point solution as

$$\begin{aligned} \left[s^c_{\epsilon\epsilon'}\right]_{(R/A)\beta} &= \frac{i}{2} \operatorname{tr} \hat{\tau}_1 \hat{I}_{(R/A)} \check{X}^{\beta 2}_{\epsilon\epsilon'} \\ \left[s^d_{\epsilon\epsilon'}\right]_{(cl/q)\beta} &= \frac{i}{2} \operatorname{tr} \hat{\sigma}_\mp \check{X}^{\beta 2}_{\epsilon\epsilon'} \\ \left[r^c_{\epsilon\epsilon'}\right]_{(R/A)\beta} &= \frac{i}{2} \operatorname{tr} \hat{\tau}_1 \hat{I}_{(R/A)} \left(\check{X}^{03}_{\epsilon\epsilon} \check{X}^{\beta 3}_{\epsilon\epsilon'} + \check{X}^{\beta 3}_{\epsilon\epsilon'} \check{X}^{03}_{\epsilon'\epsilon'} \right) \\ \left[r^d_{\epsilon\epsilon'}\right]_{(cl/q)\beta} &= \frac{i}{2} \operatorname{tr} \tau_1 \hat{\sigma}_\mp \left(\check{X}^{03}_{\epsilon\epsilon} \check{X}^{\beta 3}_{\epsilon\epsilon'} + \check{X}^{\beta 3}_{\epsilon\epsilon'} \check{X}^{03}_{\epsilon'\epsilon'} \right), \end{aligned} \tag{E.14}$$

where we have defined

$$\check{X}^{st}_{\epsilon\epsilon'} = \check{R}_\epsilon \hat{\sigma}_s \hat{\tau}_t \check{R}^{-1}_{\epsilon'} \hat{\sigma}_3 \hat{\tau}_3 \tag{E.15}$$

and $\hat{I}_{R/A} = (\hat{\sigma}_0 \pm \sigma_3)/2$. If we define $\bar{\theta}_\pm = (\theta_\epsilon \pm \theta_{\epsilon'})/2$ and $\tilde{\theta}_\pm = (\theta_\epsilon \pm \theta_{\epsilon'}^*)/2$ we can express the traces as

$$\hat{s}_{\epsilon\epsilon'}^c = \begin{bmatrix} -\cosh\bar{\theta}_+ & -F\cosh\bar{\theta}_+ \\ \cosh\bar{\theta}_+^* & -F'\cosh\bar{\theta}_+^* \end{bmatrix} \tag{E.16}$$

$$\hat{s}_{\epsilon\epsilon'}^d = \begin{bmatrix} (F'-F)\sinh\tilde{\theta}_+ & (FF'-1)\sinh\tilde{\theta}_+) \\ 0 & \sinh\tilde{\theta}_+^* \end{bmatrix} \tag{E.17}$$

$$\hat{r}_{\epsilon\epsilon'}^c = 2i \begin{bmatrix} \sinh 2\bar{\theta}_+ \cosh\bar{\theta}_- & F\sinh 2\bar{\theta}_+ \cosh\bar{\theta}_- \\ \sinh 2\bar{\theta}_+^* \cosh\bar{\theta}_-^* & -F'\sinh 2\bar{\theta}_+^* \cosh\bar{\theta}_-^* \end{bmatrix} \tag{E.18}$$

$$\hat{r}_{\epsilon\epsilon'}^d = 2i \begin{bmatrix} (F-F')e^{\tilde{\theta}_+}\cosh\tilde{\theta}_+ \sinh\tilde{\theta}_- & (1-FF')e^{\tilde{\theta}_+}\cosh\tilde{\theta}_+ \sinh\tilde{\theta}_- \\ 0 & \sinh 2\tilde{\theta}_+^* \sinh\tilde{\theta}_-^* \end{bmatrix} \tag{E.19}$$

where $F = F(\epsilon)$ and $F' = F(\epsilon')$.

E.3 Exact Parametrization of the Bosonic action for finite supercurrent

The expression for the Higgs-photon action can be put into a more familiar form, reminiscent of Ref. [153], using the parametrization

$$\theta_\epsilon = \theta_\epsilon^0 + \phi_\epsilon \tag{E.20}$$

where θ_ϵ^0 is the spectral angle for the quasi-classical Green's function in the absence of a supercurrent (c.f. Eq. (5.29)). In terms of the Ricatti parametrization introduced in Appendix E.1 we have

$$\tanh\phi_\epsilon = \frac{\Delta(1+\xi_\epsilon^2) - 2z\xi_\epsilon}{z(1+\xi_\epsilon^2) - 2\Delta\xi_\epsilon}, \tag{E.21}$$

where $z = \epsilon + i\gamma$. Using this parameterization the inverse Cooperon and diffuson propagators are

$$
\begin{aligned}
\mathcal{D}^{-1}_{\epsilon_+\epsilon_-} = & -Dq^2 + i\zeta_R(\epsilon_+)\cosh\phi_+ + i\zeta_A(\epsilon_-)\cosh\phi_-^* \\
& - \frac{\Gamma}{\zeta_R(\epsilon_+)^2\zeta_A(\epsilon_-)^2} \\
& \times \left[\zeta_R(\epsilon_+)\zeta_A(\epsilon_-) + (z_+z_-' - \Delta_0^2)\cosh(\phi_+ - \phi_-^*) - \Delta_0(\omega + 2i\gamma)\sinh(\phi_+ - \phi_-^*)\right] \\
& \times \left[(z_+z_-' + \Delta_0^2)\cosh(\phi_+ + \phi_-^*) + 2\Delta_0\epsilon\sinh(\phi_+ + \phi_-^*)\right] \\
\left[\mathcal{C}^{R}_{\epsilon_+\epsilon_-}\right]^{-1} = & -Dq^2 + i\zeta_R(\epsilon_+)\cosh\phi_+ + i\zeta_R(\epsilon_-)\cosh\phi_- \\
& - \frac{\Gamma}{\zeta_R(\epsilon_+)^2\zeta_R(\epsilon_-)^2} \\
& \times \left[\zeta_R(\epsilon_+)\zeta_A(\epsilon_-) + (z_+z_- - \Delta_0^2)\cosh(\phi_+ - \phi_-) - \Delta_0\omega\sinh(\phi_+ - \phi_-)\right] \\
& \times \left[(z_+z_- + \Delta_0^2)\cosh(\phi_+ + \phi_-) + 2\Delta_0 z\sinh(\phi_+ + \phi_-)\right]
\end{aligned}
\tag{E.22}
$$

where $z' = \epsilon - i\gamma$. The above, in combination with the matrix elements derived in Appendix E.2, can be inserted into Eq. (5.39) to obtain the Gaussian bosonic propagator to all orders in the supercurrent.

Bibliography

[1] H. Kamerlingh Onnes, "On the sudden change in the rate at which the resistance of mercury disappears", Commun. Phys. Lab. Univ. Leiden **124** (1911).

[2] F. London and H. London, "The electromagnetic equations of the supraconductor", Proc. Royal Soc. Lond. A **149**, 71 (1935).

[3] V. L. Ginzburg and L. D. Landau, "On the theory of superconductivity", Zh. Eksp. Teor. Fiz. **20**, 1064 (1950).

[4] J. Bardeen, L. N. Cooper, and J. R. Schrieffer, "Theory of superconductivity", Phys. Rev. **108**, 1175 (1957).

[5] N. N. Bogoliubov, "A new method in the theory of superconductivity. I", J. Exp. Theor. Phys. **7**, 41 (1958); V. Tolmachev and S. Tiablikov, "A new method in the theory of superconductivity. II", ibid. **7**, 46 (1958); N. N. Bogoliubov, "A new method in the theory of superconductivity. III", ibid. **7**, 51 (1958).

[6] J. G. Valatin, "Comments on the theory of superconductivity", Il Nuovo Cimento **7**, 843 (1958).

[7] A. A. Abrikosov, "On the magnetic properties of superconductors of the second group", J. Exp. Theor. Phys. **5**, 1174 (1957).

[8] L. P. Gor'kov, "On the energy spectrum of superconductors", J. Exp. Theor. Phys. **7**, 158 (1958).

[9] L. P. Gor'kov, "Microscopic derivation of the ginzburg-landau equations in the theory of superconductivity", J. Exp. Theor. Phys. **9**, 1364 (1959).

[10] J. G. Bednorz and K. A. Müller, "Possible high T_c superconductivity in the Ba-La-Cu-O system", Z. Phys. B **110**, 189 (1986).

[11] W. Meissner and R. Ochsenfeld, "Ein neuer Effekt bei Eintritt der Supraleitfähigkeit", Die Naturwissenschaften **21**, 787 (1933).

[12] A. F. G. Wyatt, V. M. Dmitriev, W. S. Moore, and F. W. Sheard, "Microwave-enhanced critical supercurrents in constricted tin films", Phys. Rev. Lett **16**, 1166 (1966).

[13] A. H. Dayem and J. J. Wiegand, "Behavior of thin-film superconducting bridges in a microwave field", Phys. Rev. **155**, 419 (1967).

[14] G. M. Eliashberg, "Film superconductivity stimulated by a high-frequency field", JETP Lett. **11**, 114 (1970).

[15] B. I. Ivlev, S. G. Lisitsyn, and G. M. Eliashberg, "Nonequilibrium excitations in superconductors in high-frequency fields", J. Low. Temp. Phys **10**, 449 (1973).

[16] K. D. Usadel, "Generalized diffusion equation for superconducting alloys", Phys. Rev. Lett **25**, 507 (1970).

[17] B. Ivlev and G. Eliashberg, "Influence of nonequilibrium excitations on the properties of superconducting films in a high-frequency field", Jetp Lett. **13**, 333 (1971).

[18] M. V. Feigel'man, A. Larkin, and M. A. Skvortsov, "Keldysh action for disordered superconductors", Phys. Rev. B **61**, 12361 (2000).

[19] K. S. Tikhonov, M. A. Skvortsov, and T. M. Klapwijk, "Superconductivity in the presence of microwaves: full phase diagram", Phys. Rev. B **97**, 184516 (2018).

[20] D. Fausti et al., "Light-induced superconductivity in a stripe-ordered cuprate.", Science **331**, 189 (2011).

[21] W. Hu et al., "Optically enhanced coherent transport in $YBa_2Cu_3O_{6.5}$ by ultrafast redistribution of interlayer coupling.", Nat. Mater. **13**, 705 (2014).

[22] R. Mankowsky et al., "Nonlinear lattice dynamics as a basis for enhanced superconductivity in $YBa_2Cu_3O_6$.5.", Nature **516**, 71 (2014).

[23] S. Kaiser et al., "Optically induced coherent transport far above T_c in underdoped $YBa_2Cu_3O_{6+\delta}$", Phys. Rev. B **89** (2014).

[24] M. Först et al., "Femtosecond x rays link melting of charge-density wave correlations and light-enhanced coherent transport in $YBa_2Cu_3O_{6.6}$", Phys. Rev. B **90**, 184514 (2014).

[25] D. Nicoletti et al., "Optically induced superconductivity in striped $La_{2-x}Ba_xCuO_4$ by polarization-selective excitation in the near infrared", Phys. Rev. B **90**, 100503 (2014).

[26] M. Mitrano et al., "Possible light-induced superconductivity in K_3C_{60} at high temperature.", Nature **530**, 461 (2016).

[27] L. Taillefer, "Scattering and pairing in cuprate superconductors", Annu. Rev. Condens. Matter Phys. **1**, 51 (2010).

[28] B. Keimer, S. A. Kivelson, M. R. Norman, S.-i. Uchida, and J. Zaanen, "From quantum matter to high-temperature superconductivity in copper oxides.", Nature **518**, 179 (2015).

[29] G. Ghiringhelli et al., "Long-range incommensurate charge fluctuations in $(Y,Nd)Ba_2Cu_3O_{6+x}$", Science **337**, 821 (2012).

[30] J. Chang et al., "Direct observation of competition between superconductivity and charge density wave order in $YBa_2Cu_3O_{6.67}$", Nat. Phys. **8**, 871 (2012).

[31] A. J. Achkar et al., "Distinct charge orders in the planes and chains of ortho-III-ordered $YBa_2Cu_3O_{6+\delta}$ superconductors identified by resonant elastic x-ray scattering.", Phys. Rev. Lett **109**, 167001 (2012).

[32] G. Coslovich et al., "Competition between the pseudogap and superconducting states of $Bi_2Sr_2Ca_{0.92}Y_{0.08}Cu_2O_{8+\delta}$ single crystals revealed by ultrafast broadband optical reflectivity.", Phys. Rev. Lett **110**, 107003 (2013).

[33] K. Fujita et al., "Direct phase-sensitive identification of a d-form factor density wave in underdoped cuprates.", Proc. Natl. Acad. Sci. U.S.A **111**, E3026 (2014).

[34] R. Comin et al., "Charge order driven by Fermi-arc instability in $Bi_2Sr_{2-x}La_xCuO_{6+\delta}$", Science **343**, 390 (2014).

[35] M. Hamidian et al., "Atomic-scale electronic structure of the cuprate d-symmetry form factor density wave state", Nat. Phys. **12**, 150 (2016).

[36] S. Sachdev and R. La Placa, "Bond order in two-dimensional metals with antiferromagnetic exchange interactions.", Phys. Rev. Lett. **111**, 027202 (2013).

[37] J. D. Sau and S. Sachdev, "Mean-field theory of competing orders in metals with antiferromagnetic exchange interactions", Phys. Rev. B **89**, 075129 (2014).

[38] J. J. Hopfield, "Theory of the contribution of excitons to the complex dielectric constant of crystals", Phys. Rev. **112**, 1555 (1958).

[39] R. H. Ritchie, "Plasma losses by fast electrons in thin films", Phys. Rev. **106**, 874 (1957).

[40] J. M. Pitarke, V. M. Silkin, E. V. Chulkov, and P. M. Echenique, "Theory of surface plasmons and surface-plasmon polaritons", Rep. Prog. Phys. **70**, 1 (2007).

[41] G. Borstel and H. J. Falge, "Surface phonon-polaritons at semi-infinite crystals", Phys. Status Solidi B **83**, 11 (1977).

[42] J. Polo and A. Lakhtakia, "Surface electromagnetic waves: a review", Laser Photonics Rev. **5**, 234 (2011).

[43] I. Carusotto and C. Ciuti, "Quantum fluids of light", Rev. Mod. Phys. **85**, 299 (2013).

[44] J. D. Plumhof, T. Stöferle, L. Mai, U. Scherf, and R. F. Mahrt, "Room-temperature bose–einstein condensation of cavity exciton–polaritons in a polymer", Nat. Mater. **13**, 247 (2014).

[45] Y. Sun et al., "Bose-Einstein condensation of long-lifetime polaritons in thermal equilibrium", Phys. Rev. Lett **118**, 016602 (2017).

[46] J. Kasprzak et al., "Bose-Einstein condensation of exciton polaritons", Nature **443**, 409 (2006).

[47] F. Li et al., "From excitonic to photonic polariton condensate in a ZnO-based microcavity.", Phys. Rev. Lett **110**, 196406 (2013).

[48] J. Rammer and H. Smith, "Quantum field-theoretical methods in transport theory of metals", Rev. Mod. Phys. **58**, 323 (1986).

[49] A. Altland and B. D. Simons, *Condensed matter field theory* (Cambridge University Press, 2010).

[50] A. Kamenev, *Field theory of non-equilibrium systems* (Cambridge University Press, 2011).

[51] K. Morawetz, *Interacting systems far from equilibrium: quantum kinetic theory* (Oxford University Press, 2018).

[52] A. Kamenev and A. Levchenko, "Keldysh technique and non-linear σ-model: basic principles and applications", Adv. Phys. **58**, 197 (2009).

[53] Z. M. Raines, V. G. Stanev, and V. M. Galitski, "Enhancement of superconductivity via periodic modulation in a three-dimensional model of cuprates", Phys. Rev. B **91**, 184506 (2015).

[54] Z. Raines, *Phase pinning and interlayer effects on competing orders in cuprates*, 2018, arXiv:1809.06879 [cond-mat.supr-con].

[55] J.-J. Chang and D. J. Scalapino, "Gap enhancement in superconducting thin films due to microwave irradiation", J. Low. Temp. Phys **29**, 477 (1977).

[56] A. Robertson and V. M. Galitski, "Nonequilibrium enhancement of cooper pairing in cold fermion systems", Phys. Rev. A **80** (2009).

[57] R. Höppner, B. Zhu, T. Rexin, A. Cavalleri, and L. Mathey, "Redistribution of phase fluctuations in a periodically driven cuprate superconductor", Phys. Rev. B **91**, 11 (2015).

[58] A. A. Patel and A. Eberlein, "Light-induced enhancement of superconductivity via melting of competing bond-density wave order in underdoped cuprates", Phys. Rev. B **93**, 195139 (2016).

[59] S. A. Kivelson, V. J. Emery, and H. Q. Lin, "Doped antiferromagnets in the weak-hopping limit", Phys. Rev. B **42**, 6523 (1990).

[60] E. Dagotto and J. Riera, "Superconductivity in the two-dimensionalt-jmodel", Phys. Rev. B **46**, 12084 (1992).

[61] D. Chowdhury and S. Sachdev, "Feedback of superconducting fluctuations on charge order in the underdoped cuprates", Phys. Rev. B **90**, 134516 (2014).

[62] A. Allais, J. Bauer, and S. Sachdev, "Auxiliary-boson and dmft studies of bond ordering instabilities of $t - J - V$ models on the square lattice", Indian J. Phys. **88**, 905 (2014).

[63] D. Pines, "Nearly antiferromagnetic fermi liquids: a progress report", Z. Phys. B **103**, 129 (1997).

[64] T. Dahm, D. Manske, and L. Tewordt, "Charge-density-wave and superconductivityd-wave gaps in the hubbard model for underdoped high-T_c cuprates", Phys. Rev. B **56**, R11419 (1997).

[65] N. M. Plakida, "Spin fluctuation superconducting pairing in copper oxides", Philos. Mag. B **76**, 771 (1997).

[66] A. V. Chubukov, D. Pines, and J. Schmalian, in *Superconductivity: conventional and unconventional superconductors*, edited by K. H. Bennemann and J. B. Ketterson (Springer Berlin Heidelberg, Berlin, Heidelberg, 2008), pp. 1349–1413.

[67] M. A. Metlitski and S. Sachdev, "Quantum phase transitions of metals in two spatial dimensions. II. Spin density wave order", Phys. Rev. B **82**, 075128 (2010).

[68] A. Allais, J. Bauer, and S. Sachdev, "Density wave instabilities in a correlated two-dimensional metal", Phys. Rev. B **90**, 155114 (2014).

[69] D. Chowdhury and S. Sachdev, "Density-wave instabilities of fractionalized Fermi liquids", Phys. Rev. B **90**, 245136 (2014).

[70] A. Thomson and S. Sachdev, "Charge ordering in three-band models of the cuprates", Phys. Rev. B **91**, 115142 (2015).

[71] T. Wu et al., "Incipient charge order observed by nmr in the normal state of $YBa_2 Cu_3 O_y$", Nat. Commun. **6**, 6438 (2015).

[72] P. A. Lee, N. Nagaosa, and X.-G. Wen, "Doping a mott insulator: physics of high-temperature superconductivity", Rev. Mod. Phys. **78**, 17 (2006).

[73] K. B. Efetov, H. Meier, and C. Pépin, "Pseudogap state near a quantum critical point", Nat. Phys. **9**, 442 (2013).

[74] Y. Wang and A. V. Chubukov, "Charge-density-wave order with momentum (2q,0) and (0,2q) within the spin-fermion model: continuous and discrete symmetry breaking, preemptive composite order, and relation to pseudogap in hole-doped cuprates", Phys. Rev. B **90**, 035149 (2014).

[75] D. J. Scalapino, "The case for $d_{x^2-y^2}$ pairing in the cuprate superconductors", Phys. Rep. **250**, 329 (1995).

[76] T. Dahm et al., "Strength of the spin-fluctuation-mediated pairing interaction in a high-temperature superconductor", Nat. Phys. **5**, 217 (2009).

[77] R. S. Markiewicz, S. Sahrakorpi, M. Lindroos, H. Lin, and A. Bansil, "One-band tight-binding model parametrization of the high-Tc cuprates including the effect of k_z dispersion", Phys. Rev. B **72**, 054519 (2005).

[78] T. Xiang and W. N. Hardy, "Universalc-axis conductivity of high-T_c oxides in the superconducting state", Phys. Rev. B **63**, 024506 (2000).

[79] A. Moor, P. A. Volkov, A. F. Volkov, and K. B. Efetov, "Dynamics of order parameters near stationary states in superconductors with a charge-density wave", Phys. Rev. B **90**, 024511 (2014).

[80] S. Chakravarty, A. Sudbø, P. Anderson, and S. Strong, "Interlayer tunneling and gap anisotropy in high-temperature superconductors.", Science **261**, 337 (1993).

[81] P. Nyhus, M. A. Karlow, S. L. Cooper, B. W. Veal, and A. P. Paulikas, "Dynamically assisted interlayer hopping in $YBa_2Cu_3O_{6+x}$", Phys. Rev. B **50**, 13898 (1994).

[82] J. D. Jorgensen et al., "Structural properties of oxygen-deficient $YBa_2Cu_3O_{7-\delta}$", Phys. Rev. B **41**, 1863 (1990).

[83] T. Honma and P. Hor, "Universal scaling of the c-axis dc conductivity for underdoped high-temperature cuprate superconductors", Solid State Commun. **150**, 2314 (2010).

[84] M. Bukov, L. D'Alessio, and A. Polkovnikov, "Universal high-frequency behavior of periodically driven systems: from dynamical stabilization to floquet engineering", Adv. Phys. **64**, 139 (2015).

[85] A. Robertson, V. M. Galitski, and G. Refael, "Dynamic stimulation of quantum coherence in systems of lattice bosons.", Phys. Rev. Lett **106**, 165701 (2011).

[86] S. J. Denny, S. R. Clark, Y. Laplace, A. Cavalleri, and D. Jaksch, "Proposed parametric cooling of bilayer cuprate superconductors by terahertz excitation.", Phys. Rev. Lett **114**, 137001 (2015).

[87] V. J. Emery and S. A. Kivelson, "Importance of phase fluctuations in superconductors with small superfluid density", Nature **374**, 434 (1995).

[88] J. Corson, R. Mallozzi, J. Orenstein, J. N. Eckstein, and I. Bozovic, "Vanishing of phase coherence in underdoped $Bi_2Sr_2CaCu_2O_{8+\delta}$", Nature **398**, 221 (1999).

[89] Z. Xu, N. P. Ong, Y. Wang, T. Kakeshita, and S.-i. Uchida, "Vortex-like excitations and the onset of superconducting phase fluctuation in underdoped $La_{2-x}Sr_xCuO_4$", Nature **406**, 486 (2000).

[90] Z. M. Raines, V. G. Stanev, and V. M. Galitski, "Hybridization of Higgs modes in a bond-density-wave state in cuprates", Phys. Rev. B **92**, 184511 (2015).

[91] J. Demsar, K. Biljaković, and D. Mihailovic, "Single particle and collective excitations in the one-dimensional charge density wave solid $K_0.3MoO_3$ probed in real time by femtosecond spectroscopy", Phys. Rev. Lett **83**, 800 (1999).

[92] J. P. Hinton et al., "Time-resolved optical reflectivity of the electron-doped $Nd_{2-x}Ce_xCuO_{4+\delta}$ cuprate superconductor: evidence for an interplay between competing orders.", Phys. Rev. Lett **110**, 217002 (2013).

[93] J. P. Hinton et al., "New collective mode in $YBa_2Cu_3O_{6+x}$ observed by time-domain reflectometry", Phys. Rev. B **88**, 60508 (2013).

[94] D. Torchinsky, F. Mahmood, A. Bollinger, I. Božović, and N. Gedik, "Fluctuating charge-density waves in a cuprate superconductor.", Nat. Mater. **12**, 387 (2013).

[95] G. L. Dakovski et al., "Enhanced coherent oscillations in the superconducting state of underdoped $YBa_2Cu_3O_{6+x}$ induced via ultrafast terahertz excitation", Phys. Rev. B **91**, 220506 (2015).

[96] P. B. Littlewood and C. M. Varma, "Gauge-invariant theory of the dynamical interaction of charge density waves and superconductivity", Phys. Rev. Lett **47**, 811 (1981).

[97] D. T. Lawson, W. J. Gully, S. Goldstein, R. C. Richardson, and D. M. Lee, "Attenuation of zero sound and the low-temperature transitions in liquid He3", Phys. Rev. Lett **30**, 541 (1973).

[98] D. N. Paulson, R. T. Johnson, and J. C. Wheatley, "Propagation of collisionless sound in normal and extraordinary phases of liquid he_3 below 3 mK", Phys. Rev. Lett **30**, 829 (1973).

[99] D. Pekker and C. M. Varma, "Amplitude/Higgs modes in condensed matter physics", Annu. Rev. Condens. Matter Phys. **6**, 269 (2015).

[100] G. E. Volovik and M. A. Zubkov, "Higgs bosons in particle physics and in condensed matter", J. Low. Temp. Phys **175**, 486 (2014).

[101] P. B. Littlewood and C. M. Varma, "Amplitude collective modes in superconductors and their coupling to charge-density waves", Phys. Rev. B **26**, 4883 (1982).

[102] D. A. Browne and K. Levin, "Collective modes in charge-density-wave superconductors", Phys. Rev. B **28**, 4029 (1983).

[103] X. Lei, C. Ting, and J. L. Birman, "Spectral function of the charge-density-wave (CDW) phonon in an anisotropic CDW superconductor", Phys. Rev. B **30**, 6387 (1984).

[104] X. Lei, C. Ting, and J. L. Birman, "Raman scattering of light from a charge-density-wave (CDW) phonon in an anisotropic CDW superconductor", Phys. Rev. B **32**, 1464 (1985).

[105] I. Tüttö and A. Zawadowski, "Theory of Raman scattering of superconducting amplitude modes in charge-density-wave superconductors", Phys. Rev. B **45**, 4842 (1992).

[106] T. Cea and L. Benfatto, "Nature and Raman signatures of the Higgs amplitude mode in the coexisting superconducting and charge-density-wave state", Phys. Rev. B **90** (2014).

[107] I. Kulik, O. Entin-Wohlman, and R. Orbach, "Pair susceptibility and mode propagation in superconductors: a microscopic approach", J. Low. Temp. Phys **43**, 591 (1981).

[108] M. Vojta and S. Sachdev, in *Advances in solid state physics* (Springer, 2001), pp. 329–341.

[109] H. Schaefer, V. V. Kabanov, and J. Demsar, "Collective modes in quasi-one-dimensional charge-density wave systems probed by femtosecond time-resolved optical studies", Phys. Rev. B **89**, 45106 (2014).

[110] E. Abrahams and T. Tsuneto, "Time variation of the ginzburg-landau order parameter", Phys. Rev. **152**, 416 (1966).

[111] A. Larkin and A. Varlamov, *Theory of fluctuations in superconductors* (Clarendon Press, 2005).

[112] S. G. Sharapov, H. Beck, and V. M. Loktev, "Finite-temperature time-dependent effective theory for the phase field in two-dimensionald-wave neutral superconductors", Phys. Rev. B **64**, 23 (2001).

[113] W. Fu, L.-Y. Hung, and S. Sachdev, "Quantum quenches and competing orders", Phys. Rev. B **90**, 24506 (2014).

[114] R. Matsunaga et al., "Higgs amplitude mode in the BCS superconductors $Nb_{1-x}Ti_xN$ induced by terahertz pulse excitation", Phys. Rev. Lett **111**, 057002 (2013).

[115] J. B. Curtis, Z. M. Raines, A. A. Allocca, M. Hafezi, and V. M. Galitski, "Cavity quantum Eliashberg enhancement of superconductivity", Phys. Rev. Lett **122**, 167002 (2019).

[116] T. M. Klapwijk, J. N. v. d. Bergh, and J. E. Mooij, "Radiation-stimulated superconductivity", J. Low. Temp. Phys **26**, 385 (1977).

[117] A. Schmid, "Stability of radiation-stimulated superconductivity", Phys. Rev. Lett **38**, 922 (1977).

[118] A. Schmid, "Superconductors out of thermal equilibrium", Le Journal de Physique Colloques **39**, C6 (1978).

[119] J.-J. Chang and D. J. Scalapino, "Nonequilibrium superconductivity", J. Low. Temp. Phys **31**, 1 (1978).

[120] A. Cavalleri, "Photo-induced superconductivity", Contemp. Phys. **59**, 31 (2018).

[121] M. Babadi, M. Knap, I. Martin, G. Refael, and E. Demler, "Theory of parametrically amplified electron-phonon superconductivity", Phys. Rev. B **96** (2017).

[122] A. Kemper, M. Sentef, B. Moritz, J. Freericks, and T. Devereaux, "Direct observation of Higgs mode oscillations in the pump-probe photoemission spectra of electron-phonon mediated superconductors", Phys. Rev. B **92**, 224517 (2015).

[123] M. A. Sentef, A. Kemper, A. Georges, and C. Kollath, "Theory of light-enhanced phonon-mediated superconductivity", Phys. Rev. B **93**, 144506 (2016).

[124] Y. Murakami, N. Tsuji, M. Eckstein, and P. Werner, "Nonequilibrium steady states and transient dynamics of conventional superconductors under phonon driving", Phys. Rev. B **96**, 045125 (2017).

[125] A. Komnik and M. Thorwart, "BCS theory of driven superconductivity", Eur. Phys. J. B **89**, 244 (2016).

[126] R. H. Dicke, "Coherence in spontaneous radiation processes", Phys. Rev. **93**, 99 (1954).

[127] E. M. Purcell, "Spontaneous emission probabilities at radio frequencies", in *Confined electrons and photons: new physics and applications*, edited by E. Burstein and C. Weisbuch (Springer US, Boston, MA, 1995), pp. 839–839.

[128] G. Baskaran, *Superradiant superconductivity*, 2012, arXiv:1211.4567 [cond-mat.supr-con].

[129] E. Jaynes and F. Cummings, "Comparison of quantum and semiclassical radiation theories with application to the beam maser", Proc. IEEE **51**, 89 (1963).

[130] T. Ebbesen, "Hybrid light-matter states in a molecular and material science perspective.", Acc. Chem. Res. **49**, 2403 (2016).

[131] H. Deng, G. Weihs, C. Santori, J. Bloch, and Y. Yamamoto, "Condensation of semiconductor microcavity exciton polaritons", Science **298**, 199 (2002).

[132] T. Byrnes, N. Y. Kim, and Y. Yamamoto, "Exciton–polariton condensates", Nat. Phys. **10**, 803 (2014).

[133] A. Blais, R.-S. Huang, A. Wallraff, S. M. Girvin, and R. J. Schoelkopf, "Cavity quantum electrodynamics for superconducting electrical circuits: an architecture for quantum computation", Phys. Rev. A **69** (2004).

[134] C. Maissen et al., "Ultrastrong coupling in the near field of complementary split-ring resonators", Phys. Rev. B **90**, 205309 (2014).

[135] M. Malerba et al., "Towards strong light-matter coupling at the single-resonator level with sub-wavelength mid-infrared nano-antennas", Appl. Phys. Lett. **109**, 021111 (2016).

[136] A. Bayer et al., "Terahertz light-matter interaction beyond unity coupling strength.", Nano Lett. **17**, 6340 (2017).

[137] M. Sentef, M. Ruggenthaler, and A. Rubio, "Cavity quantum-electrodynamical polaritonically enhanced electron-phonon coupling and its influence on superconductivity.", Sci. Adv. **4**, eaau6969 (2018).

[138] A. A. Allocca, Z. M. Raines, J. B. Curtis, and V. M. Galitski, "Cavity superconductor-polaritons", Phys. Rev. B **99** (2019).

[139] G. Mazza and A. Georges, "Superradiant quantum materials", Phys. Rev. Lett **122** (2019).

[140] F. Schlawin, A. Cavalleri, and D. Jaksch, *Cavity-mediated electron-photon superconductivity*, 2018, arXiv:1804.07142 [cond-mat.mes-hall].

[141] Z. Raines, A. A. Allocca, and V. Galitski, "Cavity Higgs-polaritons", In Preperation (2019).

[142] Weisbuch, Nishioka, Ishikawa, and Arakawa, "Observation of the coupled exciton-photon mode splitting in a semiconductor quantum microcavity.", Phys. Rev. Lett **69**, 3314 (1992).

[143] E. Wertz et al., "Spontaneous formation and optical manipulation of extended polariton condensates", Nat. Phys. **6**, 860 (2010).

[144] F. Laussy, A. Kavokin, and I. Shelykh, "Exciton-polariton mediated superconductivity", Phys. Rev. Lett **104**, 106402 (2010).

[145] O. Cotleţ, S. Zeytinoğlu, M. Sigrist, E. Demler, and A. Imamoğlu, "Superconductivity and other collective phenomena in a hybrid Bose-Fermi mixture formed by a polariton condensate and an electron system in two dimensions", Phys. Rev. B **93**, 054510 (2016).

[146] R. Matsunaga et al., "Light-induced collective pseudospin precession resonating with Higgs mode in a superconductor.", Science **345**, 1145 (2014).

[147] N. Tsuji and H. Aoki, "Theory of Anderson pseudospin resonance with Higgs mode in superconductors", Phys. Rev. B **92**, 064508 (2015).

[148] K. Katsumi et al., "Higgs mode in the d-wave superconductor $Bi_2Sr_2CaCu_2O_{8+x}$ driven by an intense terahertz pulse", Phys. Rev. Lett **120**, 117001 (2018).

[149] F. Kretzschmar et al., "Raman-Scattering Detection of Nearly Degenerate s-Wave and d-Wave Pairing Channels in Iron-Based $Ba_{0.6}K_{0.4}Fe_2As_2$ and $Rb_{0.8}Fe_{1.6}Se_2$ Superconductors", Phys. Rev. Lett. **110**, 187002 (2013).

[150] T. Böhm et al., "Balancing act: evidence for a strong subdominantd-wave pairing channel in $Ba_{0.6}K_{0.4}Fe_2As_2$", Phys. Rev. X **4** (2014).

[151] D. Jost et al., "Indication of subdominant d -wave interaction in superconducting cakfe4as4", Phys. Rev. B **98** (2018).

[152] S. Maiti and P. J. Hirschfeld, "Collective modes in superconductors with competings- andd-wave interactions", Phys. Rev. B **92**, 094506 (2015).

[153] A. Moor, A. Volkov, and K. Efetov, "Amplitude Higgs mode and admittance in superconductors with a moving condensate.", Phys. Rev. Lett **118**, 047001 (2017).

[154] S. Nakamura, Y. Iida, Y. Murotani, R. Matsunaga, H. Terai, and R. Shimano, *Infrared activation of Higgs mode by supercurrent injection in a superconductor NbN*, 2018, arXiv:1809.10335 [cond-mat.supr-con].

[155] A. Bardasis and J. R. Schrieffer, "Excitons and plasmons in superconductors", Phys. Rev. **121**, 1050 (1961).

[156] M. M. Qazilbash et al., "Electronic correlations in the iron pnictides", Nat. Phys. **5**, 647 (2009).

[157] N. Barišić, D. Wu, M. Dressel, L. J. Li, G. H. Cao, and Z. A. Xu, "Electrodynamics of electron-doped iron pnictide superconductors: normal-state properties", Phys. Rev. B **82**, 054518 (2010).

[158] D. C. Johnston, "The puzzle of high temperature superconductivity in layered iron pnictides and chalcogenides", Adv. Phys. **59**, 803 (2010).

[159] V. Cvetkovic and O. Vafek, "Space group symmetry, spin-orbit coupling, and the low-energy effective hamiltonian for iron-based superconductors", Phys. Rev. B **88**, 134510 (2013).

[160] E. F. Talantsev and J. L. Tallon, "Universal self-field critical current for thin-film superconductors", Nat. Commun. **6**, 7820 (2015).

[161] S. J. Singh et al., "Ultrahigh critical current densities, the vortex phase diagram, and the effect of granularity of the stoichiometric high-T_c superconductor $CaKFe_4As_4$", Phys. Rev. Mater. **2**, 074802 (2018).

[162] D. C. Mattis and J. Bardeen, "Theory of the anomalous skin effect in normal and superconducting metals", Phys. Rev. **111**, 412 (1958).

[163] A. Volkov and S. M. Kogan, "Collisionless relaxation of energy-gap in superconductors", Zh. Eksp. Teor. Fiz **65**, 2038 (1973).

[164] L. Sieberer, M. Buchhold, and S. Diehl, "Keldysh field theory for driven open quantum systems.", Rep. Prog. Phys. **79**, 096001 (2016).

[165] M. Galassi and B. Gough, *Gnu scientific library: reference manual*, GNU manual (Network Theory, 2009).